

# **Voortschrijdend Onderzoeks Programma Slib**

**Rapportage 2008**

Bas van Maren, Kees Kuijper, Yann Friocourt, Sofia Caires, Thijs  
van Kessel



Prepared for:  
Waterdienst

# **Voortschrijdend Onderzoeks Programma Slib**

**Rapportage 2008**

Bas van Maren, Kees Kuijper, Yann Friocourt, Sofia Caires,  
Thijs van Kessel

Report

January 2009



<b>Client</b>	Waterdienst						
<b>Title</b>	Voortschrijdend Onderzoeks Programma Slib						
<b>Abstract</b>							
<p>This report presents the results of the activities in the framework of the project 'VOP-slib' in 2008. VOP-slib research in 2008 focussed on the buffering of fines in a mud bed, improvement of the North Sea model, and testing of a new consolidation and fluid mud model. For the fine sediment buffering a literature study was conducted, and overview of sand-mud model implementations was compiled, and the sand-mud model in Delft3D-WAQ was improved. For the North Sea model, the wave forcing was improved, and a sensitivity analysis on parameters that determine mud transport was made. The fluid mud and consolidation model was tested on a simple slope and on a schematized harbour basin.</p>							
<b>References</b>			Stuurboord 2008				
Ver	Author	Date	Remarks	Review	Approved by		
	Bas van Maren,			van Kessel	Schilperoort		
<b>Project number</b>		Z4773.00					
<b>Keywords</b>		siltation, fluid mud, applied research, wave models, mud transport, numerical modelling, sand, mud					
<b>Number of pages</b>		116					
<b>Classification</b>		None					
<b>Status</b>		Final					



## Contents

<b>1</b>	<b>Introduction .....</b>	<b>1</b>
<b>2</b>	<b>Buffering of fines: a literature review .....</b>	<b>3</b>
2.1	Introduction .....	3
2.2	Mud infiltration mechanisms .....	3
2.2.1	Sedimentological processes .....	3
2.2.2	Bioturbation .....	4
2.2.3	Advective transport.....	5
2.2.4	Turbulent diffusion.....	6
2.2.5	Modelling .....	7
2.3	Residence time & infiltration rates .....	7
2.3.1	Infiltration rates.....	7
2.3.2	Mixing rates & diffusion coefficients.....	8
2.3.3	Residence time.....	9
2.3.4	Measurement methods .....	9
2.4	Erosion rate of sand-mud mixtures .....	10
2.5	The North Sea.....	11
2.5.1	Mud content.....	11
2.5.2	Bioturbation .....	12
2.5.3	Pore water flow.....	12
2.6	Discussion and conclusion .....	15
<b>3</b>	<b>Sand-mud modelling in Delft3D.....</b>	<b>19</b>
3.1	General background .....	19
3.2	Activities carried out in 2008.....	19
3.3	Implementation sand-mud interaction in WAQ.....	20
3.4	'Buffer model' .....	21
3.5	Activities elsewhere with respect to sand-mud processes and modelling.....	22
<b>4</b>	<b>Non-stationary wave computations in the North Sea .....</b>	<b>25</b>
4.1	Introduction .....	25
4.2	Model description.....	25
4.2.1	Setup of the computations .....	25
4.2.2	Description of the SWAN model .....	26
4.2.3	Default SWAN settings in Delft3d-WAVE .....	29
4.3	Description of the measurements.....	29
4.4	Description of the results .....	31
4.4.1	Initial results .....	31
4.4.2	Model calibration results .....	34

4.5	Conclusions .....	36
<b>5</b>	<b>Uncertainties in mud transport modelling of the North Sea .....</b>	<b>39</b>
5.1	Introduction .....	39
5.2	Methodology .....	39
5.3	Overview of the available measurement sources .....	40
5.3.1	In-situ measurements .....	40
5.3.2	Remote sensing data .....	41
5.3.3	Discussion of the data uncertainties .....	41
5.4	Model setup .....	42
5.5	Model results .....	43
5.5.1	Reference simulation .....	43
5.5.2	Uncertainty analysis .....	48
5.5.3	Discussion .....	54
<b>6</b>	<b>Modelling harbour siltation by fluid mud flows .....</b>	<b>57</b>
6.1	Introduction .....	57
6.2	Consolidation and fluid mud transport .....	57
6.3	Model setup .....	59
6.3.1	Model physics .....	59
6.3.2	Simple slope application .....	60
6.3.3	Schematized harbour basin .....	60
6.3.4	Sediment settings .....	62
6.4	Simple slope model .....	63
6.4.1	Introduction .....	63
6.4.2	Results .....	64
6.4.3	Discussion .....	68
6.5	Schematized harbour basin .....	69
6.5.1	Scenarios .....	69
6.5.2	Budgets .....	75
6.6	Discussion .....	75
6.6.1	Transport mechanisms .....	75
6.6.2	Implications for harbour siltation .....	77
6.7	Conclusions .....	77
<b>7</b>	<b>References .....</b>	<b>79</b>
<b>Appendices</b>		
<b>A</b>	<b>Sand-mud interaction in Delft3D-WAQ .....</b>	<b>85</b>
A.1	Definities .....	85
A.2	Niet-cohesief regime (zand gedomineerd): $p_m < p_{m,cr}$ .....	86
A.2.1	Erosiesnelheid en erosieparameter .....	86
A.2.2	Kritieke erosieschuifspanning ( $p_m < p_{m,cr}$ ) .....	88
A.3	Cohesief regime (slib gedomineerd): $p_m > p_{m,cr}$ .....	90
A.3.1	Erosieparameter $M_c$ ( $p_m > p_{m,cr}$ ) .....	91
A.3.2	Kritieke erosieschuifspanning ( $p_m > p_{m,cr}$ ) .....	91

---

A.4	Samenvatting .....	92
<b>B</b>	<b>Beschrijving Buffer model .....</b>	<b>95</b>
<b>C</b>	<b>Notulen bijeenkomst Bram van Prooijen, Kees Kuijper, Johan de Kok ...</b>	<b>101</b>
C.1	Achtergronden .....	101
C.2	Activiteiten elders.....	101
C.3	Activiteiten TUD (Bram) op gebied van zand-slib formuleringen .....	101
C.4	Buffermodel.....	102
C.5	Overig .....	103
C.6	Acties .....	103
<b>D</b>	<b>Notulen bijeenkomst Walter Jacobs, Kees Kuijper, Johan de Kok.....</b>	<b>105</b>
D.1	Achtergronden .....	105
D.2	Bulkparameters zand-slib mengsels .....	105
D.3	Erosie en consolidatie van zand-slib mengsels .....	106
D.4	Noordzee .....	106
D.5	Relaties tussen parameters.....	106
D.6	Overige zaken.....	106
D.7	Consequenties voor toekomstige ontwikkelingen .....	107
<b>E</b>	<b>Kennisvragen vanuit ingenieurspraktijk .....</b>	<b>109</b>



## 1 Introduction

Applied mud-related research has been carried out by Deltares / Delft Hydraulics in the framework of Voortschrijdend Onderzoeks Programma Slib (VOP-slib) since 2006. The objective of VOP is to carry out applied research to support managerial issues. It forms a link between more fundamental research (often carried out at Universities) and engineering applications. It focuses on the development and application of models or knowledge rules which can be readily applied to assess the impact of changes to the natural system or the autonomous development hereof.

The range of activities has been steadily increasing in the past years. In 2006, the focus was on improvement of the modelling capability of the seasonal variation in mud concentration in the North Sea (Brière and van Kessel, 2006). In 2007, the main goal was to make an inventory of the knowledge gaps that exist within the regional directorates of the Ministry of Public Works (Rijkswaterstaat). These knowledge gaps and scientific questions formed the basis of a long-term research plan 2007-2011 (Bruens et al, 2007). This research plan was composed of three main parts:

- 1) Development of models (mainly improve model parameterisations)
- 2) System analysis (i.e. detailed hydrodynamic analysis, data-model integration, required resolution)
- 3) Model application (development of operational models, implementation of new model formulations).

The VOP-slib 2008 programme was based on this long-term research programme. Its specific aims were to (van Kessel, 2008):

- 1) Further analyse the buffering of fines in a sand bed
- 2) Further develop the North Sea mud model
- 3) Disseminate knowledge and develop future plans.

This report presents the results of the work carried out in 2008. A literature review on the buffering of fines is presented in Chapter 2, while a review of sand-mud interaction model approaches is given in Chapter 3. Further developments of the North Sea model are dealt with in Chapters 4 and 5. Improvement of wave simulations with the ZUNO model are presented in Chapter 4, while a sensitivity analyses on model uncertainties is given in Chapter 5. As part of ongoing model development, the slib3D code has been verified and applied to the modelling of harbour siltation by fluid mud flows (Chapter 6). Dissemination of knowledge and developments of future plans have been postponed to VOP-slib 2009 (van Maren et al., 2009). However, Royal Haskoning has been asked to make a short inventory of mud-related issues in engineering practise (Appendix E).



---

## 2 Buffering of fines: a literature review

### 2.1 Introduction

Research on the impact of large-scale sand mining in the Dutch coastal zone in the framework of Maasvlakte-2 land reclamation has demonstrated the influence of the assumed buffer capacity of fines in the sandy seabed on the long-term behaviour of the dispersion of fines (Van Kessel et al. & Van Prooijen et al., 2007). As insufficient knowledge on this buffer capacity exist, a literature review was made as a first step towards increasing the accuracy of fine sediment dispersion models.

Fine sediments penetrate into or are released from a sandy substrate, depending on the hydrodynamic conditions. Release of fine sediments results in an increasing sediment concentration in the upper water column, while penetration of fines into the bed lowers the suspended sediment concentration. This so-called buffering of fines into a sandy substrate has been demonstrated to influence the annual variation of the suspended sediment concentration: In the North Sea, the mud concentrations 2 km offshore are larger during and after storms than before storms. It takes days to weeks for the concentrations to return to pre-storm values. The autumn sediment concentrations are lower than the spring sediment concentrations, during similar hydrodynamic conditions (Kleinhans et al., 2005).

The physical processes responsible for the buffering of fine sediments still remain to be further explored. This literature review aims to summarize the mud infiltration mechanisms in subtidal marine sediment beds, estimates of mixing rates and residence times of mud in sand beds, and state-of-the-art modelling efforts. Although primarily generic, this review is also regionally focusing on the North Sea area. The infiltration mechanisms in intertidal areas such as swash on sloping beaches (i.e. Turner and Masselink, 1998) or sand banks (Gibbes et al. 2008s, 2008b) are not evaluated here.

### 2.2 Mud infiltration mechanisms

In muddy, cohesive sediment, solutes are mainly transported by molecular diffusion, and possibly by benthic fauna. Interstitial flow is much faster in permeable sands, resulting in higher advective transport rates (see Figure 2.1). Advective transport is flow-induced material transport through sediment pores, driven by pressure gradients. Especially in the presence of bedforms, advective transport in permeable sediments may be high. Furthermore, fine sediment may be mixed or released from a sand bed through bedform migration. These mechanisms can be summarized as (1) sedimentological processes, (2) biological processes, (3), advective transport, and (4) molecular diffusion, which will be elaborated hereafter.

#### 2.2.1 Sedimentological processes

The entrainment of muds into suspension is coupled to bedform dynamics. Mobile bedforms create an active layer of sediment with a thickness approximately equal to the bedform height, to be mobilised during one or a few storms. On a timescale of 1-10 years, bedforms smaller than sandwaves, macrobenthos, and fishing determine the mobility depth (Kleinhans et al, 2005).

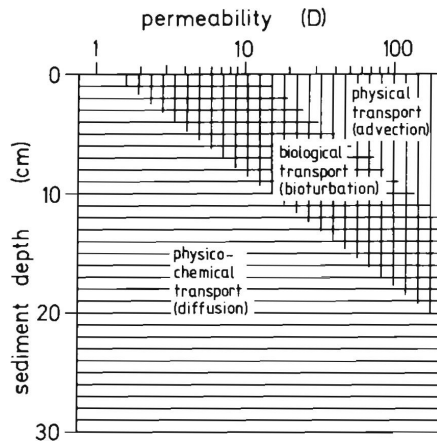


Figure 2.1 Mixing process as a function of depth and permeability ( $D$ , in  $10^{-13} \text{ m}^2$ ). From Huettel and Gust, 1992.

Mud infiltrates a sand bed by bedform dynamics through two mechanisms:

- 1) Mud drapes (consolidated or not) are covered by bedforms. In the North sea, these drapes are typically 1-5 mm thick (Kleinhans et al., 2005). Such mud drapes can probably only form during summer neap tides. Burial by large bedforms, such as sandwaves, may lead to residence times of the mud in the sand bed of 1 century.
- 2) The upper part of a sediment bed is permanently mobilised by ripples (the active layer), even during fairly tranquil conditions during which a substantial amount of fine sediment may settle towards the bed. In the North Sea, ripples generated by tidal currents bury fine sediment up to a depth of 5 cm (Kleinhans et al., 2005). Most organisms must migrate below the active layer to survive highly energetic conditions (Kleinhans et al., 2005).

Marinelli et al (1998) measured a 'reset' of tracer concentrations during the winter storm season. A single hurricane was insufficient to vertically mix and lower the tracer concentrations, from which they assumed that longer term energetic conditions are needed to reset the profile.

### 2.2.2 Bioturbation

Organisms influence sediment beds mainly through biodeposition, biostabilization, and bioturbation. Biodeposition results in increased sedimentation rates, biostabilization in reduced erosion rates, and bioturbation in increased mixing rates (which, usually, increases the erosion rate). Modelling results by Paarlberg et al. (2004) suggest that destabilizing organisms reduce the mud content in a bed, whereas stabilizing organisms *may* cause an increase in the mud content.

Biodeposition through faeces production is different for deposit feeders, which only change the characteristics of existing sediment, and filter feeders, which add new material to the sediment (Lee and Swartz, 1980). Bed sediment is stabilized through microbial binding (micro-organisms, especially polysaccharides), tubes (especially species that burrow firm tubes), roots by aquatic vegetation, and by benthic macroalgal mats. Bioturbation results in the vertical mixing of surface sediment. Mixing rate and burial depth depend on the species that occur at a typical site, which in turn relate to the hydrodynamic conditions, sediment available, nutrients and temperature. Hence, the variation of mixing by bioturbation is large. An extensive review of reworking rate and penetration depth is given by Lee and Swartz (1980).

### 2.2.3 Advective transport

Advective transport is the transport of fines by interstitial porewater flow in stationary sediment beds. Fines and the coarser sediment matrix are therefore not physically mixed: the sand matrix through which the fines percolate remains unchanged.

Mechanisms of advective transport are (Huettel and Webster, 2001):

- Current-topography interaction by steady flow as well as by oscillating wave-generated currents.
- Wave-generated pressure gradients.
- Haline or thermal convection.

#### *Current-topography interaction*

Pressure differences generated by bedforms cause inflow into the bedform troughs and outflow from the bedform crests (see Figure 2.2). Infiltration rates are highest for fines with a grain size of  $1\ \mu\text{m}$  as smaller grain sizes adhere to particles, while coarser are blocked by the pores (Huettel et al., 1996). In a shallow but calm environment (0.5 m deep, wave height less than 0.1 m), the bulk porewater flow velocity decreases from nearly 50 cm/hr or  $140\ \mu\text{m/s}$  (near-surface) to 20 cm/hr at a depth of 5 cm (Precht and Huettel, 2004). In addition to bedforms, bioroughness may also generate pressure differences sufficiently high to generate pore water flows (Huettel and Gust, 1992). Thibodeaux and Boyle (1987) measured inflow velocities of around  $50\ \mu\text{m/s}$ , and intrusion depth 5 times the bedform height. Wilson et al. (2008) estimate that under typical shelf conditions, bottom currents induce pressure gradients up to 2 Pa/cm across seafloor ripples and similar seafloor features. Resulting porewater flows can reach the upper 30 cm of sediments below the seafloor. The magnitude of this flow depends on the permeability of the sediments in question, and laboratory studies suggest that this type of flow does not affect biogeochemical processes significantly below a permeability of roughly  $10^{-12}\ \text{m}^2$  (Wilson et al., 2008).

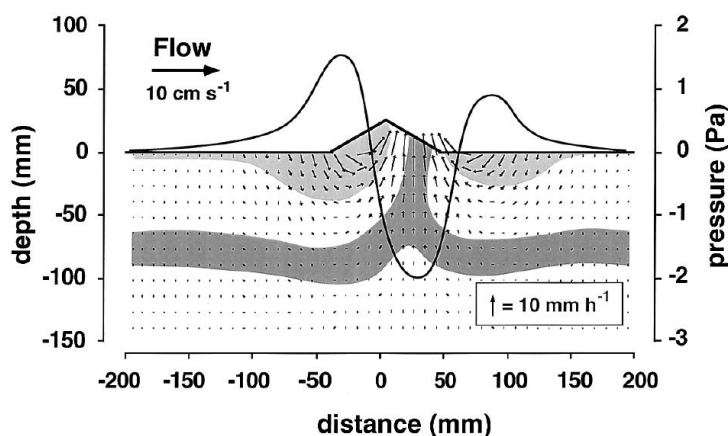


Figure 2.2 Infiltration and outflow due to pressure variations over bed-topography interaction in steady uniform flow. From Huettel et al., 1998.

### *Wave-generated pressure gradients*

Alternatively, mud infiltration into sand beds may be substantially increased by wave-generated pressure gradients (Riedl et al, 1972, Harrison et al., 1983, Shum, 1993). The dynamic pressure gradients generated by waves creates oscillating horizontal near-bed flows, as well as oscillating pressure gradients. The horizontal flow velocities produce inflow of pore water when interacting with morphologic perturbations, which is basically the mechanism described in section above. The focus here is on the effect of the time-varying pressure gradients near the bed, generating inflow and outflow of pore water.

Wave –generated pressures are highest under the wave crest, resulting in inflow, while water flows upward under the wave trough. The result is an elliptical trajectory of the porewater within the bed, more analogue to eddy diffusion than to advection (Riedl et al., 1972, Harrison et al., 1983). The resulting exchange velocity between the bed and the water column depends on wave characteristics (wave height, and length), fluid viscosity, bed permeability which was elaborated in detail by Riedl et al. (1972). The depth to which the porewater penetrates as a result of wave-driven pressure difference is not quantified. Transport of porewater within the sand bed itself were addressed by Harrison et al. (1983) and Rutgers van der Loeff (1981) Harrison et al. (1983) quantified the wave-driven mechanical dispersion whereby wave-enhanced transport is simulated with an empirical diffusion coefficient. Wave-driven mechanical dispersion is favored by large grain size or high permeability, large sediment thickness, large wave amplitude, and shallow water. However, the mechanisms by which an oscillatory flow generates net advective transport are not obvious. Solute transport in a porous medium forced by an oscillatory flow may be caused by rotational dispersion or by shear dispersion (Webster, 2003). Rotational dispersion requires that the pore water excursion exceeds the grain size diameter, and therefore there is a minimum wave height, grain diameter, and penetration depth for which this mechanism effectively contributes to pore water mixing. Shear dispersion (Webster, 2003) creates a radial concentration gradient of a solute transported by the pore water flow within the pores itself. This gradient is reduced by molecular diffusion, resulting in mixing along the length of the pores. Shear dispersion is effective for mixing of solutes within pores to greater depths than rotational dispersion, even if these may dominate the mixing close to the water-bed interface (Webster, 2003).

### *Density-driven convection*

Haline or thermal convection may play a role in areas with substantial temporal variations in salinity or temperature. When the water above the water-bed interface is more saline or colder than the porewater, the water in the upper layer enters the permeable bed as plumes, while the fresher and/or warmer porewater is expelled. Mixing rates by haline convection are substantially larger than mixing rates by molecular diffusion (Huettel and Webster, 2001).

#### 2.2.4 Turbulent diffusion

In absence of other mixing processes, fines transported in pore waters may be mixed within the sand matrix by turbulent diffusion. However, turbulent diffusion is probably several orders of magnitude lower than any of the other mechanism, and is therefore of minor importance. Advective transport dominates over diffusion processes when the Péclet Number exceeds unity. In coarse-grained ( $d = 2$  mm), shallow areas ( $H = 5$  m) with relatively large waves ( $H_s = 0.5$  m)), the wave-driven diffusivity increases 4 orders

of magnitude compared to the molecular diffusivity (Harrison et al, 1983). In a shallow area in the Mediterranean Sea with very low wave heights ( $H = 0.7$  m and  $H_s = 0.1$  m), the advective transport was observed to exceed transport by molecular diffusion by at least 3 orders of magnitude (Precht and Huettel, 2004). The importance of molecular diffusion is higher at impermeable sediments and absence of biological and/or physical mixing mechanisms (see also Figure 2.1).

### 2.2.5 Modelling

Several numerical models exist that compute the grain size distribution of sediment beds using different sediment fractions. In these models, sediment is deposited as distinct layers which are vertically mixed within the bed through a diffusion coefficient representing bioturbation. Harris and Wiberg (1996), for instance, apply a double-layer sediment transport model to account for the effect of bed armouring. The upper layer may be resuspended, while sediment from the lower layer may be mixed upward by biodiffusion. The depth of the active layer is related to the excess shear strength and the grain size. Sanford (2008) developed a 1DV numerical (MATLAB) model simulating the effect of bioturbation on the vertical distribution of sand and mud. Van Ledden (2003) developed a sand-mud model as part of the Delft3D model suite that model the vertical and spatial segregation of sand-mud mixtures. A distinguishing aspect of van Ledden's model is that it also models the effect of mixtures on erosion rates. Paarlberg et al (2004) extended the sand-mud model developed by Van Ledden (2003) with biotic stabilization and mixing.

A two layer mud buffering model is developed by van Prooijen et al. (2007) and van Kessel et al. (submitted) to simulate fine sediment transport in a sandy environment. The first layer is representative for the thin fluff layer on the bed surface that forms during slack tide and that is easily resuspended by tidal currents. The total sediment mass in this layer tends to be small and the residence time of sediment in this layer is short because of the large flux between the fluff layer and the water column. The second layer is representative for the sandy seabed into which fines may entrain and temporarily be stored. Resuspension from this buffer layer is only significant during highly dynamic conditions, such as spring tide or storms. A user-defined fraction of the fine sediment is transported from the water column into the layer 1 and 2, and eroded when the bed shear stress exceeds a critical value  $\tau_{cr}$ . Since  $\tau_{cr}$  of the layer 2 (lower layer) is higher than the layer 1 (upper layer), sediment is transported from layer 1 to layer 2 when  $\tau_{cr,1} < \tau < \tau_{cr,2}$ . An alternative method to transport sediment from layer 1 to layer 2 is through a so-called burial term in which a user defined percentage of fines in the upper layer is transported to the deeper layer. This latter is more in analogy to diffusion coefficients representing bioturbation used in other models. The erosion rates in van Kessel's and van Prooijen's model is not influenced by the composition of the sand-mud mixtures. Also, it only simulates the transport of mud, and not of sand.

## 2.3 Residence time & infiltration rates

### 2.3.1 Infiltration rates

Infiltration rates are highest for fines with a grain size of  $1 \mu\text{m}$  because smaller grain sizes adhere to particles, while coarser are blocked by the pores (Huettel et al., 1996). Field measurements of Reimers et al. (2004) of flow intrusion at a water depth of 13 m yielded intrusion velocities up to 53 cm/hr near the seabed surface, decreasing rapidly

to nearly 0 approximately 2 cm below the seabed surface. The intrusion velocity is episodic, depending on the wave height and current velocity. Intrusion velocities rapidly decline with depth and time. Thibodeaux and Boyle (1987) measured inflow velocities of around 50  $\mu\text{m/s}$  in the field. Measured inflow velocities are lower in laboratory conditions: intrusion velocities over 1 cm/hour near the surface were measured by Huettel et al. (1996, 1998) due to flow-topography interactions. More typical inflow velocities are displayed in Figure 2.3 (Precht and Huettel, 2004).

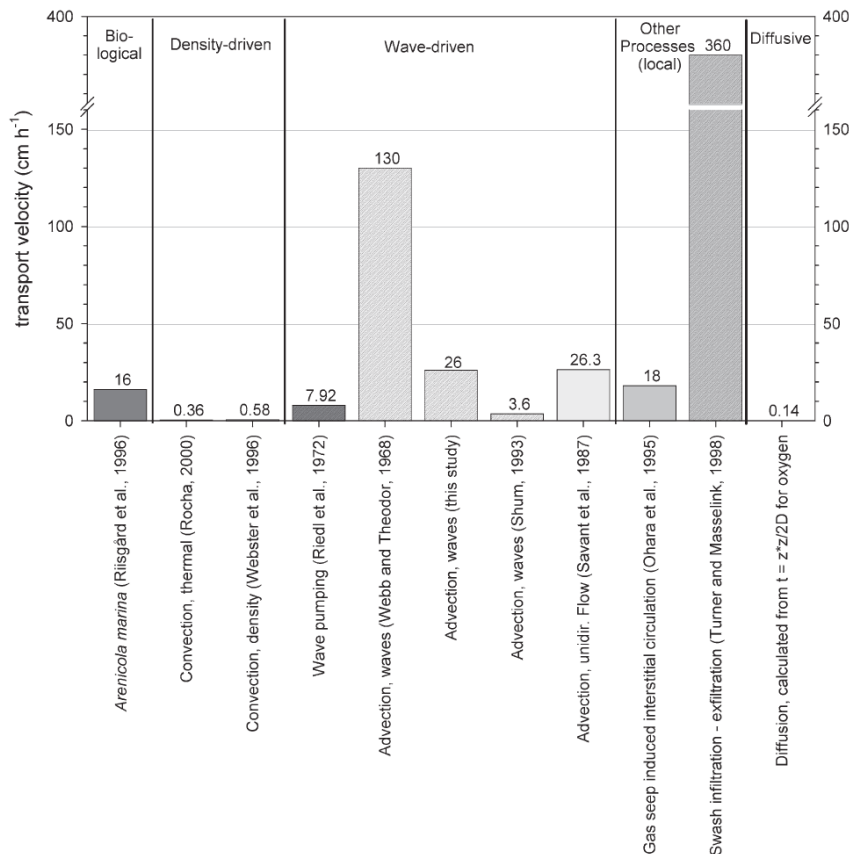


Figure 2.3 Flow velocity in permeable sediment, based on different sources (Precht and Huettel, 2004).

Infiltration rates are determined by hydrodynamics and sediment dynamics. Especially the permeability is important for the inflow velocity. The inflow velocity scales linearly with permeability, but at different locations around the world the permeability differs several orders of magnitude. Wilson et al. (2008) related existing measurements of permeability obtained worldwide to the grain size. The permeability correlates reasonably with grain size as long as the nearshore zone (< 10 m water depth) is separated from the continental shelf (>10 m water depth). The lowest permeability observed in undisturbed samples is  $2 \cdot 10^{-12}$  m/s (at a median grain size  $D_{50}$  of 150  $\mu\text{m}$ ). The permeability in the nearshore zone is consistently lower than that on the continental shelf, despite a similar grain size class.

### 2.3.2 Mixing rates & diffusion coefficients

Dellapenna et al. (1998) measured mixing coefficients in two strongly contrasting environments. One site had biological mixing rates of 80 to 172  $\text{cm}^2/\text{year}$ , with mixing

depths of 17 to 25 cm. The other site had less intense mixing rates of 6-30 cm<sup>2</sup>/year, but mixing depths were greater, 21-40 cm. Heberta et al. (2007) measured in situ pore water mixing at a depth of 10 m below the water surface on a flat sandy seafloor. No infaunal burrows were observed in cores. The wave height was up to 1.2 m, and near-bed current velocities less than 20 cm/s. The measured diffusivity scales reasonably with the wave height, and is 3-4 orders of magnitude higher than the molecular diffusion rate: between 10<sup>-2</sup> to 10<sup>-3</sup> m<sup>2</sup>/hr. A field study on an intertidal mud flat by Rusch et al (2000) on the seasonal dynamics of Particulate Organic Matter in the top sediment layer resulted in a  $D_s$  between 0.18 10<sup>-6</sup> and 1.43 10<sup>-6</sup> cm<sup>2</sup>/s. They concluded that in an area with only minor influence of macrofauna, the biodiffusion coefficient of 1.85 10<sup>-6</sup> cm<sup>2</sup>/s is responsible for half of the total mixing rate. Forster et al. (1999) measured a diffusion coefficient  $D_s$  around 6.5 10<sup>-6</sup> cm<sup>2</sup>/s by applying a Bromide Tracer to measure benthic mixing in the bed sediments of the Skagerrak and the North Sea.

### 2.3.3 Residence time

The time that fines remain buried in the bed can be expressed in terms of a half life, and as a residence time. Decadal measurements of various contaminants have been used by Laane et al. (1999) to compute an average half life of sediments in the active layer of the North Sea. For the Dutch coastal zone North of the Rhine, the half life is 1.9 years. This means that half of the sediment in the active layer is resuspended in 1.9 years. This is a fundamentally different approach from the residence time used by Dellapenna (1998), which is defined as the time for sediments to be permanently buried. This residence time is estimated by dividing the mixing depth by the accumulation rate. Hence, the residence time is defined as the time required for the sediments to be permanently deposited.

From a geological point of view, bioturbation is a slow and continuous process, and therefore biological mixing dominates sedimentary strata on longer timescales (Dellapenna, 1998). The duration, depth, and degree of sediment disturbance by biological processes depend on the benthic community structure and its temporal and spatial variability. Physical mixing is episodic (event-driven), and modulated on a variety of frequencies and depths, depending on the driving forces (e.g. wind, waves, tides, surges).

### 2.3.4 Measurement methods

Measurement methods which can be used to measure the flux of mud into or out of the sediment bed are basically (1) to determine the mixing rates from sediment cores, using some sort of natural tracer, (2) active field measurements during which the decay of a substance injected into the bed is monitored, and (3) indirect measurements such as sediment concentration time series.

Examples of the first are Dellapenna et al. (1998, 2003), who measured particle residence time and mixing using radioactive tracers. Biological mixing is identified by a constant decrease in tracer activity with depth, while the absence of biological mixing results in distinct layers of constant or decreasing activity. Laane et al (1999) used existing decadal measurements of various contaminants to compute an average half life of sediments in the active layer of the North Sea. Rusch et al. (2000) used profiles of particulate organic matter concentrations to estimate the porewater flows and mixing rates in an area relatively little influenced by macrofauna.

The redox potential discontinuity (RPD) layer separates the oxidized surface water from the reduced pore water, resulting from the balance between metabolic demand of sediment biota oxidizing organic matter, and the delivery rate of nutrients. The RPD is therefore a proxy for the penetration depth of the seawater (Riedl et al., 1972). In the North Sea, the RPD layer is approximately 2.5 cm below the seabed (Rutgers van der Loeff, 1980). Near Hawaii, at a site exposed to large swell waves, the depth of the RPD layer was between 15 and 50 cm (Falter and Sansone, 2000). More moderate depths of around 10 cm were observed by Marinelli et al (1998) in the South Atlantic Bight. Riedl et al. (1972) use the depth of the redox potential discontinuity layer as an indication of the penetration depth, which in their study area (the West Atlantic shelf North of Florida) amounts to 20 cm at shallow depth (3 m) to 2-5 cm at 10 m water depth, and less further offshore.

Field experiments during which the decay of an injected substance is measured vary considerably. Forster et al. (1999) applied a Bromide Tracer to measure benthic mixing in the bed sediments of the Skagerrak and the North Sea, and Marinelli et al (1998) et al used Bromide in the South Atlantic Bight (US). Heberta et al. (2007) injected a neutrally buoyant dye 15 cm below the bed level, and the concentration decay measured with a spectrometer attached on a tripod. Reimers et al. (2004) executed field measurements of flow intrusion in the top 2 cm of the seabed using iodide injected from a tripod, at a water depth of 13 m. Precht and Huettel (2004) injected dye in a sandy substrate in a shallow water and low energy environment, and measured the concentration decay with optical instruments.

Krishnappan and Engel (2006) measured the entrapment of fines in coarse sediment beds in the laboratory using an annular flume. With a calibrated flocculation and settling model the concentration variation in the flume as a function of time could be reproduced. A systematic study is planned to determine the entrapment coefficient for various bed material types and bulk hydraulic parameters.

Sediment concentration measurements can be used as an indirect method to determine the buffering of fines through data analysis (Kleinhans et al., 2005) or in combination with numerical modelling tools (van Kessel et al., submitted, and van Prooijen et al., 2007).

## 2.4 Erosion rate of sand-mud mixtures

The network structure of a sediment bed determines the erosion type and rate significantly. A conceptual framework for the erosion behaviour of sand–mud mixtures was proposed by van Ledden et al. (2004), identifying a cohesive and non-cohesive sand-dominated network structure, a cohesive and non-cohesive silt-dominated network structure, a non-cohesive mixed structure, and a cohesive clay-dominated structure. The transitions between silt–sand–clay domination are determined by the volume fractions of the different sediment types, and the total water content  $n$ . The behaviour of the sediment bed is dominated by a sand skeleton when at least 40% of the volume fraction (including sediment and water) consists of sand. The sand content needed for a sand-dominated skeleton increases with porosity (or water content), see van Ledden et al. (2004) or Winterwerp & van Kesteren (2004) for more details. Mastbergen & van den Berg (2003) analysed the effect of permeability on the erosion rate of sand beds. A moderately packed sand bed needs to increase its pore volume in order to release individual sand particles (shear dilatancy). This shear dilatancy results

in negative pore pressures, which decrease the effective erosion rate of the bed. Sediment beds with a low permeability are compacted silts or very fine sands, but also sand in which the pores are blocked by clay.

The critical clay or mud content for a sediment bed to become cohesive can be determined through experiments. Both Mitchener & Torfs (1996) and Houwing (1999) used the mud content ( $D_{50} < 63 \mu\text{m}$ ) as a discriminator, finding critical mud contents of 3% to 15% and 20%, respectively. However, cohesive properties are determined mainly by the clay fraction (defined as  $D_{50} < 4 \mu\text{m}$ ) and the clay mineral and, therefore, the clay content is probably a better discriminator than the mud content. Experimental results show that the critical clay content varies from 5% to 10% (Mitchell, 1976; Raudviki, 1990) to 11% to 14% (Panagiotopoulos et al., 1997). Van Ledden et al. (2004) concluded that a clay fraction of 7.5% results in a transition of cohesive to non-cohesive properties.

In addition to the clay content or mud content, the erosion rate is also strongly influenced by biological activity. Biostabilization (i.e. by micro-organisms, vegetation, and algae mats) reduce erosion rates, while bioturbation increases the mixing rate (which, usually, increases the erosion rate). The biological activity therefore also influence the sediment composition of the bed: destabilizing organisms reduce the mud content in a bed, whereas stabilizing organisms *may* cause an increase in the mud content (Paarlberg et al., 2004).

## 2.5 The North Sea

### 2.5.1 Mud content

The mud content in the top one meter varies of a larger part of the Dutch nearshore zone varies between 0.25 and 4% (Figure 2.4 and Figure 2.5); it may exceed 10% or locally 20% close to the shore line (Figure 2.4). The mud content in the lower meter (1-2 m below the seabed) is slightly higher (Figure 2.5), but this may be attributed to the large number of grab samples used in the surface sampling. Fines are easily flushed out during grab sampling, resulting in underestimated fine fractions. This is supported by observations by Rutgers van der Loeff (1980) in the North Sea that the bed sediment in the nearshore region is frequently covered by a mud layer. However, this mud layer is only found when collecting samples with a box core and a Van Veen grab, because the North Sea corer disturbs the sea surface too much. Additionally the grain size analyses done previously on the cores frequently did not sample mud layers within the bed sediment. Therefore the maps in Figure 2.4 provide a lower estimate for the mud content.

Surface sediment data presented by Creutzberg (1979) of a larger part of the North Sea (Figure 2.6) shows that larger mud contents are found further north of the Dutch Coast. The location of this mud deposit is the same in winter and in summer, and was already described at that location since 1904. The distinct boundary between the mud field north of the  $53.5^\circ$  latitude and the sandy Southern Bight is principally determined by spring tide current velocities. In the mud field net deposition of mud is possible because the increase of erosion velocity by consolidation proceeds faster than the increase of current velocity after slack tide.

### 2.5.2 Bioturbation

In the North Sea, bioturbation especially occurs in the upper 10-20 cm (0.01-0.1 m for Bivalvia, 0.05 – 0.2 m for Polychaeta). Mollusca, especially bivalves (shellfish) occur on the shoreface and the sandwave troughs. Polychaeta (bristle worms) and Echinodermata (e.g sea-urchins) are found further offshore (Kleinhans et al., 2005). Typical sediment reworking rates are 0.3 g/m<sup>2</sup>/day for Bivalvia to 1 g/m<sup>2</sup>/day for segmented worms such as Polychaeta, but are strongly seasonally varying. Bioturbation occurs most on the shoreface and the sandwave troughs where the Mollusca thrive. The amount of mud per m<sup>2</sup> is estimated at 1 kg/m<sup>2</sup>, which is probably mixed within the active layer in one week.

### 2.5.3 Pore water flow

A simple model to estimate the pore water velocity due to flow-topography interaction was introduced by Thibodeaux and Boyle (1987), which can be used to estimate pore water inflow velocities in the North Sea. Combining a simple model to account for the pressure drop behind simple bedforms with the Darcy's law yields an estimate of inflow at the seabed surface::

$$v_0 = \frac{K}{\nu} \left( \frac{c_p V^2}{\lambda} + gs \right) \quad (1)$$

where  $K$  is the permeability,  $\nu$  the pore water viscosity,  $c_p$  the pressure coefficient, estimated as  $c_p = \left( \frac{\Lambda}{2h} \right)^{3/8}$ ,  $h$  is the water depth and  $\Lambda$  the bedform height,  $\lambda$  is the bedform length,  $V$  is the flow velocity,  $s$  the water level slope, and  $g$  the gravitational acceleration. In their laboratory experiments, this formulation would yield an intrusion velocity of 0.24 cm/s, which underestimates the measured intrusion velocity with a factor 2. Using eq. 1 and typical shelf conditions with ripples (bedforms with a length of 20 cm and a height of 2 cm, a water depth  $h$  of 30 m, permeability between  $1 \cdot 10^{-10} \text{ m}^2$  and  $1 \cdot 10^{-11} \text{ m}^2$ , a flow velocity  $V$  of 1 m/s, a viscosity of  $1 \cdot 10^{-6} \text{ m}^2/\text{s}$ ,  $s = 1 \cdot 10^{-5}$ ) yields  $c_p = 0.05$  and  $v_0 = 2.5$  to  $25 \text{ } \mu\text{m/s}$ . Using the same formulation but different settings, Kleinhans et al. (2005) estimated the mud infiltration into the bed to be  $1 \cdot 10^{-6} \text{ m/s}$  (or 1-10 m/year). But they also concluded that as pores will be blocked by the infiltrating mud, the infiltration velocity gradually decreases. A typical amount of mud on the sandy surface deposited during tranquil conditions would then take approximately one year to infiltrate into the bed. They therefore concluded that mud infiltration into the bed is primarily caused by bedform migration.

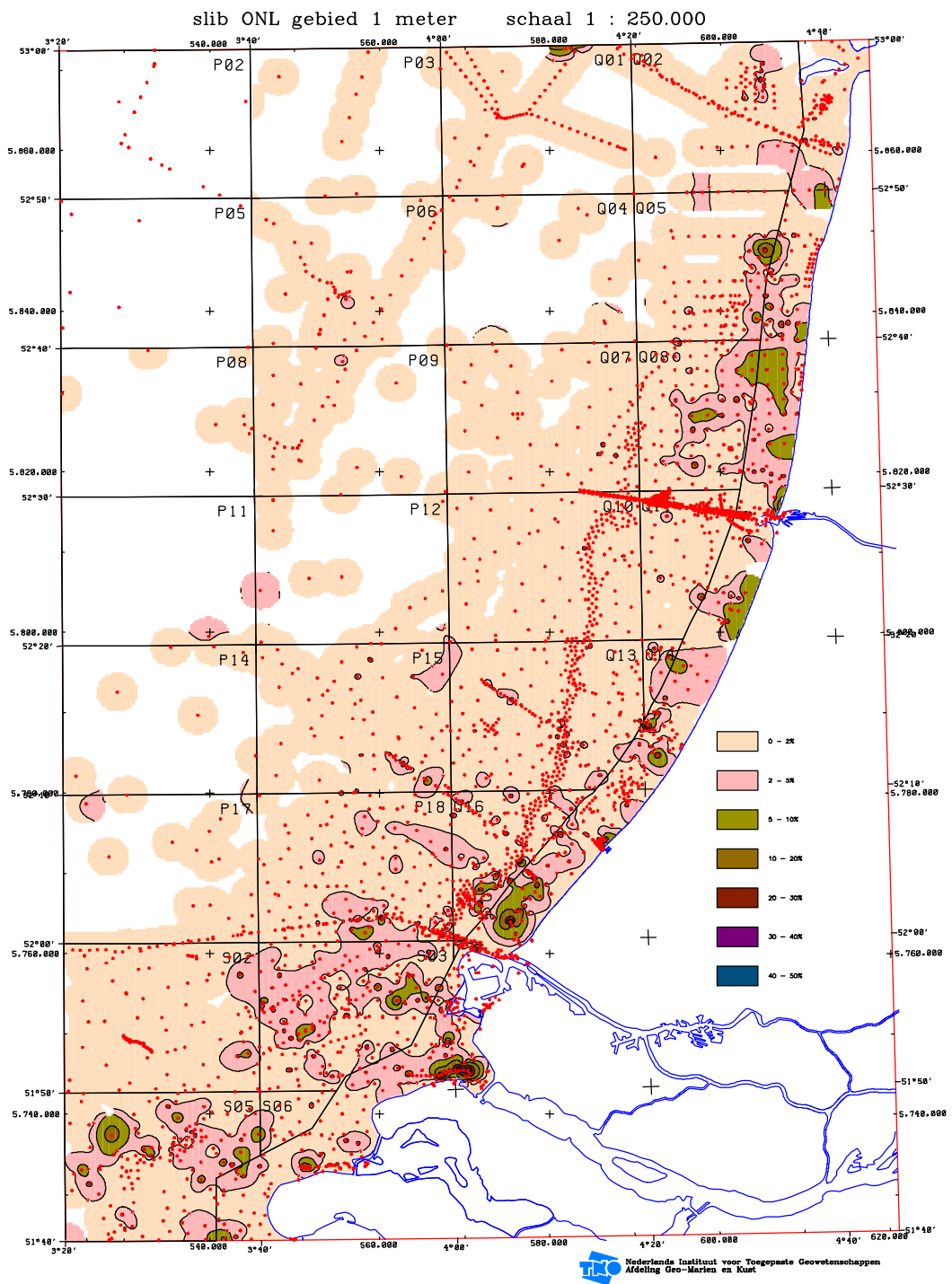


Figure 2.4 Mud content in the Dutch Coastal waters (TNO).

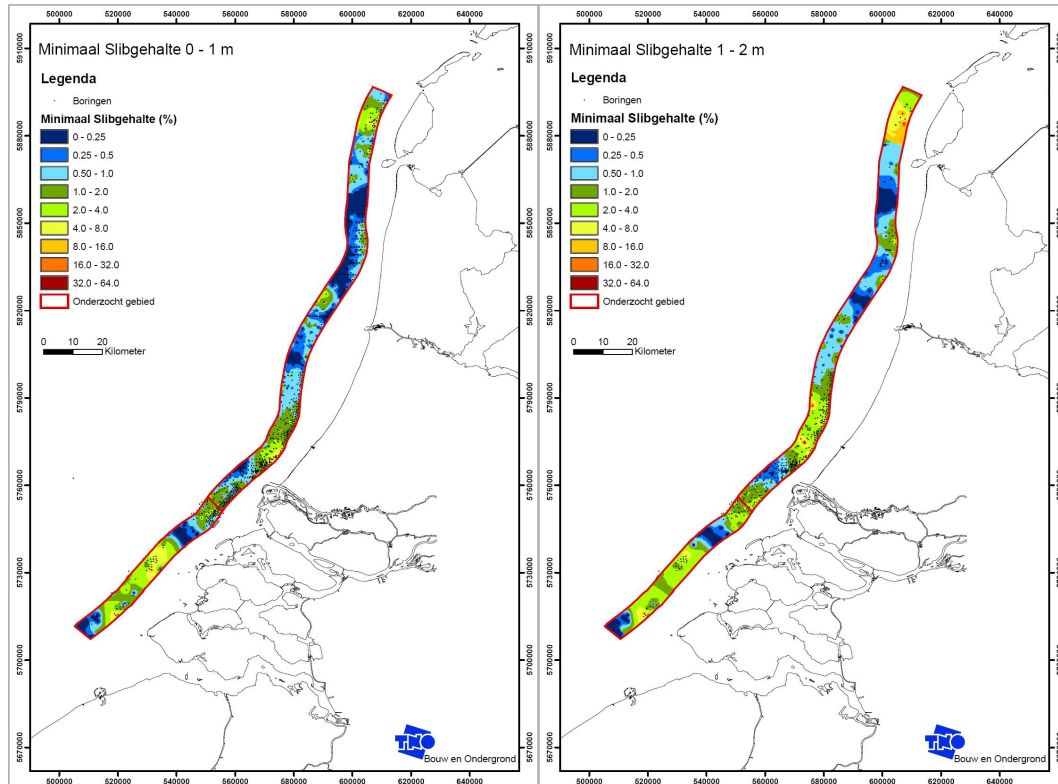


Figure 2.5 Mud content in the Dutch coastal waters between the 20 m depth contour and 7 km seaward of the 20 m depth contour (van Heteren et al., 2007)

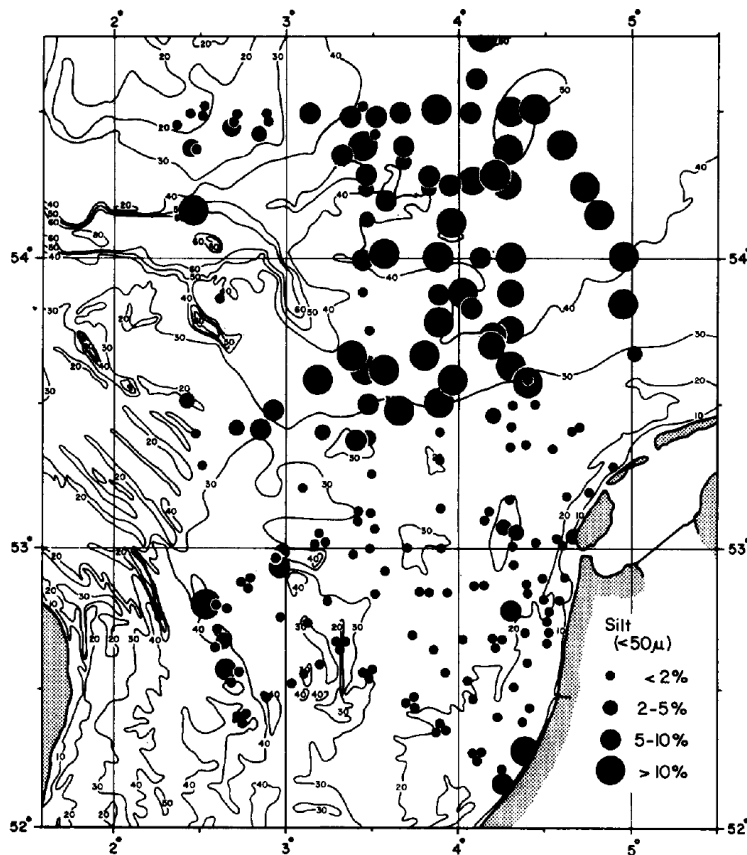


Figure 2.6 Mud content in the North Sea, from Creutzberg (1979).

Riedl et al. (1972) quantified the exchange of water between the bed and the water column through wave-generated pressure gradients. The exchange velocity between the bed and the water column depends on wave characteristics (wave height, and length), fluid viscosity, and bed permeability. The wave length can be determined from the wave period and the local water depth through linear wave theory. Considering the same shelf area as above (30 m water depth and permeability between  $1 \cdot 10^{-10} \text{ m}^2$  and  $1 \cdot 10^{-11} \text{ m}^2$ , a wave period of 6 seconds, and a wave height of 3 m, their formulations predict pore water flow velocities of 1 to 10  $\mu\text{m/s}$ . This flow velocity decreases with the wave height. At higher wave heights the upper layer of the sediment bed is probably permanently mobilised, during which sedimentological processes will probably dominate the vertical distribution of fine sediments in the bed.

It therefore seems that both flow-topography interaction and wave-generated pressure gradients in the order of 1-25  $10 \mu\text{m/s}$ , or around 0.1 to 2 m/day. This seems sufficient to transport mud into the bed. However, the permeability sand-mud mixtures increases with the mud content, and therefore mud infiltration rates are substantially less than computed with existing formulas for pore water flows.

## 2.6 Discussion and conclusion

Mud infiltration into a sand bed is caused by reworking of the bed (through bioturbation and sedimentological processes; mainly bedform dynamics) or by mixing within the pores of a sand matrix (pore water flow or diffusion). Turbulent diffusion is of lesser importance in dynamic marine areas. The question then remains to what extent release and infiltration is related to mixing processes or to interstitial pore water flows.

On the short term, interstitial pore water flows are probably important. Estimated pore water flow velocities at the sand-sea surface are in the order of 0.1 to 2 m/day in typical shelf sea conditions. However, this velocity is oscillating and does not lead to advective transports in the same order. Also, the intrusion velocity in the pores strongly depends on the permeability which strongly decreases with the mud content of the bed. This is supported by the observation that the permeability of the nearshore zone, defined by the 10 m water depth, is lower than in the open shelf, while the median grain size of the sediments is equal. The penetration depth of the pore water flow is limited, in the order of cm's to tens of cm's per year.

While pore water flow may lead to influx of mud into the bed within a relatively short time span, the amount of mud that can penetrate is probably limited because the permeability decreases. To further increase the mud content in the bed, biological and sedimentological processes are probably import. Bioturbation mixes segregated sand and mud layers, while sedimentological processes (bed form migration) lead to increased segregation. Bedforms are generated by bedload transport of sand, and therefore all mud is eroded from the upper layer when a bedform migrates. The erosion depth is determined by the size of the bedform, which may be several cm's (ripples) to decimetres (megaripples/dunes). Fine sediment eroded from the bed is brought into suspension, and deposited on the rippled bed surface. On a short timescale, this leads to a reduction of the mud content. This mud layer is subsequently slowly mixed again with the sand through percolation or bioturbation. However, if the mud layer is slightly consolidated, the mud layer may be buried by a bedform. This leads to the formation of mud layers or lenses within the sand, and is a very fast influx mechanism into the bed.

Observations and modelling shows that progressively more sediment is brought into suspension during the course of the storm season, i.e. a single storm is insufficient to rework the entire active upper layer (Marinelli et al., 1998, Kleinhans, 2005, van Kessel et al, submitted). It is not likely that subsequent storms rework progressively deeper sediment: this reworking depth is determined by the bedforms, which are in turn related to the hydrodynamics (assuming that during a storm all mud is in suspension, and the sand is non-cohesive; otherwise the bedform type and migration rate depend on the mud content). All mud present in the active layer will be resuspended during a storm, and therefore additional mechanism must play an additional role. Probably, a combination of mixing processes is responsible for the progressive increase of the sediment concentration. The most important element probably is that the sediment release depth (during a storm) is smaller (between 5 and 10 cm) than the depth up to which substantial mixing (through bioturbation or pore water flow) takes place (up to 20 to 30 cm).

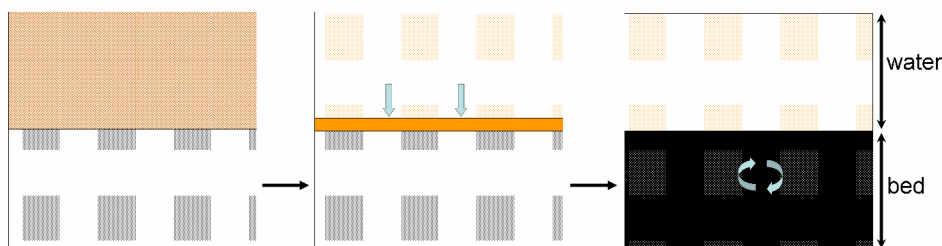


Figure 2.7 Transport of fines into the bed during summer: Suspended sediment is deposited on the clean sand bed and gradually mixed, resulting in clear water and high mud content in the bed.

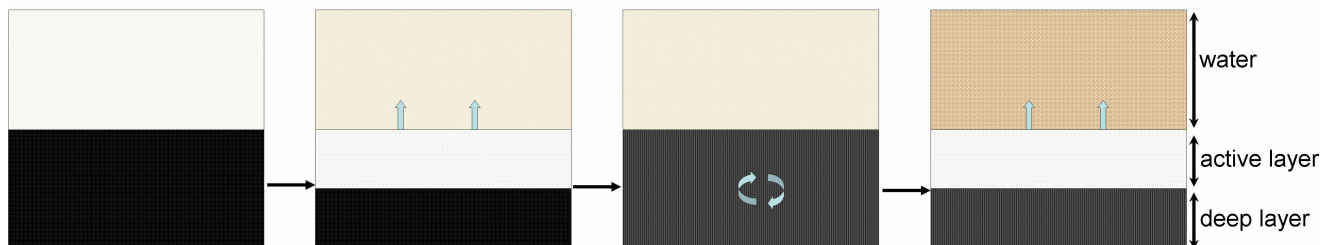


Figure 2.8 Fine sediment released during winter storms: fine sediment is washed out from the active layer, with a thickness depending on the bedform height, resulting in more turbid water, a sandy active layer, and a muddy deeper layer. Mud is transported from the muddy lower layer into the active layer through bioturbation or pore water flow. During a following storm, more fine sediment can be eroded from the upper layer, resulting in an increase in turbidity.

At the beginning of summer / end of winter, the sand bed is clean and all mud is suspended in the water column (left panel in Figure 2.7). This sediment is deposited as a thin mud layer on a clean sand bed (middle panel), which can be remobilized during spring tides or during storms only. During summer neap tides, this mud layer is mixed within the sand bed by a combination of pore water flow, bioturbation, and possibly bedform migration (right panel). During the first winter storm, all mud in the active layer (5 to 10 cm, depending on the bedform size) is washed from the sand bed due to bedform migration and brought in suspension (Figure 2.8). Due to more or less permanent higher turbulence levels in the water column, the suspended sediment concentration remains high. The upper layer devoid of fines is subsequently mixed with lower layer (between 10-20 cm), which still contains a large amounts of fines, through bioturbation or pore water flow. Overall, the mud content in the combined upper layer is

lower than at the end of summer. Because more mud is now available in the top layer, more mud can be entrained from the seabed during the following storm. Note that during slack tide some of the mud may be temporarily deposited on the sand bed in a mud layer. In contrast with summer, during which the periods that this layer exists for substantial periods of time and therefore mix with underlying sand, the period that this mud layer exists is short.

The amount of sediment in suspension can then be computed as the maximum amount of sediment the flow can at that moment carry in suspension, as long as sufficient amount of sediment is available. The sediment availability is the summation of

- 1) The amount of sediment already in suspension;
- 2) The amount of sediment available in the mud layer (if existing at that time)
- 3) The amount of mud available in the active layer. The mud content of this active layer depends on its history, and the depth on the bedform height. This bedform height can be estimated using a bedform roughness diagram (e.g van Rijn, 1993).

The amount of sediment in the active layer depends on the sedimentation / erosion flux as described above, and on supply from the deeper layer. The amount of mud transported from the deeper layer to the active layer depends on the mud fraction in both the active layer and the lower layer (sediment is transported by diffusion processes, which act on the concentration gradient), and the mixing rates. The mixing rates are determined by biological activity, wave-induced pressure gradient, or flow-topography interaction. Their relative importance varies in time and with, with diffusion due to wave-induced pressure gradients peaking in winter and bioturbation-induced mixing highest in summer. These diffusion coefficients can be computed for rotational shear due to wave-induced pressure gradients (Rutgers van der Loeff, 1981; Harrison et al., 1983; Shum, 1993), shear dispersion due to wave-induced pressure gradients (Webster, 2003), bioturbation (Lee and Schwartz, 1980; Forster et al., 1999; Rusch et al., 2000; Heberta et al., 2007), and current-bedform interaction. Although the diffusion coefficients may be based on the actual physics, for numerical modelling of mud exchange a constant value may be preferred, to be used as a calibration parameter. In somewhat different form this is the burial term in Van Kessel's model.



## 3 Sand-mud modelling in Delft3D

### 3.1 General background

Research on transport of *non-cohesive* sediment has a long history. Transport formulas have been developed in the past by a large number of scientists such as Einstein and Bagnold, later followed by Engelund and Hansen, Van Rijn and many others. Regarding the transport of *cohesive sediment*, research on sedimentation and erosion was initiated by Krone and Partheniades in the sixties of the 20<sup>th</sup> century, followed by for instance Mehta, Soulsby and Winterwerp. For many years both disciplines acted more or less independently from each other. Given the fact that nature seldom exhibits fully non-cohesive or fully cohesive behaviour of sediment, it was inevitable that sooner or later research would have to focus on mixtures of sand (non-cohesive) and mud (cohesive). Also during the years, managerial issues more and more related to the quality of the water bed as part of environmental impact assessment studies requiring prediction on bed composition, particularly on mud content. This societal relevance has led recently to research focusing on the interaction between sand and mud, see for instance Torfs (1995) and Van Ledden (2003). Small quantities of fines, with particle sizes less than 2 microns, may already affect the erosion and transport of sand and, vice versa, sand present in a mud bed will alter the properties of the bed and consequently erosion. It is common practice to consider the deposition of sand and mud independently from each other. This is justifiable as long as suspended sediment concentrations are relatively low. It is thus apparent, that a profound understanding of the behaviour of the bed, as influenced by the mud content, is crucial for sand-mud modelling. The mud content itself is governed by the transport of sand and mud in the water column and subsequent deposition. Erosional behaviour of the bed is a function of consolidation, influenced by physico-chemical properties, and biological effects such as bioturbation and the presence of algae. The work described in this report only deals with water beds characterized by the mud content, which is according to the methodology followed by Van Ledden. This review aims to provide an overview of sand-mud model approaches that are currently implemented, or being implemented, in the Delft3D model.

### 3.2 Activities carried out in 2008

Van Ledden developed his methodology on sand–mud interaction as part of his Ph.D. work at the Delft University of Technology (Van Ledden, 2003); an outline will be given in the next section. Process formulations were implemented by him in a ‘special’ of Delft3D and simulations were made for a number of estuaries and tidal basins giving insight into the complexity of the processes, but also showing the feasibility of his approach. Although many physical, chemical and biological processes are not yet understood, there is an urge to make available the current knowledge in an operational version of software code of Deltares. The purpose of this implementation is twofold:

- To gain experience with the modelling of sand-mud processes giving directions for future improvement and development;
- To be able to address managerial questions.

The following considerations led to the decision to implement sand-mud interaction in the software package WAQ of Deltares:

- Some formulations and model concepts, developed as part of specific projects, were already present in WAQ. Thus, a relatively minor effort was needed to make the software code operational.
- The policy at Deltares Software Centre (DSC) is to include the formulations of processes in the so-called process library of WAQ. For many processes this has been accomplished but sediment transport and morphology, still included in Delft3D, will be transferred to WAQ in the nearby future.

As mentioned above modelling of the water-bed exchange of sand and mud has been done as part of previous projects. The so-called Buffer model was set up for the extension of the Maasvlakte to reproduce the release of fines into the water column. These fines are present within the interstitial pores of the sand bed and are washed out during the erosion of the sand bed. The inclusion of the Buffer model in WAQ has also been accomplished as part of the present project.

During recent years, various initiatives at institutes and universities have been undertaken to study sand-mud interaction. The findings of some of these studies are already available and can be made operational the forthcoming years for use in consultancy projects. Other research projects are in their initial stage or still need approval. An inventory of these activities will be given hereafter.

### 3.3 Implementation sand-mud interaction in WAQ

The following assumptions for implementation of sand-mud interaction in WAQ are made:

- Only suspended mud is transported in the water column; while sand is considered as an inactive substance. As such there is only deposition of mud, changing the mud content of the bed.
- The bed is characterised by means of the actual mud content, the critical shear stress for erosion of a 100% sand bed and the critical shear stress for erosion of a 100% mud bed.
- A critical mud content separates the non-cohesive (sand-dominated) regime from the cohesive (clay-dominated) regime.
- For a mud content lower than the critical value, the erosion rate of mud is proportional to the erosion rate of sand. The proportionality is given by the ratio of mud mass to sand mass within the bed, which assumes that mud is washed out of the pores of the sand matrix during erosion. The erosion of sand is based on formulations for non-cohesive sediment available from literature. In the equations the critical erosion shear stress is taken as a function of the mud content; the erosion parameter is constant and equal to that of sand.
- For a mud content larger than the critical value, the bed behaves cohesively. The layer is considered homogeneously so that also in this regime the erosion rate of mud is proportional to the erosion rate of sand. The proportionality is given by the ratio of mud mass to sand mass in the bed. The critical erosion shear stress and the erosion parameter are both a function of the actual mud content of the bed.
- The foregoing implies, that erosion of sand and mud in the non-cohesive and erosion in the cohesive regime do not affect the mud content of the bed.
- In WAQ the bed consists of two sediment layers. In total three mud fractions are distinguished.

Detailed descriptions of the process formulations are given in Appendix A.

### 3.4 'Buffer model'

The 'Buffer model' is a schematisation of the bed with a sand and mud layer, an overlying water layer and prescribed interactions between these layers, see Figure 3.1. The top layer in the bed (S1) only consists of mud, whereas the sandy layer underneath (S2) includes mud within the pores of the soil skeleton formed by the sand grains. As this second layer is sand-dominated, its behaviour can be treated as non-cohesive. The 'Buffer model' is specifically meant for conditions where the top layer is relatively thin. If the mass of mud per unit of area is below some critical value (in that case the layer thickness is smaller than a critical value) the erosion rate  $E_1$  is assumed proportional to the sediment mass per  $m^2$ . This behaviour is addressed as first-order erosion and mimics the occurrence of patches in a sandy environment. If the patches grow in size erosion  $E_1$  will increase proportionally until the critical mass is attained. From that moment the erosion rate is zero-order, which implies that it is independent of the sediment mass in the top layer.

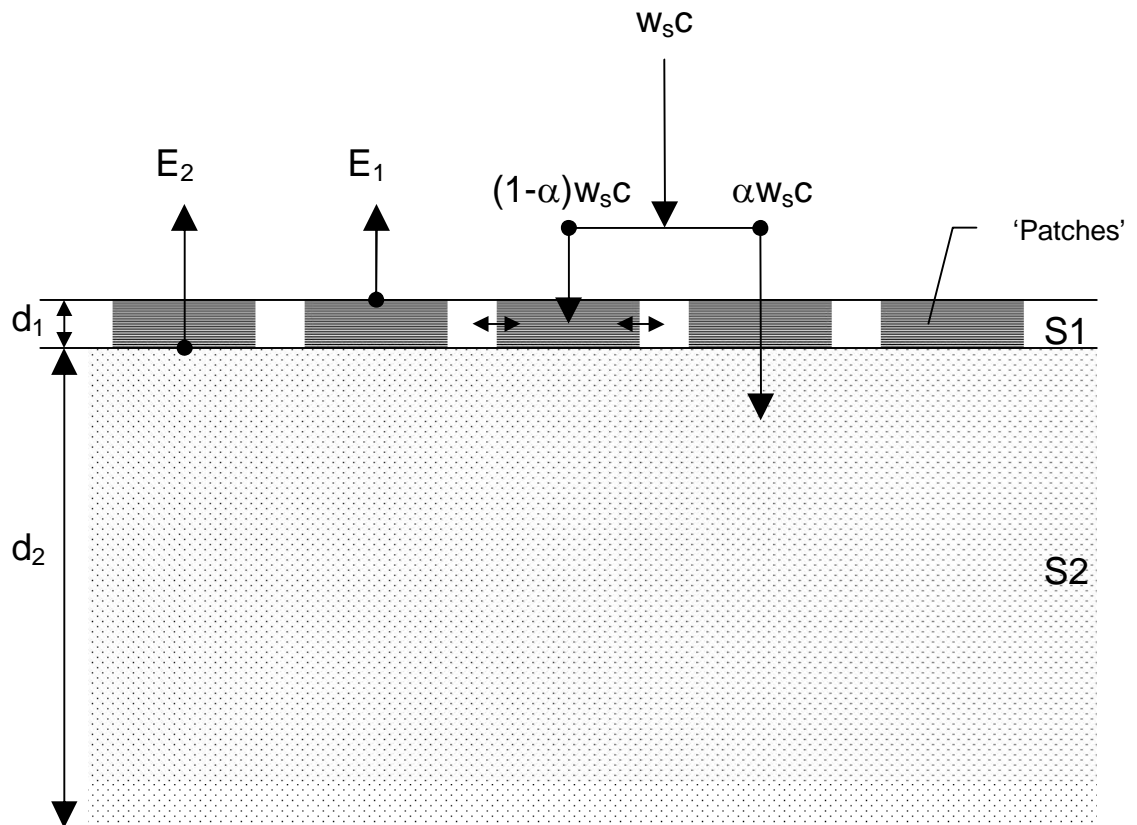


Figure 3.1 Schematisation of bed and fluxes according to the 'Buffer model'.

Further characteristics of the model are:

- The sand layer (second layer) is passive, which means that no transport of sand in the water column in horizontal direction occurs. However, erosion of the second layer results in changes of the mud fraction.

- In the water column settling of mud takes place. A fraction  $\alpha$  of the settling flux contributes to the mud mass in the second layer, while the remaining portion ( $1-\alpha$ ) contributes to the top layer. Usually,  $\alpha$  is much smaller than 1.
- Storage (buffering) of mud within the pores of the sand layer is stopped, if the mud fraction, i.e. the ratio of mud mass to sand mass, exceeds a threshold.
- A mud flux due to settling towards the second layer may also occur if the first layer completely covers the second layer. The physical processes accounting for this are consolidation, bioturbation and reworking of the bed due to the propagation of bed forms. In the previous version of the 'Buffer model' this was the only option. Presently, the user may specify whether or not the sediment flux to the second layer is zero if this layer is completely covered.
- The erosion flux of mud  $E_2$  from the second layer to the water column is governed by the erosion of the sand as given by a pick-up function for sand only. In the previous version of the 'Buffer model' the pick-up function of Van Rijn (1993) was used. Mud erosion was computed in proportion to the ratio of the mud mass and the sand mass (per  $m^2$ ) in layer 2. The critical shear stress for erosion remained unaffected by the presence of mud and erosion proceeded even if the layer was completely covered. For the present implementation the user may specify whether or not the critical erosion shear stress is a function of the mud content and if erosion stops for a complete coverage of the second layer.

A detailed description of the 'Buffer model' is given in Appendix B.

### 3.5 Activities elsewhere with respect to sand-mud processes and modelling.

Presently, a large number of activities is going-on or anticipated at various institutes with respect to research on sand-mud interaction including effects of biota. A brief summary is given below:

- NIOZ has made a proposal (NTW 3.1) as part of the program Building with Nature. It is related to the execution of field measurements of the mud flux along the Dutch coast. Use will be made of the hydrodynamic model GETM and applications will focus on the ecosystem of the North Sea.
- Delft University of Technology will finalise STW project Eco-morphology of estuaries and tidal lagoons) in 2009. Deliverables of the project are: data of laboratory measurements (see the description of the work of Walter Jacobs hereafter), analyses of collected field data and models.
- NIOO has proposed to carry out measurements on water-bed exchange processes as part of the Building with Nature program (proposal 2.3)
- Deltares proposed, also as part of the Building with Nature program, the implementation in models of various concepts regarding water-bed exchange processes.
- University of Twente (Borsje) is working on the effects of biology on erosion.

Delft University of Technology (Van Prooijen) will investigate the feasibility for a workshop early 2009 with the various institutes currently involved in sand-mud transport processes. The development of a generic open source water-bed exchange bed module could be of interest for all parties.

For information regarding activities at the Delft University of Technology reference is made to Appendix C and Appendix D. Van Prooijen (App. C) has made an inventory of various pick-up functions for sand. He also used the erosion function by Jacobs (see

hereafter) to simulate the erosion of a mud bed. Modelling the erosion of sand-mud beds is foreseen for the nearby future. Van Prooijen and Winterwerp also investigated the erosion of a sediment bed, where the erosion rate gradually decreases in time. A stochastic description of the bed shear stress and the bed properties is applied in this case.

Appendix D presents results of the work by Jacobs as part of his Ph.D research. Jacobs focused on the erosion of sand-mud beds and developed an erosion function with a more physical characterisation of the bed, i.e. using the degree of packing of the sand grains and the plasticity index to indicate the cohesiveness of the bed.



---

## 4 Non-stationary wave computations in the North Sea

### 4.1 Introduction

Long-term computations for silt dispersion on the North Sea have been carried out in the past. The presence of wind waves was included in those hydrodynamic computations, but in a somewhat simplified manner, i.e. in stationary mode and using spatially uniform wind fields. The goal of this study is to setup a model to properly hindcast wave fields to be input flow and subsequent silt dispersion simulations for the North Sea.

The study focus on a one year period, namely 2006. For this year spatial and time-varying HIRLAM wind fields wave been made available. These fields were input in Delft3D-WAVE to calculate the wave height fields for the North Sea area. Delft3D-WAVE was run in non-stationary mode. Furthermore, Delft3D-WAVE computations were stand-alone and no input or results from the hydrodynamic computation were used.

The computed wave conditions were assessed using available wave measurements offshore the Netherlands.

### 4.2 Model description

#### 4.2.1 Setup of the computations

The goal of the study was to produce non-stationary wave fields to be communicated to the silt dispersion computations inside Delft3D. The computations were therefore carried out in Delft3D. The WAVE module was run in non-stationary mode with time and space varying wind fields. The wind fields considered were HIRLAM (high resolution local area model) fields from KNMI (the Royal Netherlands Meteorological Institute). The fields cover the whole North Sea and have a spatial resolutions of 22 km x 22 km and a temporal resolution of 3 hours. No other input /boundary conditions were fed in the Delft3D-WAVE.

In order to input time and space varying wind fields in Delft3d-WAVE, the fields need to be available in a communication file. Therefore, before running the Delft3d-WAVE, Delft3D-FLOW was run in order to create the communication files. Only the wind information was communicated to the WAVES computations. The model considered both in the FLOW and in the WAVES computations was the model shown in Figure 4.1, which is known as the ZUNO model, and is also the model on which the silt dispersion computations are to be carried out. The wave model in WAVES is the SWAN (Simulation of Waves in Nearshore Areas) model which is briefly described in the following.

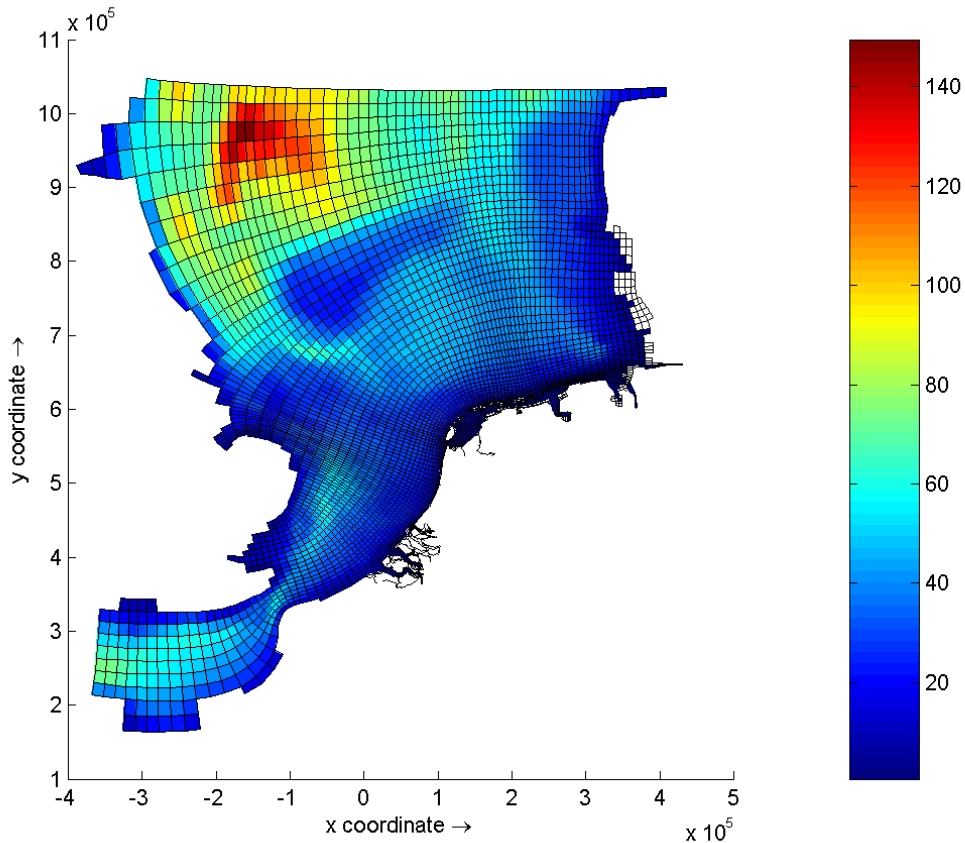


Figure 4.1 ZUNO model geographical domain, grid (black lines) and bathymetry.

#### 4.2.2 Description of the SWAN model

The SWAN model is freely available and was developed at Delft University of Technology. A detailed description of the model as it was initially developed can be found in Ris et al. (1999) and description of the latest version in [http://vIm089.citg.tudelft.nl/swan/online\\_doc/swantech/swantech.html](http://vIm089.citg.tudelft.nl/swan/online_doc/swantech/swantech.html).

The model solves the action balance equation, in Cartesian or spherical coordinates, without any *ad hoc* assumption on the shape of the wave spectrum. In Cartesian coordinates the equation is

$$\frac{\partial N}{\partial t} + \frac{\partial}{\partial x}(c_x N) + \frac{\partial}{\partial y}(c_y N) + \frac{\partial}{\partial \sigma}(c_\sigma N) + \frac{\partial}{\partial \theta}(c_\theta N) = \frac{S_{tot}}{\sigma}, \quad (1)$$

where  $N(\sigma, \theta)$  is the action density,  $t$  is the time,  $\sigma$  is the relative angular frequency and  $\theta$  the wave direction.

The first term on the left-hand side of Eq. (1) represents the local rate of change of action density in time. The second and third terms represent propagation of action in geographical space. The fourth term represents shifting of the relative frequency due to variation in depth and currents. The fifth term represents depth-induced and current-induced refraction. The quantities  $c_x$ ,  $c_y$ ,  $c_\theta$  and  $c_\sigma$  are the propagation speeds in the

geographical x- and y-space, the  $\theta$ - and the  $\sigma$ -space, respectively. The expressions of these propagation speeds are taken from linear wave theory.

In (1)  $S_{tot}$  is the sum of separate source terms representing different types of processes: wave energy growth by wind input, wave energy transfer due to wave-wave non-linear interactions (both quadruplets and triads), the decay of wave energy due to whitecapping, bottom friction, and depth-induced wave breaking.

#### *Wind input*

The wind input source term is given by the sum of a linear and an exponential term. The linear term represents Philips' resonance mechanism and is given by the expression of Cavaleri and Malanotte-Rizzoli (1981),

$$S_{w,lin} = \frac{\alpha}{2\pi g^2} \exp\left(-\left(\frac{\sigma}{\sigma_{PM}}\right)^4\right) \left(U_* \max(0, \cos(\theta - \theta_w))\right)^4, \quad (2)$$

where  $\alpha$  is the proportionality coefficient,  $g$  is the acceleration of gravity, the subscript PM denotes the value of the variable for fully developed sea states according to Pierson and Moskowitz (1964) and  $U_*$  is the wind friction velocity. The exponential term accounts for Miles' feedback mechanism. In SWAN the expressions of Komen et al. (1984) and Janssen (1991) have been implemented. The former is a function of the friction velocity divided by the phase speed of the waves ( $U_*/c_{ph}$ ) and the second of  $(U_*/c_{ph})^2$ .

#### *Wave-wave non-linear interactions*

In deep water, quadruplet wave interactions dominate the evolution of the spectrum; These nonlinear wave-wave interactions transfer energy from the peak frequency to lower frequencies (moving the peak to lower frequencies) and to higher frequencies (where it is dissipated by whitecapping). The expression of the quadruplet source term can be obtained theoretically without using poor fundamental hypotheses or approximations. However, its full computation is extremely time consuming. Therefore, a discrete operator introduced by Hasselmann and Hasselmann (1985) is also available in SWAN to take into account the quadruplet non-linear energy transfer.

In very shallow water triad wave interaction transfer energy at two frequency components to both the sum-frequency, resulting in higher harmonics, and the difference frequency, resulting in lower harmonics. In SWAN this phenomenon is taken into account only with respect tot the generation of higher harmonics by means of the lumped triad approximation of Eldeberky (1996).

#### *Whitecapping*

The wave dissipation term is still the less known in the wave balance equation. SWAN's formulation of dissipation by whitecapping is based on the pulse-based model of Hasselmann (1974), as adapted by the WAMDI group (1988):

$$S_{ds}(\sigma, \theta) = -\Gamma \bar{\sigma} \frac{k}{k} E(\sigma, \theta), \quad (3)$$

where

$$\Gamma = C_{ds} \left( (1 - \delta) + \delta \frac{k}{\bar{k}} \right) \left( \frac{\bar{s}}{\bar{s}_{PM}} \right)^4, \quad (4)$$

a bar over a variable denotes its mean,  $k$  is the wavenumber and  $s$  the wave steepness. The remaining parameters in  $\Gamma$  depend on the wind input formulation that is used and are determined by closing the energy balance of the waves in fully developed conditions. For situations for which the exponential wind growth expression of Komen et al. (1984) is used,  $C_{ds} = 2.36 \cdot 10^{-5}$  and  $\delta = 0$ , and when the formulation of Janssen (1991) is used  $C_{ds} = 4.10 \cdot 10^{-5}$  and  $\delta = 0.5$ . In SWAN's default settings the exponential wind growth expression of Komen et al. (1984) and the corresponding whitecapping formulations is used. There has however been some studies showing that this formulation tends to produce erroneous SWAN hindcast. Rogers et al. (2003) reports that using such settings SWAN underpredicts of low- and medium-frequency energy in the wind sea portion of the spectrum (0.12-0.19 Hz) and dissipates swell (0.05-0.12 Hz) in the presence of wind sea. In order to describe better what is going on, following Komen et al. (1994, p.145) they rewrite Eq. (3) in the form

$$S_{ds}(\sigma, \theta) = C_{ds} \left( \frac{\bar{s}}{\bar{s}_{PM}} \right)^4 \bar{\sigma} \left( \frac{k}{\bar{k}} \right)^n E(\sigma, \theta). \quad (5)$$

For  $n=1$  the righthand side of (5) is proportional to  $k/\bar{k}$ , as in SWAN's default whitecapping formulation that is used in combination with the exponential wind growth expression of Komen et al. (1984). Increasing the parameter  $n$  above 1 has the effect of reducing dissipation at lower frequencies while increasing dissipation at higher frequencies. With  $n=1.5$  the dependence of  $S_{ds}$  on  $k/\bar{k}$  is close to that in SWAN default whitecapping formulation that is used in combination exponential wind growth expression of Janssen (1991). Rogers et al. (2003) note that in above formulation the wind sea has an illogical and physically unjustified impact on swell. They suggested an effective way of reducing dissipation of lower frequency energy in SWAN which consisted of using the exponential wind growth expression of Komen et al., setting  $n=2$  in (5) and leaving  $C_{ds} = 2.36 \cdot 10^{-5}$ . Because the value of  $C_{ds}$  used is the same as in the default SWAN setting; consequently, for fully developed seas the total energy levels will differ from those of the default setting. In fact, Rogers et al. (2003) vent criticisms on the tuning of the dissipation terms in order that the bulk parameters match and empirically based quasi equilibrium target value at the model infinite-duration and -fetch asymptote. They argue that, in a temporal sense, the asymptotes of these models may be well tuned, but the accuracy of the rate at which the models approach these asymptotes is uncertain. In their hindcasts using the above mentioned settings results compared better with the measurements than those based on the default setting.

As Rogers et al. (2003) had done, Van der Westhuysen et al. (2007) report that when using SWAN's default configuration to hindcast pure wind sea, the energy density at lower frequencies is typically underpredicted, whereas energy levels in the high-frequency tail are generally overpredicted. When hindcasting a combined swell-sea situation, SWAN predicts more dissipation of swell in the presence of wind sea than in its absence and a reduced dissipation of wind sea in the presence of swell, leading to accelerated wave growth. In order to improve SWAN's hindcasts they propose using a whitecapping dissipation source term based on Alves and Banner (2003) with no dependence on spectral mean quantities, and a wind input source term based on that of Yan (1987) which depends on both  $(U_*/c_{ph})$  and  $(U_*/c_{ph})^2$ . In order to obtain a  $f^{-4}$  high frequency spectral tail they build a dependence of the whitecapping source term

on wave age. The resulting combination of wind input and whitecapping source terms was calibrated against fetch- and depth-limited growth curves and implemented in SWAN.

#### *Bottom friction and depth-induced wave breaking.*

For the dissipation by bottom friction, three models can be used: the empirical JONSWAP model of Hasselmann et al. (1973), the drag law model of Collins (1972), and the eddy-viscosity model of Madsen et al. (1988). Depth induced wave breaking is taken into account using the bore-based model of Battjes and Janssen (1978).

#### *Numerical approach*

As to SWAN's numerical approach, the integration of the propagation and the source terms of Eq. (1) has been implemented with finite difference schemes in all five dimensions (time, geographical space and spectral space). The model propagates wave action density of all components of the spectrum across the computational area using implicit schemes in geographical and spectral space, supplemented with a central approximation in spectral space. In geographical space the scheme is upwind and applied to each of the four directional quadrants of wave propagation in sequence. Three of such schemes are available in SWAN: a first-order backward space, backward time (BSBT) scheme, a second-order upwind scheme with second order diffusion (the SORDUP scheme) and a second order upwind scheme with third order diffusion (the S&L scheme). The numerical schemes used for the source term integration are essentially implicit.

#### *Limiter*

In order to match physical scales at relatively high frequencies and to ensure numerical stability at relatively large time steps a limiter (Ris, 1997) controlling the maximum total change of action density per iteration at each discrete wave component is imposed.

#### 4.2.3 Default SWAN settings in Delft3d-WAVE

The following SWAN settings are default in Delft3d-WAVE:

- Wave growth and whitecapping according to Komen et al. (1984).
- Quadruplets on and triads off.
- Bottom friction according to the empirical JONSWAP model of Hasselmann et al. (1973) with a bottom friction coefficient of  $0.067 \text{ m}^2/\text{s}^3$ .
- Depth induced wave breaking according to the bore-based model of Battjes and Janssen (1978) with a breaker parameter of 0.73.
- Numerical integration using the BSBT numerical scheme (see Caires et al, 2006).

#### **4.3 Description of the measurements**

North Sea wave measurements offshore the Netherlands for 2006 have been obtained from <http://www.waterbase.nl/>. The locations of the considered measuring stations is given in Table 4.1

Table 4.1 Buoy locations (cf. <http://www.golfklimaat.nl/index.cfm?page=uitleg.meetlocaties>).

Buoy	Code	RD x	RD y	Latitude	Longitude	water depth (m MSL)
K13a platform	K13	10.176	583.334	53°13'04"	03°13'13"	30
Schiermonnikoog noord	SON	206.527	623.483	53°35'44"	06°10'00"	19
Eierlandse Gat	ELD	106.514	587.985	53°16'37"	04°39'42"	26
IJmuiden mun.stortplaats	YM6	64.779	507.673	52°33'00"	04°03'30"	21
Euro platform	EUR	9.963	447.601	51°59'55"	03°16'35"	32

Table 4.2 Availability of the buoy measurements.

Buoy	Variable	Nr. of observations	Jan	Feb	Mar	Abr	May	Jun	Jul	Aug	Sep	Oct	Nov	Dec
K13	H <sub>s</sub>	total	591	611	697	630	744	720	742	743	709	0	0	0
		hourly	591	611	697	630	744	720	742	743	709	0	0	0
		% hourly	79.44	90.92	93.68	87.5	100	100	99.73	99.87	98.47	0	0	0
	T <sub>m0,2</sub>	total	592	611	699	601	744	720	742	557	709	0	0	0
		hourly	592	611	699	601	744	720	742	557	709	0	0	0
		% hourly	79.57	90.92	93.95	83.47	100	100	99.73	74.87	98.47	0	0	0
SON	H <sub>s</sub>	total	462	672	742	719	744	719	399	743	720	744	907	4459
		hourly	462	672	742	719	744	719	399	743	720	744	717	743
		% hourly	62.1	100	99.73	99.86	100	99.86	53.63	99.87	100	100	99.58	99.87
	T <sub>m0,2</sub>	total	462	672	744	719	744	719	399	549	720	744	907	4459
		hourly	462	672	744	719	744	719	399	549	720	744	717	743
		% hourly	62.1	100	100	99.86	100	99.86	53.63	73.79	100	100	99.58	99.87
ELD	H <sub>s</sub>	total	468	157	743	719	744	715	741	743	720	744	907	4459
		hourly	468	157	743	719	744	715	741	743	720	744	717	743
		% hourly	62.9	23.36	99.87	99.86	100	99.31	99.6	99.87	100	100	99.58	99.87
	T <sub>m0,2</sub>	total	468	157	743	719	744	715	741	557	720	744	907	4459
		hourly	468	157	743	719	744	715	741	557	720	744	717	743
		% hourly	62.9	23.36	99.87	99.86	100	99.31	99.6	74.87	100	100	99.58	99.87
YM6	H <sub>s</sub>	total	744	662	738	717	695	694	742	743	510	178	908	445
		hourly	744	662	738	717	695	694	742	743	510	178	718	743
		% hourly	100	98.51	99.19	99.58	93.41	96.39	99.73	99.87	70.83	23.92	99.72	99.87
	T <sub>m0,2</sub>	total	744	662	738	717	695	694	742	557	510	178	908	4458
		hourly	744	662	738	717	695	694	742	557	510	178	718	743
		% hourly	100	98.51	99.19	99.58	93.41	96.39	99.73	74.87	70.83	23.92	99.72	99.87
EUR	H <sub>s</sub>	total	549	369	743	655	248	720	740	743	719	744	547	0
		hourly	549	369	743	655	248	720	740	743	719	744	547	0
		% hourly	73.79	54.91	99.87	90.97	33.33	100	99.46	99.87	99.86	100	75.97	0
	T <sub>m0,2</sub>	total	549	369	744	655	248	720	740	557	719	744	547	0
		hourly	549	369	744	655	248	720	740	557	719	744	547	0
		% hourly	73.79	54.91	100	90.97	33.33	100	99.46	74.87	99.86	100	75.97	0

The available wave parameters are restricted. We have downloaded the timeseries of both the significant wave height ( $H_s$ ) and the zero-upcrossing wave period ( $T_{m0,2}$ , the only integral period parameter available).

The data is mostly hourly, although for some buoys after November 2006 measurements are available every 10 minutes. In the comparisons with the Delft3D hindcasts only the hourly data was used. Table 4.2 shows the total availability of data per month and the total and percentage per month of valid hourly observations. As it can be observed in Table 4.2 there are some gaps in the hourly timeseries and the gaps in  $H_s$  data do not always coincide with gaps in  $T_{m0,2}$  data, and vice-versa.

#### 4.4 Description of the results

The Delft3D computations were carried out as follows:

- Delft3D-FLOW computations were first carried out with the sole objective of creating communication files with the space and time varying wind fields to be input the Delft3D-WAVE runs using the communication file.
- Then the Delft3D-WAVE computations were carried out using SWAN version 40.51AB.
- The integration timestep used in the SWAN computations was of 20 minutes following the advise of Caires et al. (2008). This is also the timestep used to write the wind fields in FLOW. The wind field time interpolation is therefore carried out in FLOW and WAVE assumes a time constant wind field in the 20 minutes integration period, the wind field at the start of the period considered.
- Given the limitation of 4 GBytes for the communication and output files of Delft3D the computations were not carried out continuously for the whole 2006 period but divided in smaller periods.
- There were four Delft3D-FLOW computations carried out, each for a three months period. There where 12 Delft3D-WAVE computations carried out, each for a one month period and with a spin-up of one day.

The Delft3D-WAVE provide for each timestep integral wave parameters for each considered buoy location in standard TABLE format SWAN files, and it also provide a Delft3D output file with several wave parameters at every model grid point. Initially comparisons were made between the results from the TABLE files and those from the Delft3D output file at the nearest by gridpoint and the measurements. It was concluded that the SWAN results at the nearest by grid point do not differ much from those interpolated to the buoy location and therefore the TABLE results were not considered further. All comparisons to be show in this memo are for hindcasts at the gridpoint nearest to the respective buoy location.

##### 4.4.1 Initial results

The differences between the Delft3D hindcasts and the measurements were quantified by computing some standard statistics such as the bias ( $\bar{y} - \bar{x}$ ), the root-mean-square error ( $RMSE = \sqrt{n^{-1} \sum (y_i - x_i)^2}$ ), the scatter index ( $SI = \sqrt{n^{-1} \sum [(y_i - \bar{y}) - (x_i - \bar{x})]^2} / \bar{x}$ ), the correlation coefficient ( $\rho = \sum (x_i - \bar{x})(y_i - \bar{y})$ ) and the symmetric slope ( $r = \sqrt{\sum x_i^2 / \sum y_i^2}$ ). In all these formulae the  $x_i$ 's represent the observations, the  $y_i$ 's represent the Delft3D

hindcasts and  $n$  the number of observations. An overview of these results is presented in Table 4.3 and Table 4.4. Figure 4.2 to Figure 4.6 show the scatter plot comparisons for each buoy location.

Table 4.3  $H_s$  error statistics for the hindcasts using the standard settings in WAVES.

Buoy	$n$	$\bar{x}$ (m)	bias (m)	RMSE (m)	SI (%)	$\rho$	$r$
<b>K13</b>	6187	1.21	-0.08	0.11	8.44	0.90	1.05
<b>SON</b>	8124	1.12	-0.06	0.10	8.42	0.92	1.05
<b>ELD</b>	7954	1.34	-0.07	0.11	8.15	0.93	1.03
<b>YM6</b>	7884	1.29	-0.11	0.09	6.04	0.95	1.06
<b>EUR</b>	6777	1.18	-0.06	0.07	5.28	0.94	1.03

Table 4.4  $T_{m0,2}$  error statistics for the hindcasts using the standard settings in WAVES.

Buoy	$n$	$\bar{x}$ (s)	bias (s)	RMSE (s)	SI (%)	$\rho$	$r$
<b>K13</b>	5975	4.45	-1.94	4.27	11.41	0.55	1.74
<b>SON</b>	7932	4.42	-2.07	4.91	14.41	0.57	1.84
<b>ELD</b>	7768	4.56	-1.99	4.42	10.34	0.65	1.72
<b>YM6</b>	7698	4.48	-1.99	4.43	10.02	0.66	1.75
<b>EUR</b>	6592	4.27	-1.83	3.71	8.12	0.65	1.71

Analysing the errors statistics and scatter plots one can conclude that:

- In terms of significant wave height the hindcasts are rather good. Both the bias and RMSEs are low and the correlation is quite high. There is some underestimation of the high events, but that is already what was to be expected from the model, not only due to model limitations but also since on wave boundary conditions are imposed in model. In severe storms it is expected that the energy propagating into the North Sea from the North Atlantic not to be negligible.
- In terms of zero-upcrossing wave period the comparisons are rather poor. The RMSEs are in excess of 4 s. This severe underestimation of the wave period may be in part due to the lack of input wave energy at the boundaries of the Delft3D model, but seems also to point to excessive whitecapping of low/mid frequency energy in the SWAN model (as observed in the previous studies mentioned above).

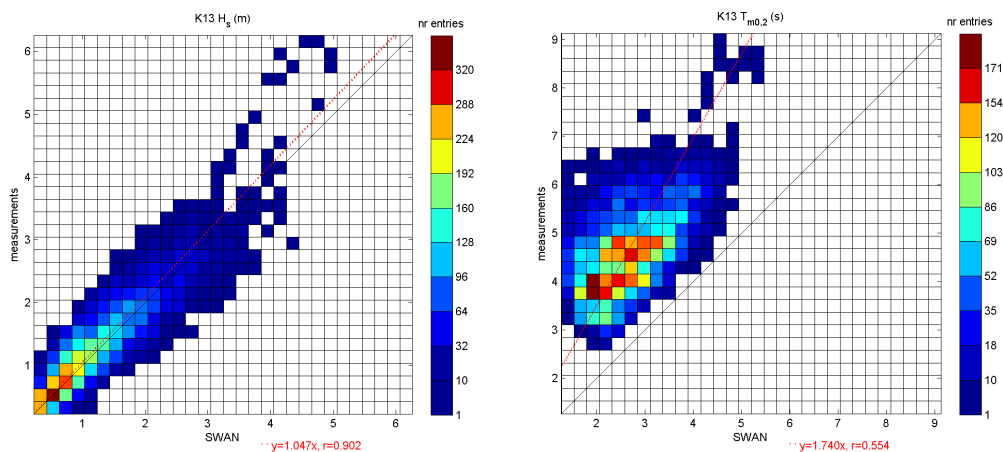


Figure 4.2 Scatter plot comparisons at K13 between  $H_s$  (left) and  $T_{m0,2}$  (right) measurements and Delft3D hindcasts using the standard settings in WAVE.

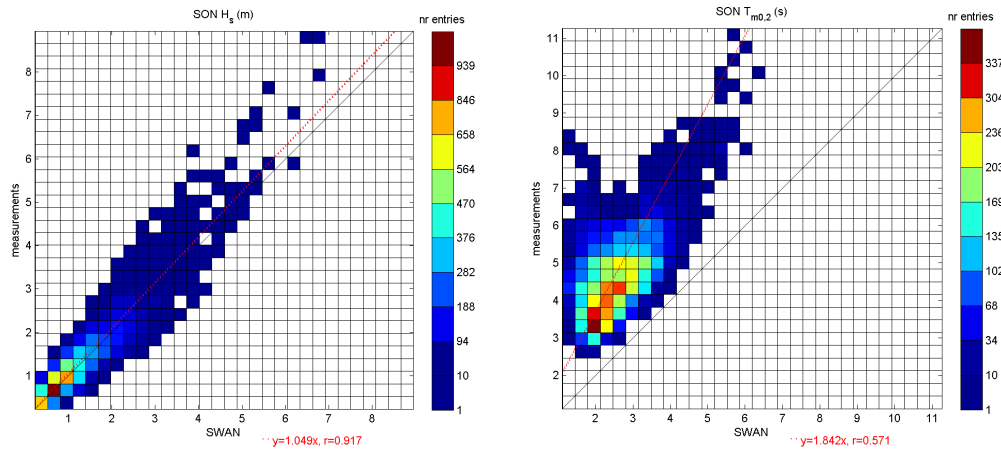


Figure 4.3 Scatter plot comparisons at SON between  $H_s$  (left) and  $T_{m0,2}$  (right) measurements and Delft3D hindcasts using the standard settings in WAVE.

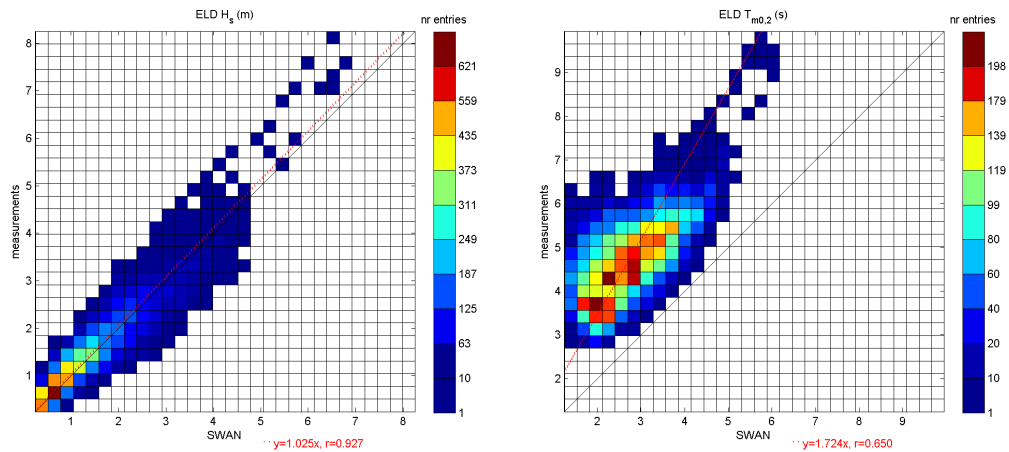


Figure 4.4 Scatter plot comparisons at ELD between  $H_s$  (left) and  $T_{m0,2}$  (right) measurements and Delft3D hindcasts using the standard settings in WAVE.

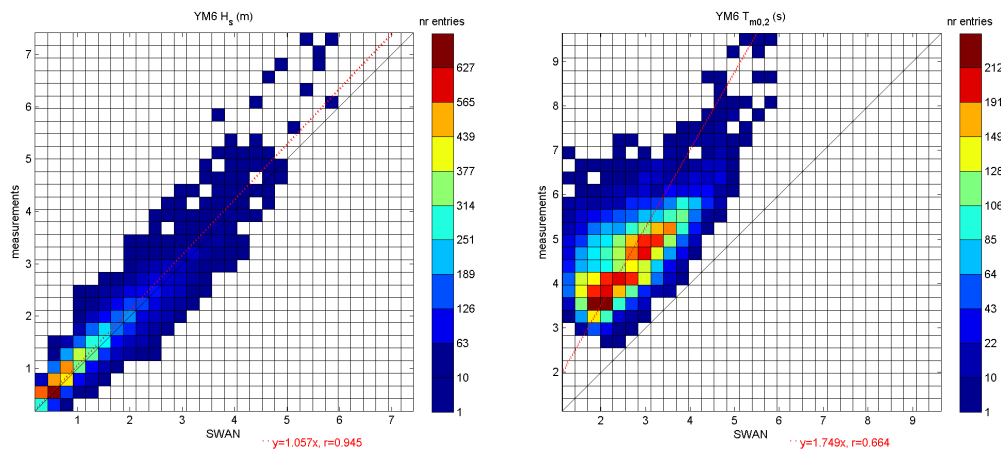


Figure 4.5 Scatter plot comparisons at YM6 between  $H_s$  (left) and  $T_{m0,2}$  (right) measurements and Delft3D hindcasts using the standard settings in WAVE.

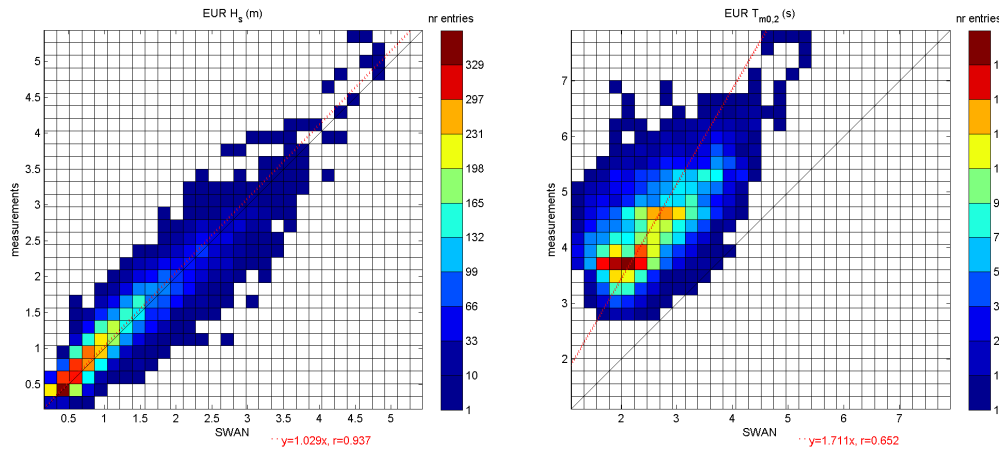


Figure 4.6 Scatter plot comparisons at EUR between  $H_s$  (left) and  $T_{m0,2}$  (right) measurements and Delft3D hindcasts using the standard settings in WAVE.

#### 4.4.2 Model calibration results

Assuming that the model poor results are due to excessive whitecapping of low/mid frequency energy, the SWAN whitecapping settings were adjusted and the SWAN computations re-run. Caires et al. (2008) also noted that SWAN North Sea hindcasts using the standard Komen et al. (1984) formulation severely underpredicted wave period measurements and have therefore carried out computations using the formulation of Van der Westhuysen et al. (2007) and the mentioned above Rogers et al. (2003) adjustment of the Komen et al. (1984) formulation by setting  $n = 2$  in (5) and leaving  $C_{ds} = 2.36 \cdot 10^{-5}$ . Their results show that when using the formulation of Van der Westhuysen et al. (2007) the wave period hindcasts improve, but substantial improvements are only obtained when using the settings suggested by Rogers et al. (2003). The Delft3D-WAVE computations were therefore re-run leaving all default SWAN settings in Delft3d-WAVE and adjusting the wave growth and whitecapping settings according to Rogers et al. (2003). The error statistics for the adjusted hindcasts are presented in Table 4.5 and Table 4.6 in terms of significant wave height and zero-upcrossing wave period, respectively. Figure 4.7 to Figure 4.11 show the scatter plot comparisons for each buoy location.

Table 4.5 –  $H_s$  error statistics for the hindcasts using adjusted settings in WAVE.

Buoy	$n$	$\bar{x}$ (m)	bias (m)	RMSE (m)	SI (%)	$\rho$	$r$
<b>K13</b>	6187	1.21	0.02	0.10	8.28	0.91	0.98
<b>SON</b>	8124	1.12	0.03	0.10	8.48	0.92	0.98
<b>ELD</b>	7954	1.34	0.03	0.11	8.34	0.93	0.96
<b>YM6</b>	7884	1.29	-0.01	0.08	6.25	0.95	0.99
<b>EUR</b>	6777	1.18	0.03	0.06	5.09	0.94	0.96

Table 4.6 –  $T_{m0,2}$  error statistics for the hindcasts using adjusted settings in WAVE.

Buoy	$n$	$\bar{x}$ (s)	bias (s)	RMSE (s)	SI (%)	$\rho$	$r$
<b>K13</b>	5975	4.45	-0.64	1.14	16.42	0.65	1.14
<b>SON</b>	7932	4.42	-0.95	1.71	18.45	0.66	1.23
<b>ELD</b>	7768	4.56	-0.67	1.26	17.88	0.71	1.13
<b>YM6</b>	7698	4.48	-0.75	1.33	17.20	0.73	1.16
<b>EUR</b>	6592	4.27	-0.64	1.00	13.72	0.73	1.14

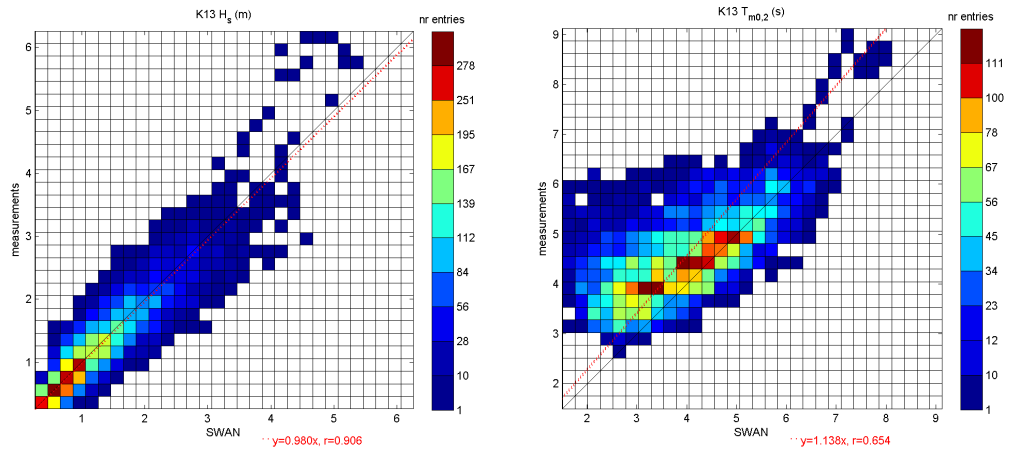


Figure 4.7 – Scatter plot comparisons at K13 between  $H_s$  (left) and  $T_{m0,2}$  (right) measurements and Delft3D hindcasts using adjusted settings in WAVE.

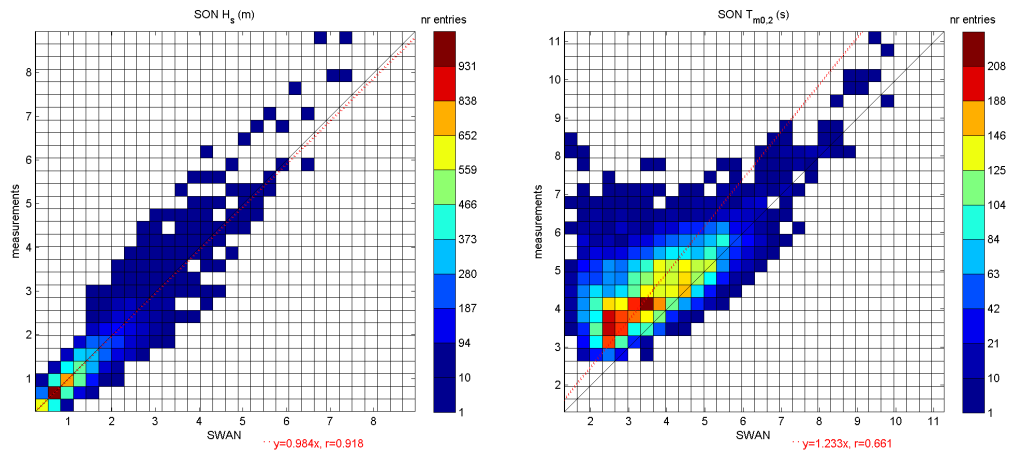


Figure 4.8 – Scatter plot comparisons at SON between  $H_s$  (left) and  $T_{m0,2}$  (right) measurements and Delft3D hindcasts using adjusted settings in WAVE.

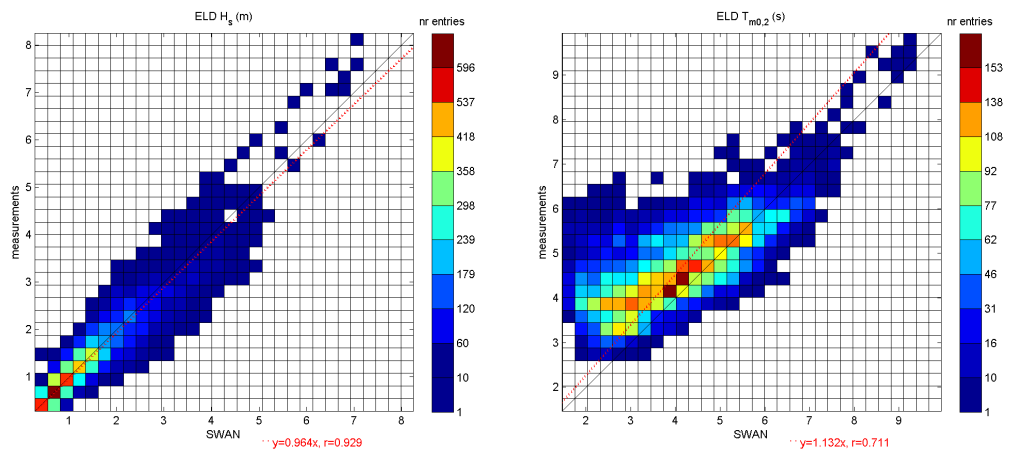


Figure 4.9 – Scatter plot comparisons at ELD between  $H_s$  (left) and  $T_{m0,2}$  (right) measurements and Delft3D hindcasts using adjusted settings in WAVE.

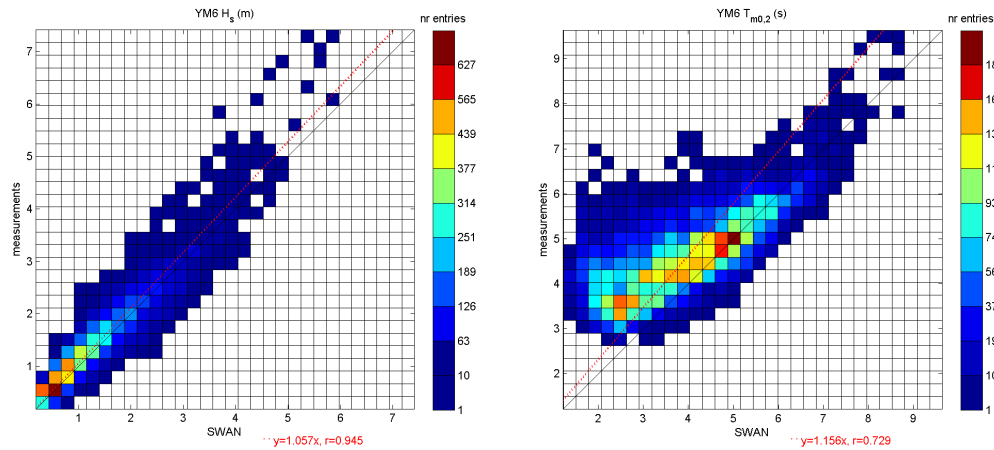


Figure 4.10 – Scatter plot comparisons at YM6 between  $H_s$  (left) and  $T_{m0,2}$  (right) measurements and Delft3D hindcasts using adjusted settings in WAVE.

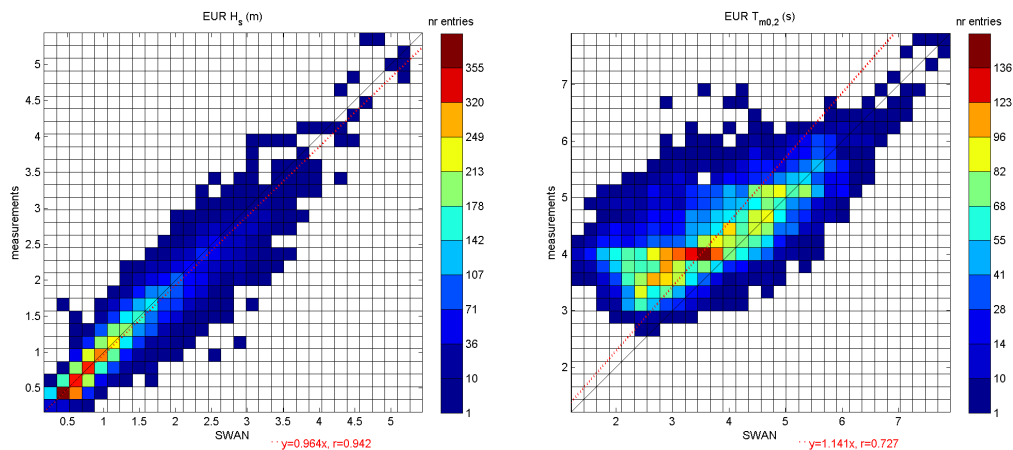


Figure 4.11 – Scatter plot comparisons between at EUR  $H_s$  (left) and  $T_{m0,2}$  (right) measurements and Delft3D hindcasts using adjusted settings in WAVE.

Analysing the errors statistics and scatter plots one can conclude that:

- In terms of significant wave height the adjusted hindcast compare marginally better with the measurements than the initial hindcasts using the standard settings in WAVE.
- In terms of zero-upcrossing wave period the adjusted results compare significantly better with the measurements. There is still a mismatch between the hindcasts and the measurements, mostly an underestimation, with associated RMSEs between 1 and 1.7 s in the considered comparisons. However, it is thought that the underestimation in these computations is mostly due to the lack of input wave energy at the boundaries of the Delft3D model, the situation being only improved if reliable and time-varying wave boundary conditions are used in the computations.

## 4.5 Conclusions

The objective of this study was to setup a model to compute accurate North Sea wave hindcasts using time and space varying HIRLAM wind fields as input. The hindcasts are to be used as input for silt dispersion simulations for the North Sea and therefore the computations were to be carried out using Delft3D.

The study focus on a one year period, namely 2006. The study results show that using the standard settings in Delft3D-WAVE the hindcasts although comparing well with significant wave height measurements, lack a considerable amount of low frequency energy. Adjusting the Delft3D-WAVE settings reliable hindcasts are obtained which compare rather well with the measured significant wave heights, but still underestimate, although much less, the measured wave periods.

As a result, resuspension at deeper water will be underestimated using the Delft3D-WAVE results. Waves with a shorter period (i.e. a shorter wave length) result in a lower wave-induced bed shear stress at deeper water. Some correction of the wave period is therefore recommended, for example by data assimilation.

Further improved North Sea wave hindcasts are expected to be obtained if time varying boundary wave information is also input in the computations. It is recommended that a pilot study is carried out using the model wave information available in the MATROOS database as boundary condition.



---

## 5 Uncertainties in mud transport modelling of the North Sea

### 5.1 Introduction

Modelling of fine sediment transport at the North Sea is an ongoing activity in the framework of multiple (but connected) projects. Results until 2008 are reported Van Kessel and Brière (2006), Van Kessel et al. (2008) and Bruens et al. (2007). These results are based on a two-fraction mud model including sediment buffering calibrated using MWTL-data (e.g. silt atlas by Suijlen and Duin, 2001) and CEFAS smartbuoy and minipod data at Noordwijk 10, 5 and 2 km in the period 1999 – 2001. Calibration has therefore been focussed on the Dutch coastal zone.

The present work focuses on the whole Southern North Sea, as remote sensing data have become available and also smartbuoy data at location farther off the Dutch coast (e.g. Oyster grounds, Dogger bank and close to the Thames estuary). A third sediment fraction has been added with a very low settling velocity to maintain realistic concentration levels (about 2 mg/l) farther offshore during calm weather. It is noted that the three fraction model used for the sensitivity analysis described below has not yet been calibrated. Therefore, initially a worse performance is expected compared to the calibrated two-fraction model, notably in the Dutch coastal zone.

### 5.2 Methodology

As a preliminary stage to the actual use of data assimilation (data-model integration, DMI) in the numerical model of suspended solids in the southern North Sea, it was decided that an uncertainty analysis would be carried out on some key parameters in the model.

Data assimilation is a method that allows to use observations of the past and current state of a system within a model in order to compute the best estimate of the current state of the system (usually referred to as the forecast). It uses the fact that both observations and models depict a certain image of the underlying truth of the system. This method relies on the fact that there are uncertainties in both the observations and the model computation, and that these uncertainties can be combined to compute the best estimate of the forecast.

However, the quality of the model forecasts relies on the knowledge of the uncertainties of the observations and model computations. The uncertainties in the observations generally depend on the measuring device and the conditions in which the measurement was performed and can often be estimated from the information provided along with the data. The hydrodynamic and transport models contain several sources of uncertainties. The governing equations may contain inaccuracies due to limited knowledge of the physical processes and their interactions. Simplifications must also be made to avoid high computational costs and because of the discretisation of continuous equations on a finite grid. Uncertainties may also arise from incorrect or incomplete model forcings, such as initial and boundary conditions, meteorological data, wave data, or bathymetry. In particular, a numerical model relies heavily on the choice of certain key parameters that are required in the rendering of several processes. Although most of these parameters exist in the real world, they are often very difficult, if

not impossible to measure. Thus, their determination often results from empirical relations derived from limited datasets or from laboratory experiments. The resulting uncertainties in these parameters translate into uncertainties in the model results.

An uncertainty analysis aims at quantifying the uncertainty that arises in the model results as a consequence of uncertainties in the parameters. The methodology relies on the fact that the typical range for each parameter value is known. Thus, for each parameter, a mean value and a standard deviation are known. By varying a given parameter within its uncertainty range, the model results may or may not vary. The uncertainty in the model results provides an indication of how sensitive the model is to the choice of this parameter. In general, an uncertainty analysis consists of running an ensemble of simulations in which all parameters are the same except one. The ensemble is built in such a way that the uncertainty range of the parameter is covered. The range covered by the results of the ensemble enables to estimate how sensitive the model is to the uncertainty of the chosen parameter.

Of course, the number of parameters in the model increase with the model complexity. In the current study, it was decided that the uncertainty analysis would focus on four key parameters in the sediment model (Van Kessel and Brière, 2006):

- the Shields shear stress for resuspension pick-up
- the factor for resuspension pick-up
- the sedimentation velocity;
- the value of the critical shear stress above which resuspension occurs;

In the current study, each member of the ensembles is compared to measurements of suspended sediments in the southern North Sea. In order to quantify how well a model run performs compared to the measurements, a simple cost function is built.

### **5.3 Overview of the available measurement sources**

Two main types of suspended solid measurements are available for the southern North Sea, with different spatial and temporal coverages: in-situ measurements and remote sensing data.

#### **5.3.1 In-situ measurements**

Each country neighbouring the southern North Sea (Netherlands, Belgium, United Kingdom, Germany) collects data at several locations. These in-situ measurements generally have different properties depending on whether they have been obtained during measurement campaigns at sea or through devices moored to the seabed.

Data collected during measurement campaigns at sea generally have a rather broad spatial coverage but a scarce temporal coverage, with rarely more than one or two value per location and per month. However, records for these data often cover several decades. Such records enable to derive seasonal patterns and low frequency trends but generally do not allow to identify the effect of short-lived events (such as a storm).

On the contrary, records data collected through moored devices are usually shorter but measurements are obtained with a much higher frequency. Such records therefore enable to identify the effect of high-frequency events on the measured parameters.

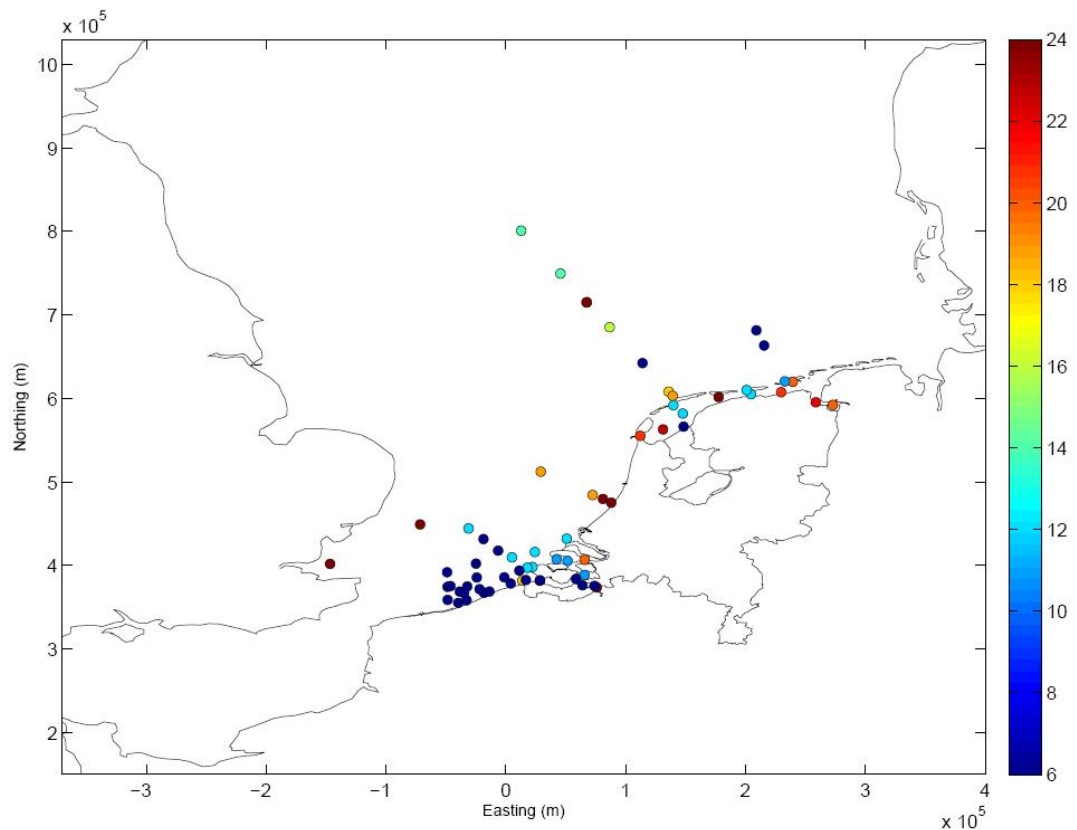


Figure 5.1 Location of the in-situ measurements and number data points available for the year 2006.

The location and number of available in-situ measurements for the year 2006 are indicated in Figure 5.1. For that year, no German measurements could be obtained. Most of the data gathered by MUMM includes less than 10 measurements per location. The frequency of the Dutch data is generally higher, with about 12 to 24 values per year. The CEFAS data points have a high frequency, with measurements every two hours for most of the year.

### 5.3.2 Remote sensing data

### 5.3.3 Discussion of the data uncertainties

The uncertainty ranges for the data depend significantly on the way the measurement method. For instance, a distinction should be made between measurements with optical devices and measurements by samplings. Optical devices measure the backscattering of light by suspended particles and derive concentrations from it. However, backscattering may be caused by organic particles that should not be considered as suspended sediments. Similarly, after several weeks or months of operation the accuracy of devices moored at sea may be altered by the growth of living organisms on the device. The uncertainty of measurements can usually be estimated by studying the

way the data is processed by the institute who provides them, and by comparing concomitant data from different sources.

#### 5.4 Model setup

The model setup is very similar to that used in the previous VOP slib project (van Kessel and Brière, 2006). The southern North Sea is modelled by combining a series of numerical models: the hydrodynamic model Delft3D-FLOW, the surface wave model SWAN, and the sediment transport model Delft3D-WAQ. All models make use of the curvilinear grid shown in Figure 5.2. The horizontal resolution is the highest in the Dutch coastal zone (about 2x2 km), and the coarsest in the northern part of the model domain (about 20x20 km). The hydrodynamic simulations include a representative tide based on astronomic components, and the actual forcing of rivers discharges, wind and atmospheric pressure.

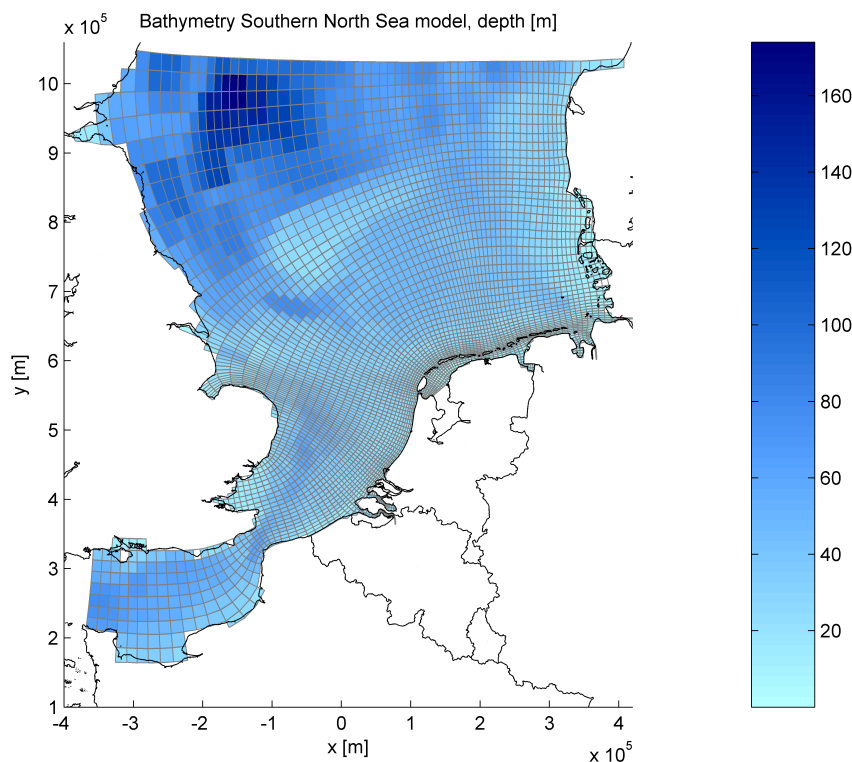


Figure 5.2 Bathymetry and curvilinear grid of the Southern North Sea (ZUNO-grof) model application. Both the Delft3D FLOW and Delft3D WAQ applications discussed in this report operate on this grid.

In the previous study, 10  $\sigma$ -layers were used in the vertical, where this number was extended to 12  $\sigma$ -layers. This discretisation enables to follow the seabed while maintaining the same number of layers throughout the domain. Each layer represents a certain percentage of the local depth. The vertical resolution is the finest at the depths where the largest velocity shear is expected, i.e. near the bottom for tidal flows and near the surface for the wind-forced circulation. The maximum velocity shear due to salinity corresponds to the depth with the largest vertical salinity gradient, which is located relatively close to the surface in the case of river plumes entering coastal seas. In order to maintain a fine enough vertical resolution to accurately model the salinity stratification

in the Dutch coastal zone, 12 layers with relative thicknesses of 4.0, 5.6, 7.8, 10.8, 10.9, 10.9, 10.9, 10.8, 7.8, 5.6, and 4.0 % of the total water depth from bottom to surface were used.

In the following, the year 2006 is considered because additional measurements were available for this year. Thus, the wind forcing was updated.

Unlike in the previous study, the silt model used now includes a three-fraction description of sediment characteristics (with three spatial- and temporal-constant settling velocities, respectively for each fraction). The third fraction corresponds to very fine silt ( $w_s = 10^{-6}$  m/s). With two fractions, it was found that the concentrations near the Dutch coast were satisfying, but that they were much too low offshore. For further information on parameter settings is referred to the input file of the simulation with runID f2\_37. As remarked in the introduction, the three-fraction model is still uncalibrated, so the model performance with the initial settings is likely to be worse than that of the calibrated two-fraction model.

For more details on the general model setup, we refer to Van Kessel and Brière (2006).

## 5.5 Model results

### 5.5.1 Reference simulation

The parameters for the reference simulation are based on the various studies and calibrations carried out with the ZUNO-coarse model within WL | Delft Hydraulics and Deltares in the past years.

In a first stage, the model results are compared to remote sensing and in-situ data. Since all available measurements for 2006 focus on the upper water column, the comparison only focuses on concentrations of suspended sediments in the upper water column. However, three types of quantities are considered:

- 1 the actual SPM concentrations in the water column. The comparison either focuses on timeseries of measured vs. modelled concentrations at several locations, or on snapshots of horizontal maps of measured vs. modelled concentrations;
- 2 the spatial patterns in the maps of temporal mean concentrations and the spatial patterns in the standard deviation of the concentrations compared to the mean;
- 3 an overall cost function, which takes into account the integrated effect of spatial differences between the time-averaged modelled  $\langle Y \rangle$  and observed concentrations  $\langle X \rangle$ . This cost function is defined as follows:

$$CF_{mean} = \sum_{space} (\langle X \rangle - \langle Y \rangle)^2 \quad (5.1)$$

The cost function on the temporal means enables to quantify the differences between the modelled mean state and the observed mean state. A similar cost function is built for the standard deviations. It gives an indication of how the modelled time variability compares with the observed one.

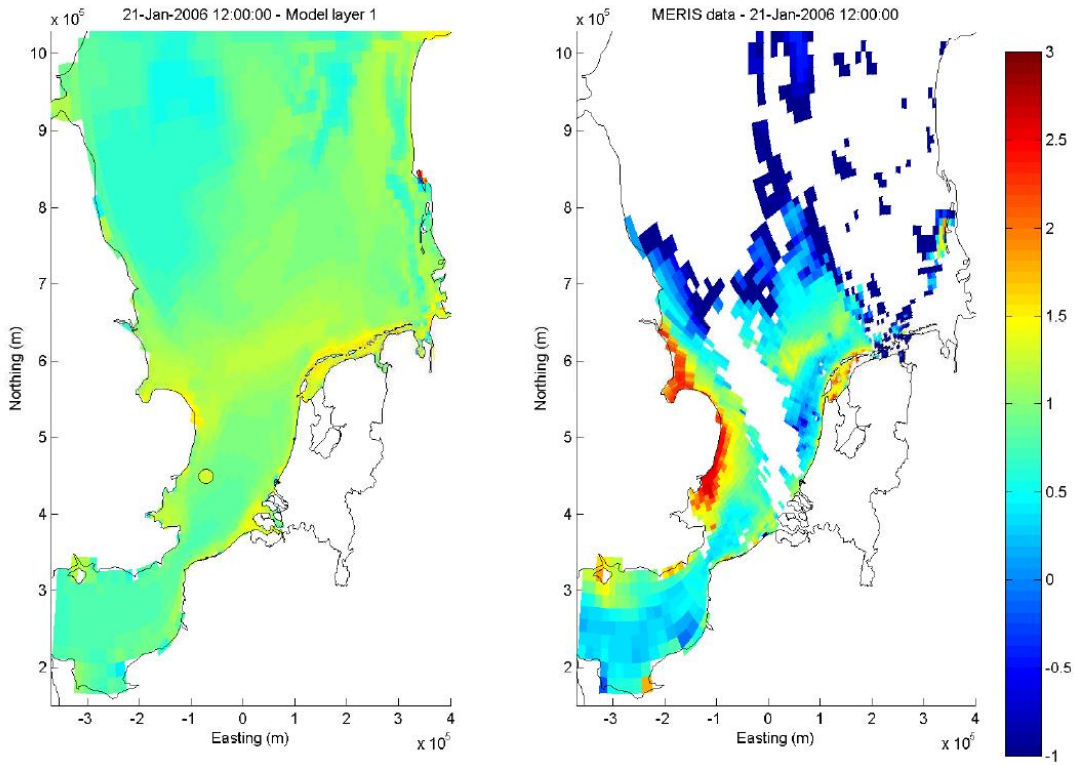


Figure 5.3 Snapshot of the suspended sediment concentrations near the surface (in  $\log_{10}$  mg/L) on the 21/01/2006 in the reference simulation (left) and obtained by remote sensing (right).

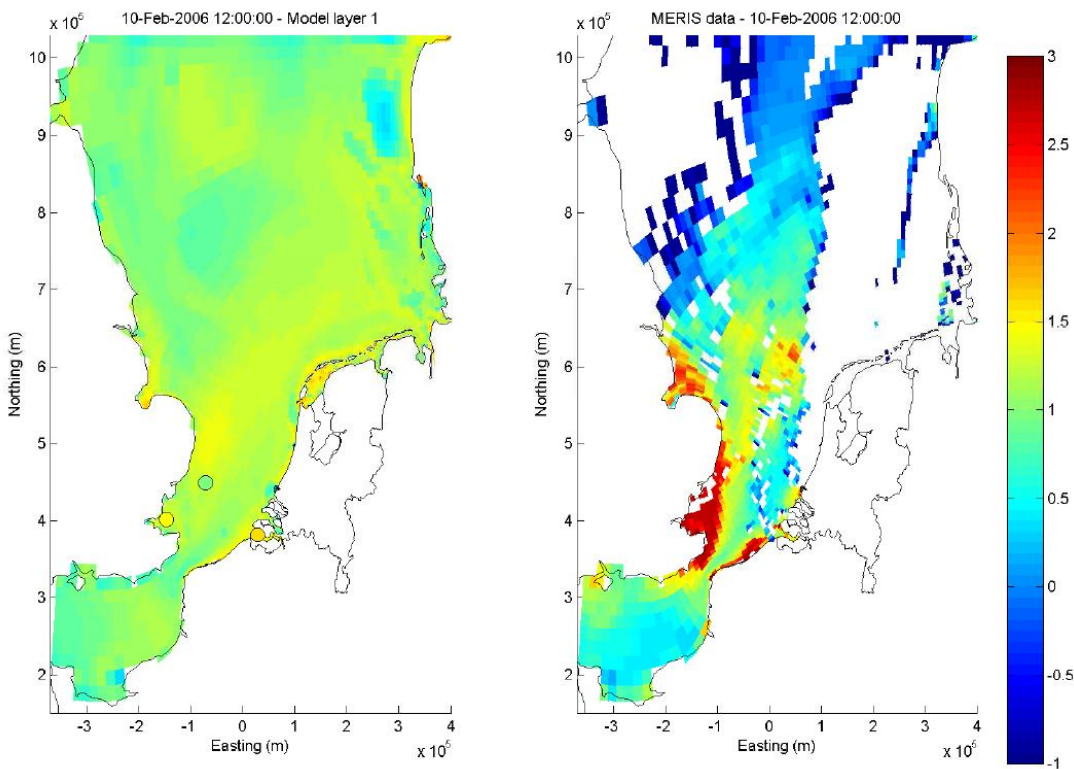


Figure 5.4 As in Figure 5.3 on 10/02/2006.

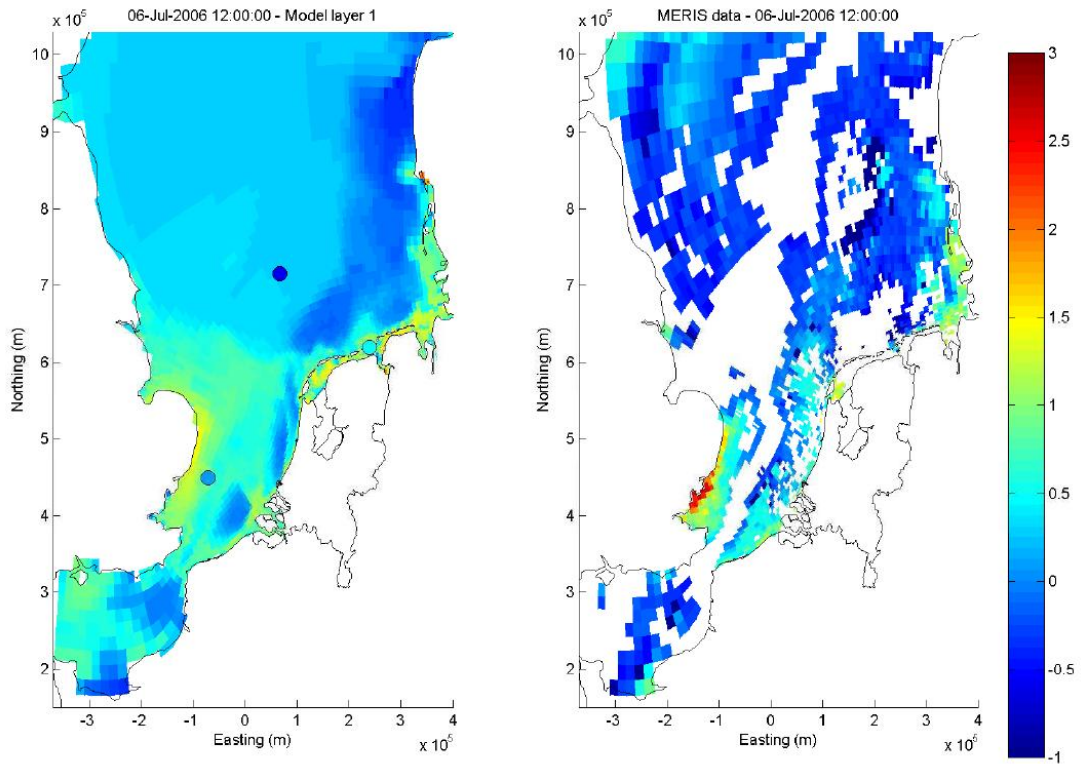


Figure 5.5 As in Figure 5.3 on 06/07/2006.

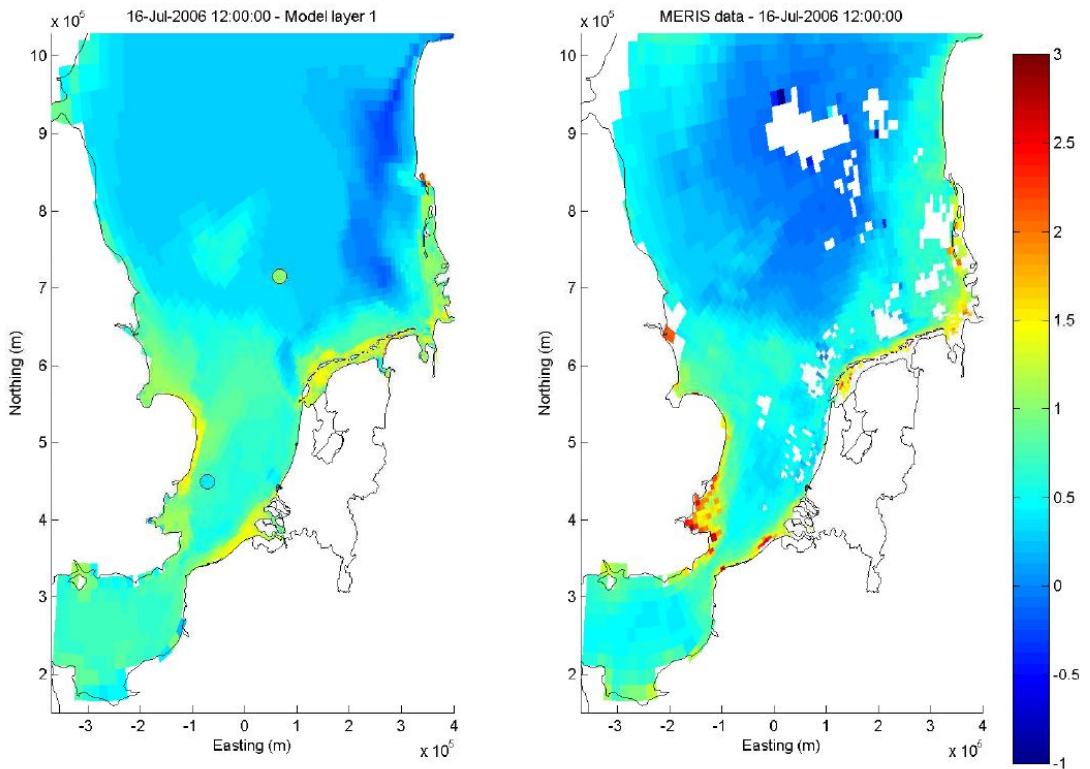


Figure 5.6 As in Figure 5.3 on 16/07/2006.

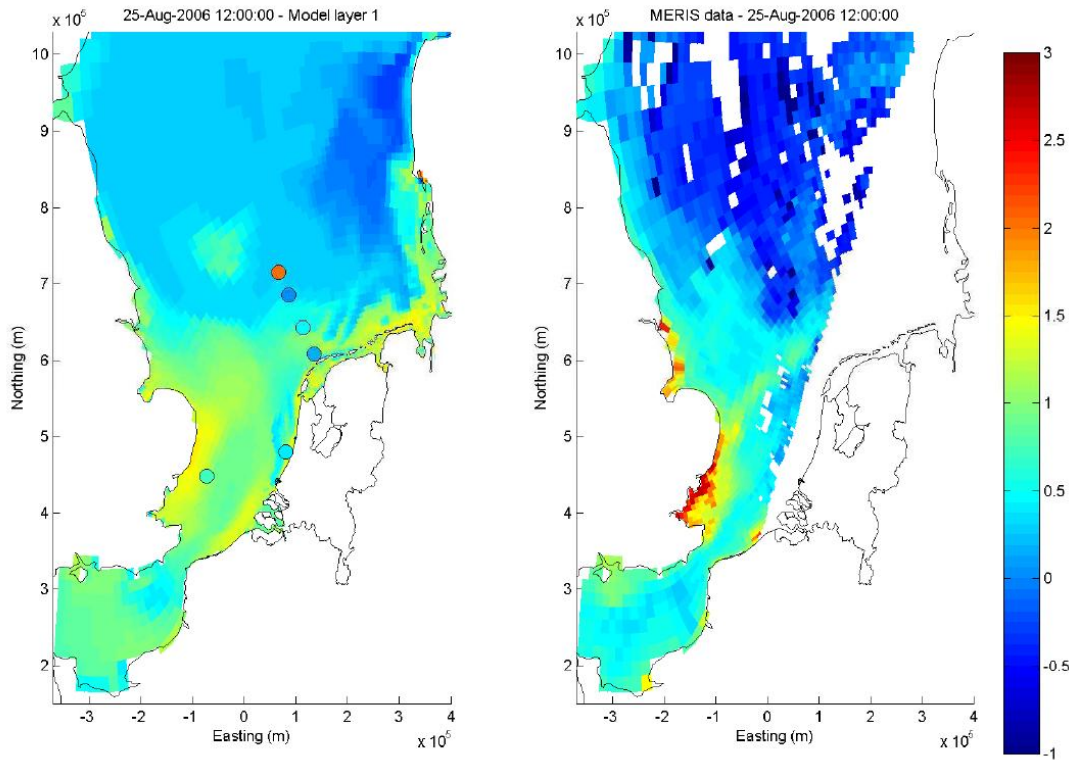


Figure 5.7 As in Figure 5.3 on 25/08/2006.

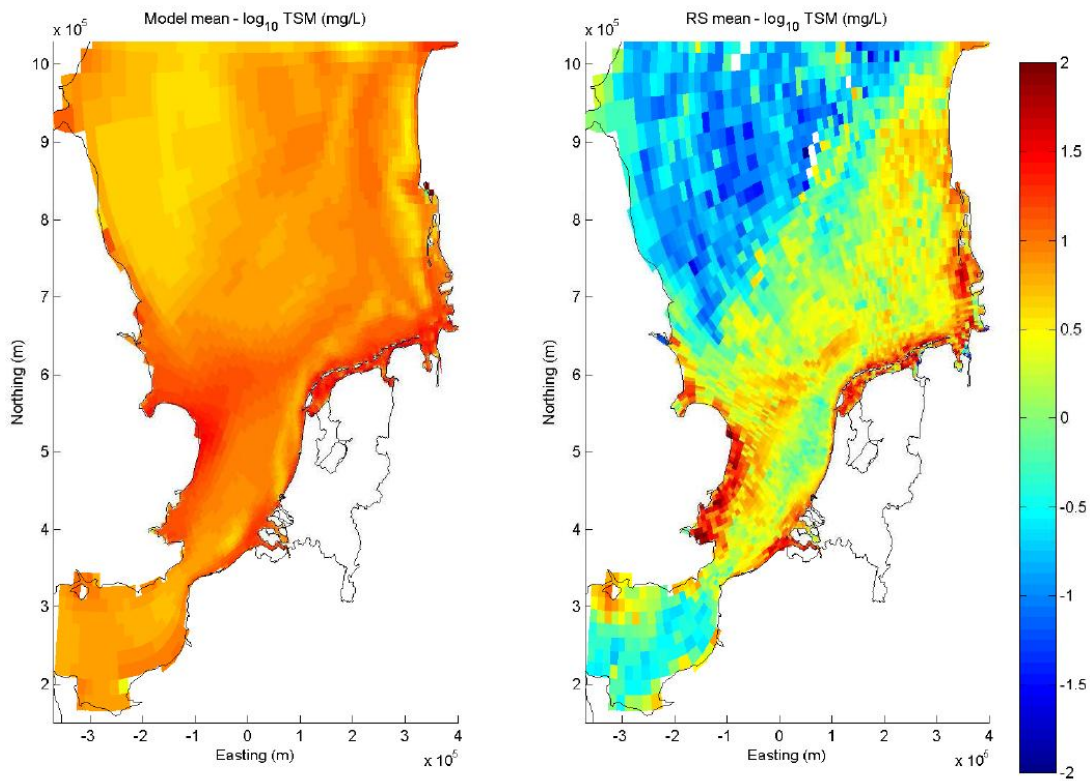


Figure 5.8 Comparison of the time-averaged modelled concentration in the reference simulation (left) with the time-averaged concentration measured by remote sensing (right).

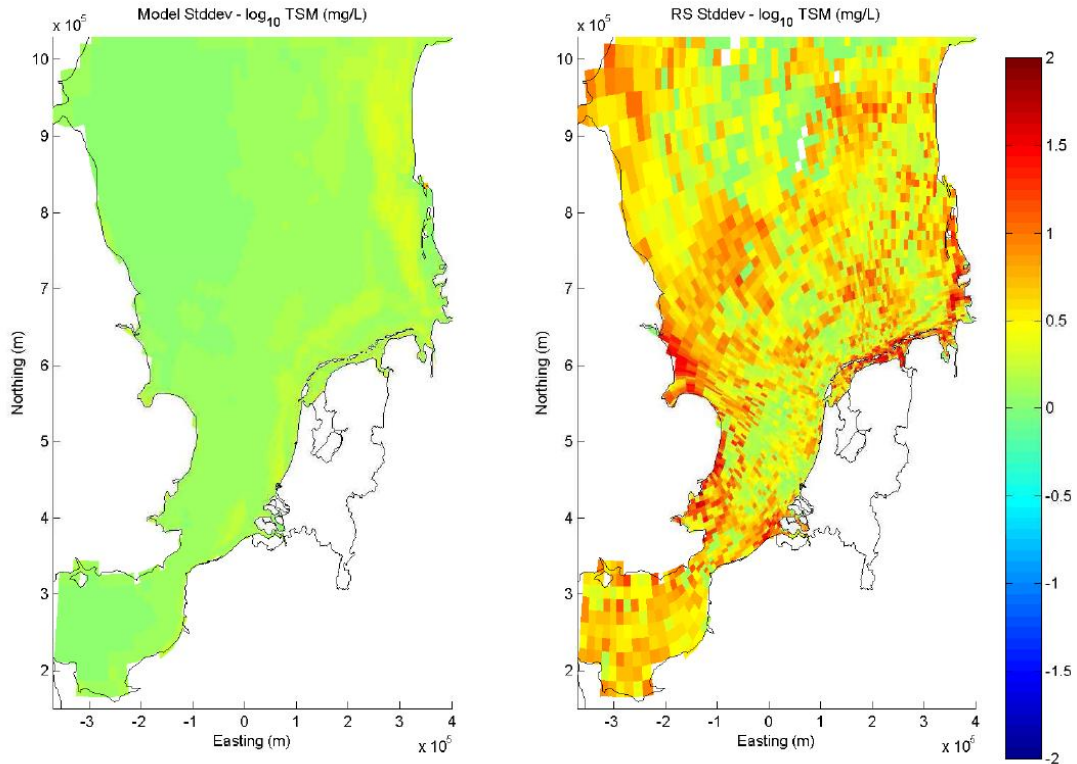


Figure 5.9 Comparison of the modelled standard deviation from the temporal mean in the reference simulation (left) with that measured by remote sensing (right).

In addition, it should be noted that the comparison focuses on the base 10 logarithm of the concentrations and not on the concentrations themselves. The reason is that the concentrations follow a log-normal distribution, so that comparing the logarithms of the concentrations gives more insight on the patterns.

Comparisons of snapshots of suspended sediment concentrations near the surface as obtained in the model and according to remote sensing data are presented in Figure 5.3 to Figure 5.7. Whenever available, concentrations according in-situ measurements have also been included on the snapshots.

The remote sensing data indicate that suspended sediment concentrations are the largest along the East Anglian, Belgian, Dutch, and German coasts. The model manages to reproduce similar patterns, though generally with much smaller concentrations than those measured. On some occasions (Figure 5.6) the model reproduces very well the situation obtained from remote sensing, but in general the satellite images exhibit a strong variability that the model only partially manages to mimic.

Figure 5.8 and Figure 5.9 present comparisons of the time-averaged and standard deviation from the mean for the modelled concentrations with those measured from remote sensing. They indicate that the model suffers from three systematic biases:

- 1 typically, the modelled concentrations in the coastal areas are too low;
- 2 typically, the modelled concentrations in the offshore areas are too high;
- 3 the modelled variability is too small.

---

These biases can be reduced to some extent by model calibration.

### 5.5.2 Uncertainty analysis

For the uncertainty analysis, 4 ensembles of 20 members each were defined. In total, 80 simulations (in addition to the reference simulation described above) were carried out. For each member of each ensemble, the monthly means and corresponding standard deviations were computed and used to calculate cost functions.

#### *Sedimentation velocity*

In reality, only the sedimentation velocity for a limit situation in which the flocculation and salinity are zero is changed. The actual sedimentation velocities for each sediment fractions are proportional to this term. Thus, changing this term affects all sediment fractions.

The cost functions for the means and standard deviations of the 20 members of the ensemble are presented in Figure 5.10 and Figure 5.11, respectively. First of all, it should be noted that the cost functions as a function of the sedimentation velocity behave similarly for each month. Increasing the settling velocity to 27.8 m/day for the first fraction (instead of 10.8 m/day) reduces the value of the cost function by about 20%. However, it only slightly improves the rendering of the time variability. In addition, it appears that the optimal sedimentation velocity for the mean state lies outside the uncertainty range that was initially chosen.

Increasing the sedimentation velocity facilitates the settling of sediments and therefore tends to decrease the concentration of suspended sediments in the water column. Thus, it improves the quality of the model simulation in offshore areas where the modelled concentrations are too high, but brings it even further from the observations in coastal regions where the concentrations were already too low (Figure 5.12). The variability is not significantly improved (Figure 5.13).

#### *Critical shear stress for resuspension*

The cost functions for the means and standard deviations of the 20 members of the ensemble are presented in Figure 5.14 and Figure 5.15, respectively. These results indicate that increasing the critical shear stress improves the mean concentrations but barely affects the temporal variability. As for the sedimentation velocity, the optimal value for the mean state lies outside the initial uncertainty range of the parameter.

By increasing the critical shear stress, a larger current velocity is required for resuspension to occur. Thus, the suspended sediment concentration in the water column decreases in areas of moderate currents but remains generally high in the areas with strong currents. Thus, the modelled concentrations tend to decrease mostly offshore but remain higher in coastal areas (Figure 5.16).

#### *Shields shear stress for the resuspension pick-up*

The cost functions for the means and standard deviations of the 20 members of the ensemble are presented in Figure 5.17 and Figure 5.18, respectively. As for the previous parameters, the mean concentrations are slightly improved but the time-variability is not affected. As for both previous parameters, the optimal Shields shear stress for the mean state seems to be located outside the initial uncertainty range.

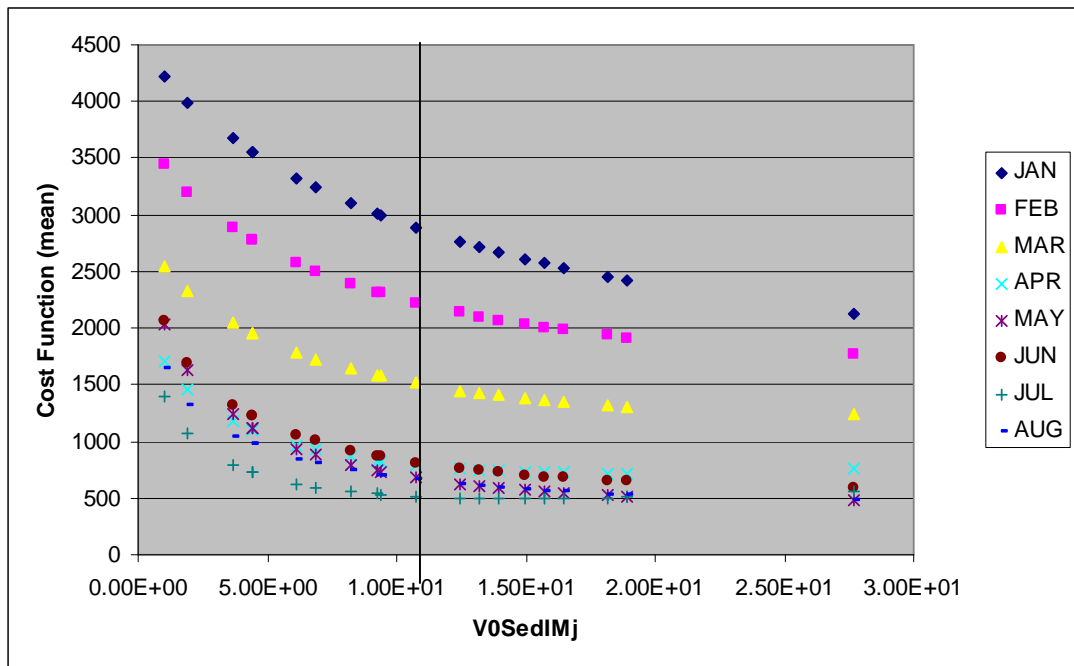


Figure 5.10 Evolution of the cost function for the mean as a function of the vertical sedimentation velocity (in m/day) for the first sediment fraction. The vertical line indicates the value chosen in the reference run.

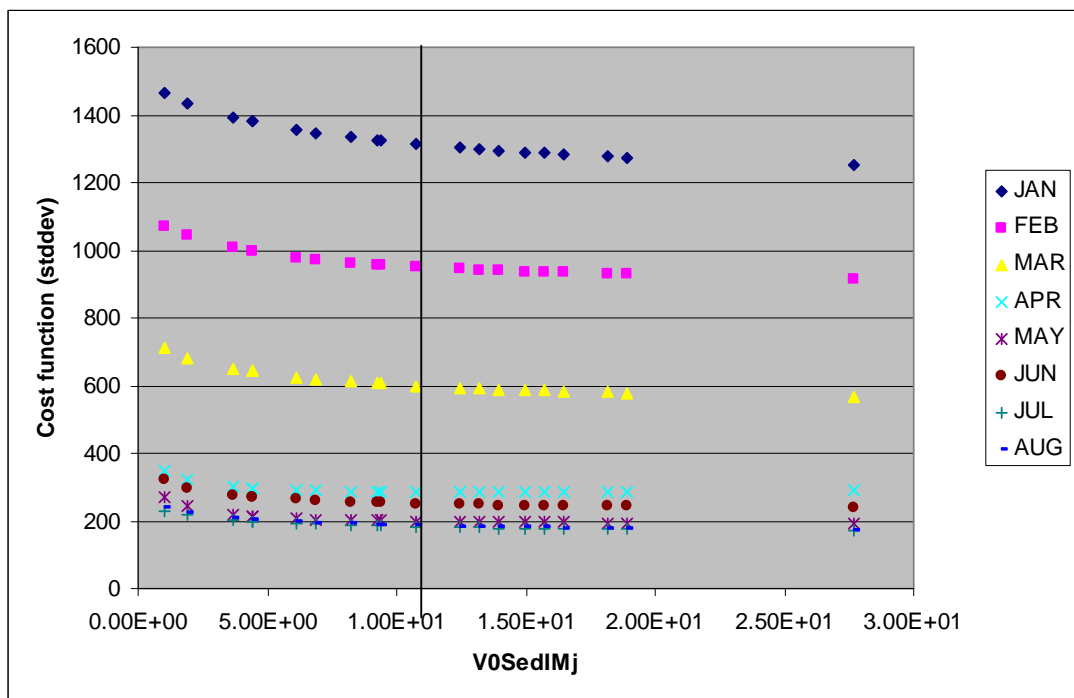


Figure 5.11 Evolution of the cost function for the standard deviation as a function of the vertical sedimentation velocity (in m/day) for the first sediment fraction. The vertical line indicates the value chosen in the reference run.

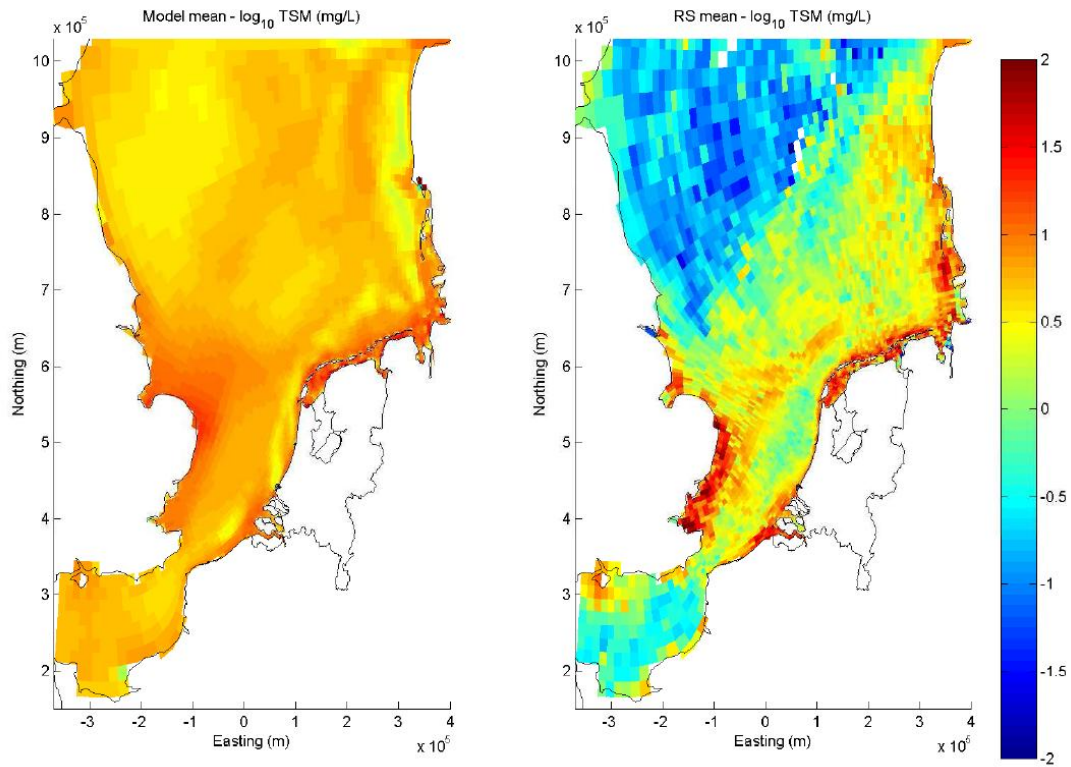


Figure 5.12 As in Figure 5.8 for the maximum sedimentation velocity.

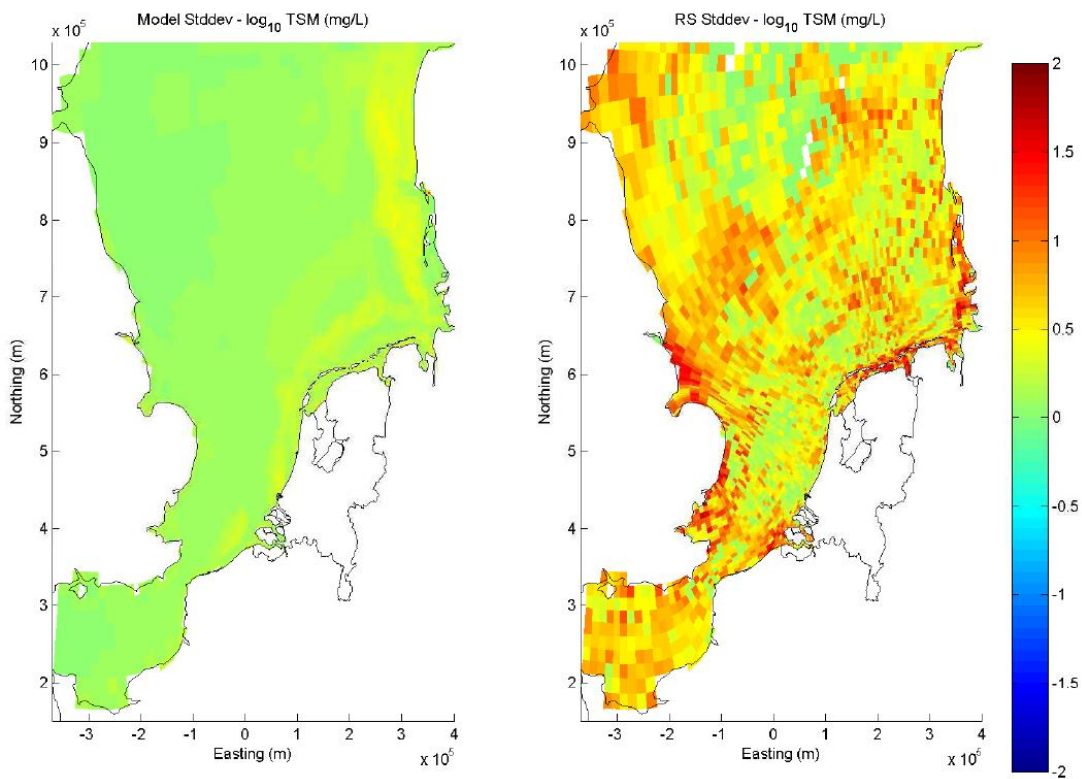


Figure 5.13 As in Figure 5.9 for the maximum sedimentation velocity.

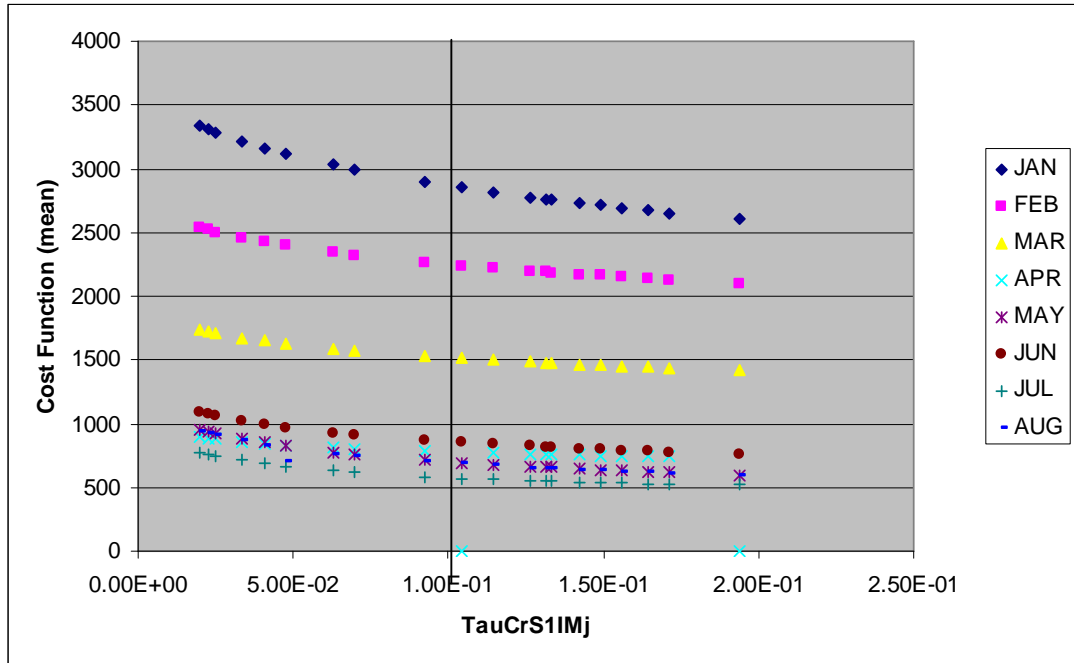


Figure 5.14 As in Figure 5.10 as a function of the critical shear stress for resuspension.

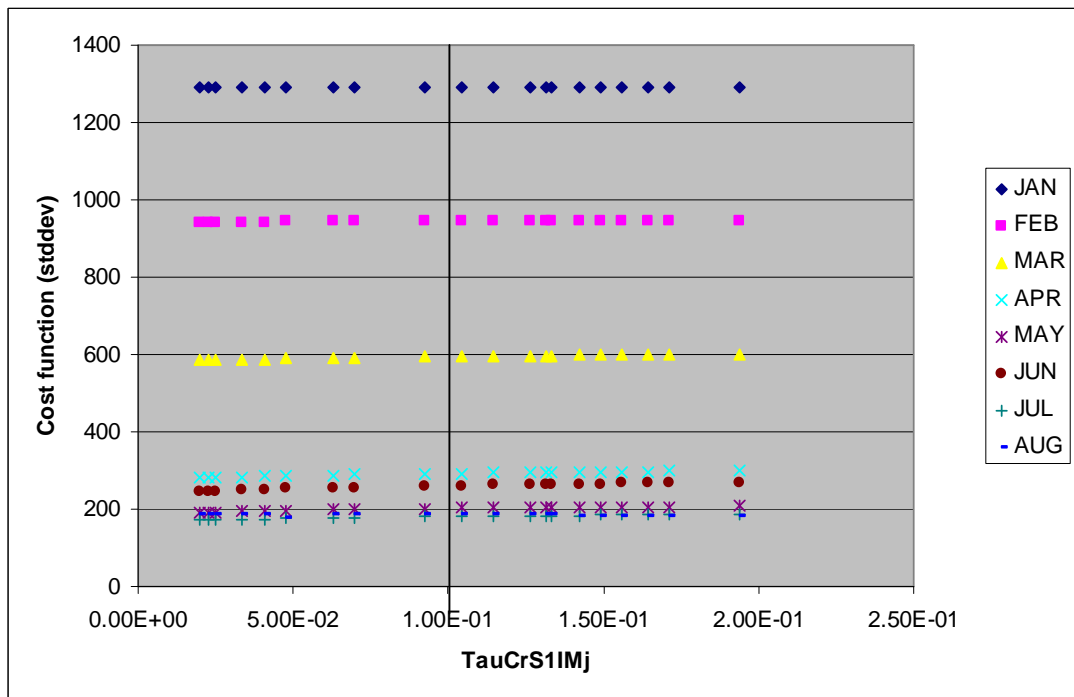


Figure 5.15 As in Figure 5.11 as a function of the critical shear stress for resuspension

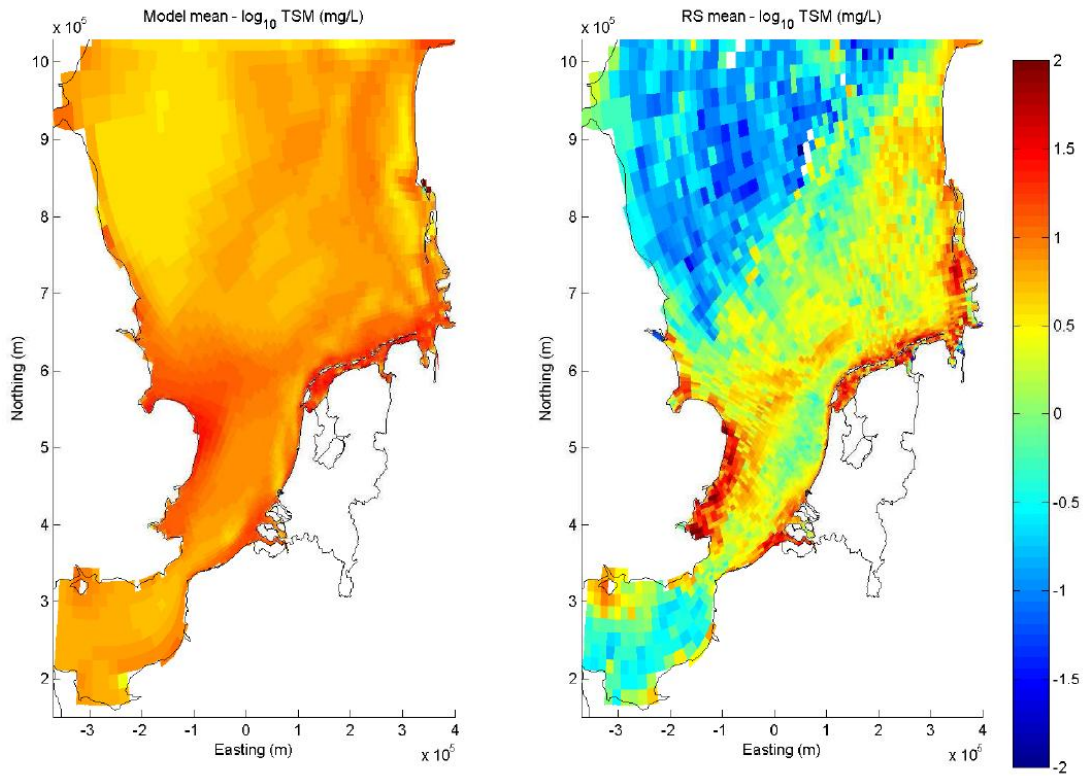


Figure 5.16 As in Figure 5.8 for the maximum critical shear stress.

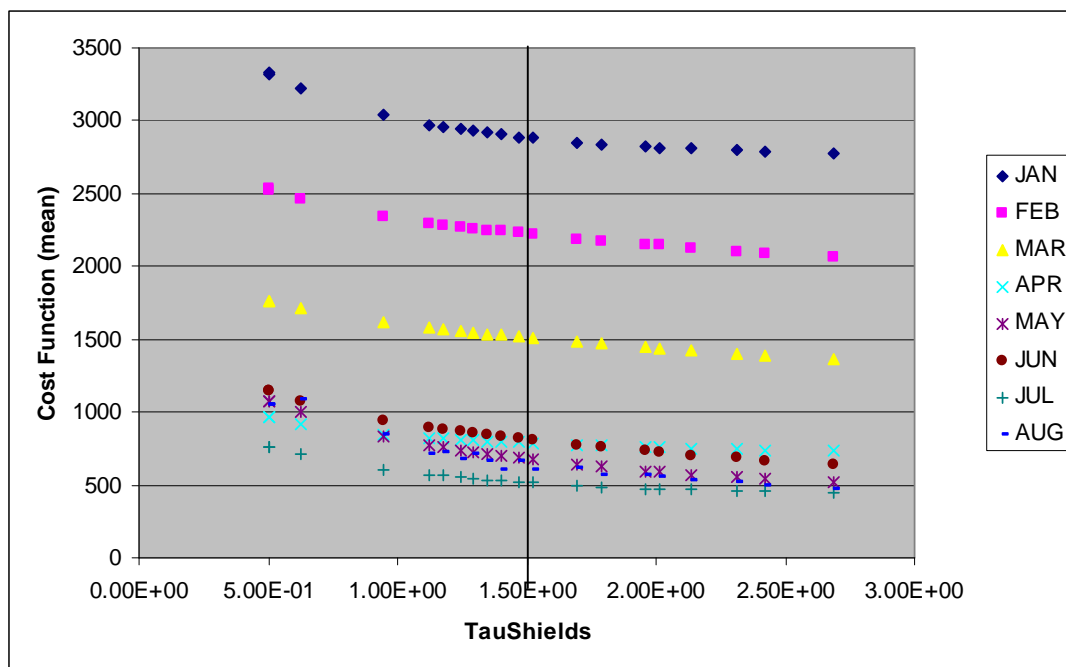


Figure 5.17 As in Figure 5.10 for the Shields shear stress resuspension pick-up.

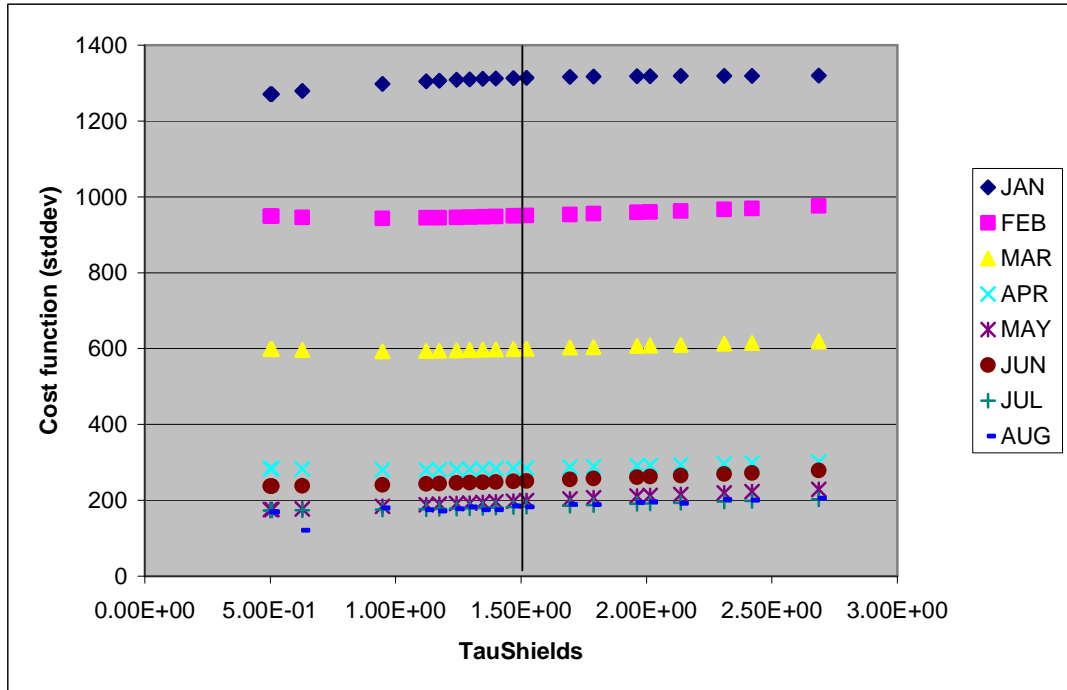


Figure 5.18 As in Figure 5.11 for the Shields shear stress for resuspension pick-up.

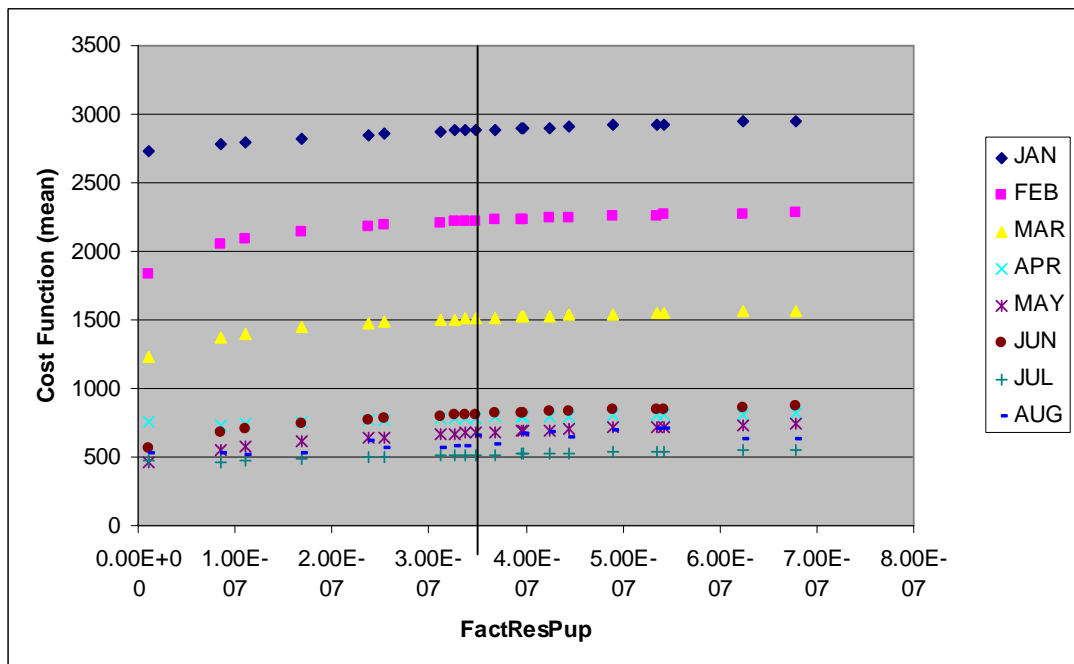


Figure 5.19 As in Figure 5.10 for the factor for resuspension pick-up.

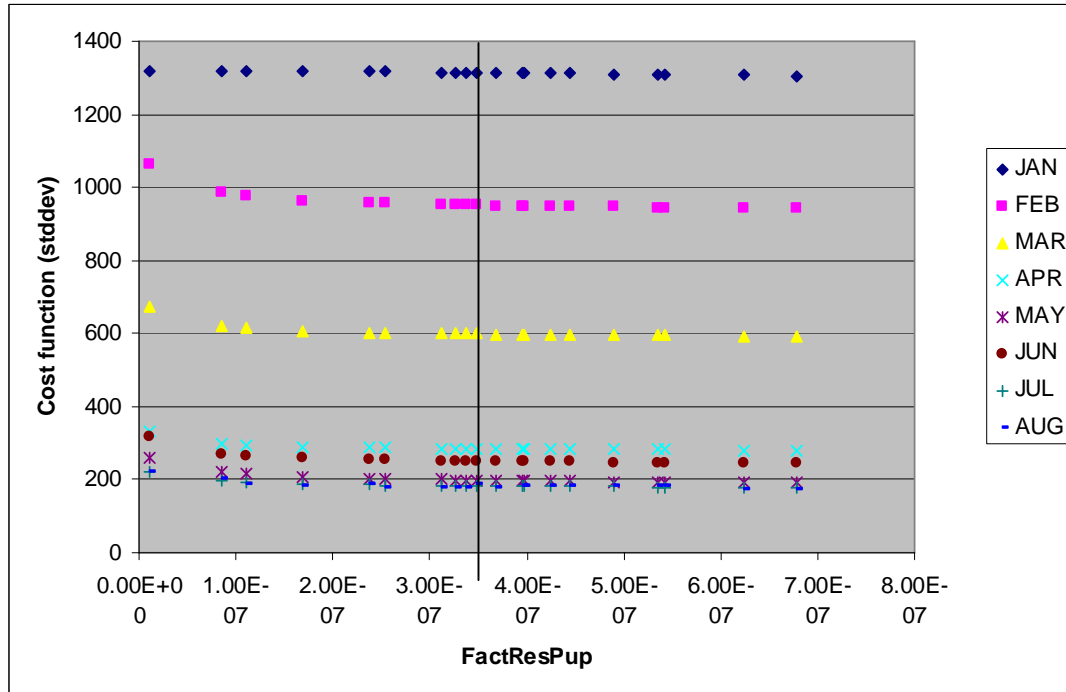


Figure 5.20 As in Figure 5.11 for the factor for resuspension pick-up.

*Factor for resuspension pick-up*

The results of the ensemble members for this parameter are rather comparable to the other parameters: it is possible to improve the mean concentrations by changing the parameter value but the time variability of the model remains unaffected. In addition, the uncertainty analysis does not clearly indicate which value for this parameter is the optimal one for the mean state.

5.5.3 Discussion

A comparison of the modelled concentrations for the reference simulation as well as for the best member of each ensemble with the measured concentrations at three Cefas locations are presented in Figure 5.21 to Figure 5.23. This comparison confirms the results of the cost functions: the model results are sensitive to the values set to each of the four parameters presented above, and the overall quality of the model will be improved by adapting some parameters.

However, it appears that in general the model is able to reproduce satisfactorily average summer conditions but performs poorly in average winter conditions and that the model biases differ in coastal and offshore areas. Thus, the ideal situation would consist in improving the model significantly for winter conditions without quality loss in summer conditions. On the other hand, changing any one of the four investigated parameters (at least without changing the others) tends to offset the suspended sediment concentrations in the water column one way or another, regardless of spatial patterns or time variability.

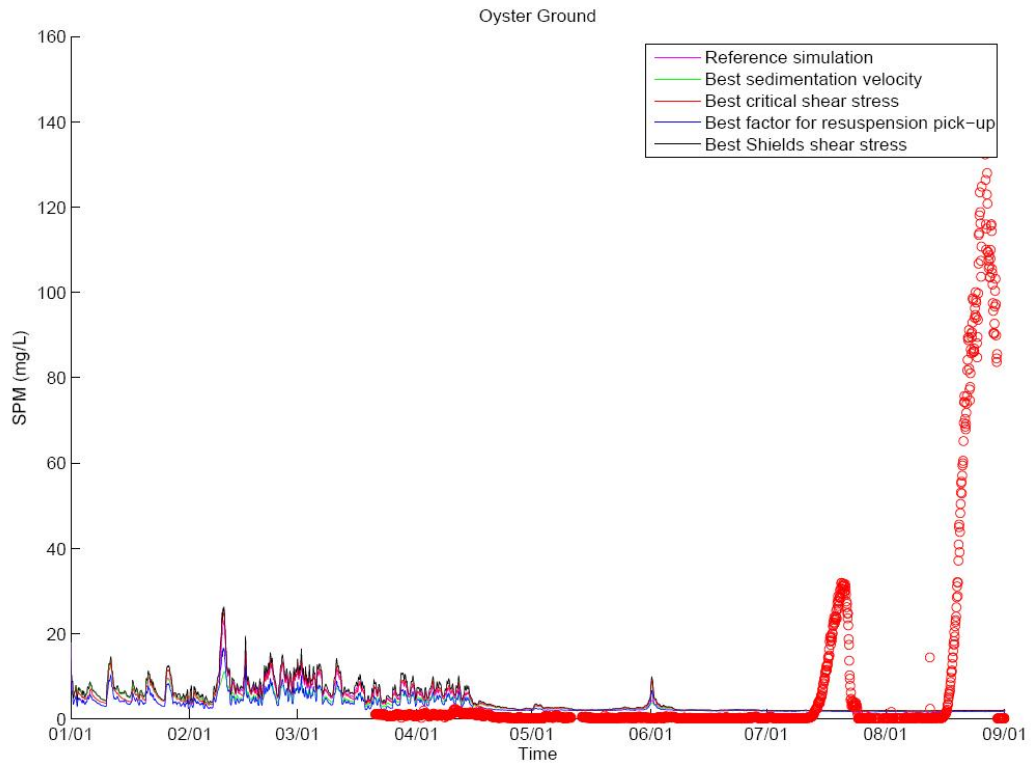


Figure 5.21 Modelled SPM concentrations near the surface at Oyster Ground for the reference simulation and each of the best ensemble member. The in-situ measurements are indicated by the red circles.

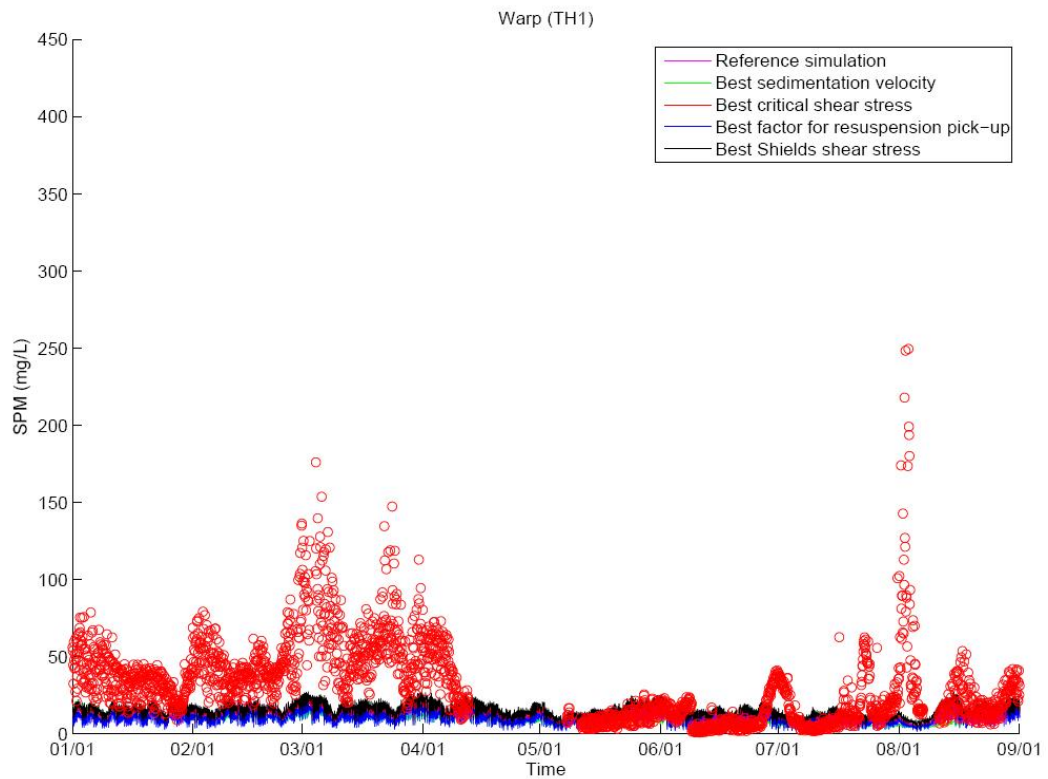


Figure 5.22 As in Figure 5.21 at Warp.

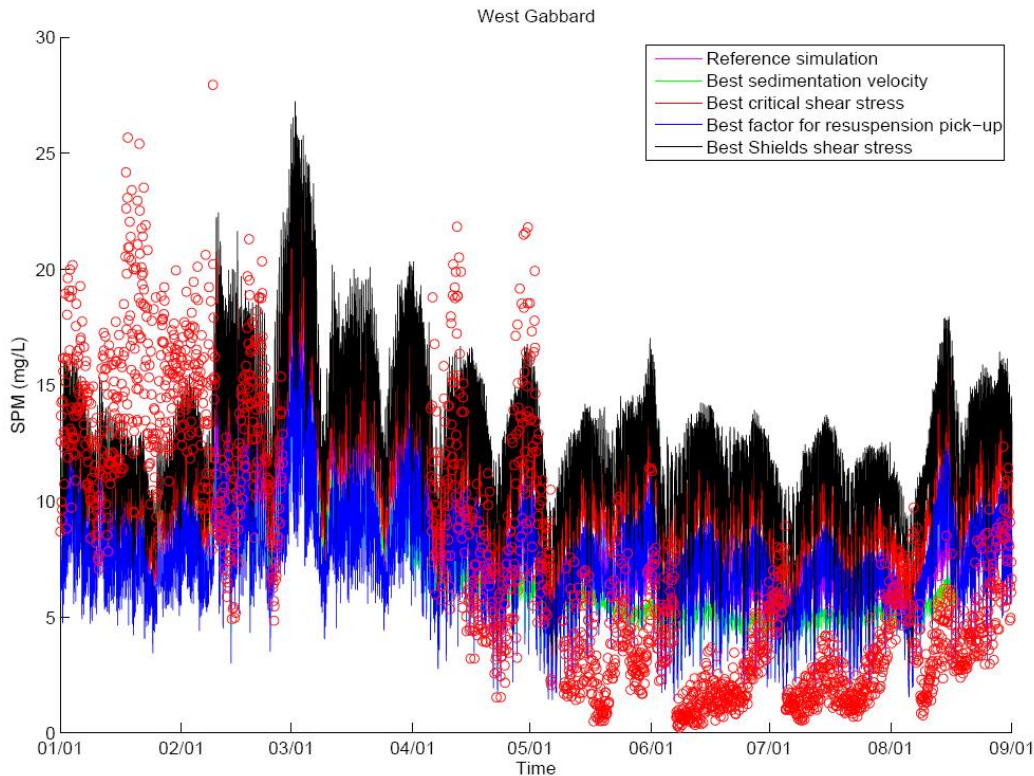


Figure 5.23 As in Figure 5.21 at West Gabbard.

In addition, the initial uncertainty ranges for the four parameters were based on bibliographical studies and ranges derived from measurements. The fact that in each case the optimal parameter appears to be located outside the initial range raises the issue of whether our knowledge of the uncertainty ranges needs to be improved or whether some other, more critical parameters of the model should be improved first. Indeed, applying non-realistic values to certain parameters for the sake of improving the model results is definitely not the way to proceed, since the model needs to be driven by realistic physical processes.

Therefore, it appears essential to extend the analysis presented above to other key parameters while keeping in mind the underlying physics. In particular, the following model developments and improvements should focus primarily on sets of parameters and forcings that are responsible for seasonal patterns.

For example, the rendering of winter conditions could be improved without altering that of summer conditions by varying the critical Shields shear stress and the factor for resuspension pick-up together, since the ratio of both quantities determines the amount of sediments that are resuspended in the water column during storms.

Similarly, relating the observed events of high concentrations to the time variability of the wind and wave forcings and improving the realism of the wave model may significantly improve the quality of the model simulations. In addition, the realism of the boundary conditions for the input of sediments in the North Sea could be improved. In particular, the input of sediments from the English and French cliffs could be made dependant on the wave-induced erosion and therefore follow a seasonal cycle, instead of being continuously released in the system the way they are now (Van Kessel and Brière, 2006).

## 6 Modelling harbour siltation by fluid mud flows

### 6.1 Introduction

Harbours are frequently located in estuaries, and often characterized by high siltation rates. Exchange of water masses between the harbour basin and the estuary is governed by (1) horizontal exchange flows (eddies), (2) tidal filling and emptying, and (3) density-driven flows (Winterwerp, 2005). Density-driven flows may be generated by salinity, temperature and/or suspended sediment. Flows with a sediment concentration of only several g/l may substantially contribute to harbour siltation (Winterwerp and van Kessel, 2003). However, when a fluid mud layer is formed close to the entrance of the basin, the contribution of sediment-driven flows may become excessive.

Transport of these fluid muds is caused by interfacial shear, gravity and/or pressure gradients. Interfacial shear is generated by the velocity difference between the two layers, shear by gravity is caused by the density difference between the fluid mud and the ambient water and the bed slope, while shear may also be generated by horizontal pressure gradients. Transport will occur if their combined shear exceeds the yield strength of the fluid mud layer, and therefore the transport depends on ambient conditions as well as on the sediment properties. Depending on the ambient conditions and sediment properties, one or more mechanisms may contribute to the transport of fluid mud. Here we aim to establish the conditions for which near-bed transport becomes the dominant contribution to harbour siltation, and assess the dominant processes for fluid mud transport.

We start out with further elaborating the processes governing the transport of fluid mud. Next the physics of the mud model is introduced, which is tested on a simple geometry model consisting of a sloping bed. The model is then applied to a schematized harbour basin geometry.

### 6.2 Consolidation and fluid mud transport

During consolidation, sediments that were initially supported by the turbulence in the fluid, become supported by the grain matrix of the deposit. The effective stress  $\sigma'$  is the stress carried by the grain skeleton, and is equal to the difference between the total pressure and the pore water pressure. In a dilute suspension, the pore water pressure equals the overall pressure and therefore the effective stress is zero. During consolidation, the excess pore pressure decreases while the total pressure remains unchanged, i.e. the effective stress increases. Consolidation ends when the pressure of the pore water becomes equal to the hydrostatic pressure, and pore water outflow stops. The time required for consolidation mainly depends on the permeability  $k$  and the thickness of the deposit  $h$ .

Fluid mud is defined as a suspension with a concentration that is sufficiently high to prevent lutocline formation when it is left at rest, and in which the effective stress is negligible compared to excess pore pressure. Generally, fluid mud is generated by failure of loosely packed sediments (e.g. by waves), or by a settling flux of fine particles that exceed the consolidation rate of the bed. The concentration of fluid muds

generated by the first mechanism is generally higher than that of the second. Fluid mud left at rest will eventually consolidate and hence disappear. However, mild disturbance by e.g. ships, waves, dredging, or water flow will reduce consolidation rates. Too much agitation will result in total resuspension of the fluid mud. Fluid mud layers are displaced by gravity or by surface forces. Generally, three mechanisms are responsible for fluid mud displacement:

(1) Gravity.

The gravity force can be computed from the excess density, thickness, and bed level gradient. Surface forces are the pressure gradients (normal stress) and the shear stress. Shear stress generated by gravity amounts to  $\tau_g = \Delta\rho gh \sin\alpha$ , with  $\Delta\rho$  the density difference between HCBS layer and water,  $h$  the HCBS layer thickness and  $\alpha$  the bed slope.

(2) Pressure gradients.

Pressure gradients are generated by hydraulic gradients, surface waves, and turbulence. Shear stresses are generated by near-bed velocity gradients and by turbulence. A horizontal pressure gradient  $dp/dx$  generates a shear stress  $\tau_p = h (dp/dx)$ .

(3) Interfacial shear.

Interfacial shear is generated the interface roughness and the velocity difference between the two layers considered:  $\tau_i = f_i \rho (u_1 - u_2)^2$ .  $\tau_i$  has the same order the bed shear stress.

Depending on the ambient conditions, one or more mechanisms may contribute to the transport of HCBS. When the forces exerted on the fluid mud layer are known, its transport rate can be calculated assuming a certain rheological behaviour, i.e. the relation between stress and strain. This is complex because

(a) The rheology of a fluid mud is complex, with a yield strength and viscosity depending on the shear rate, shear history, and sediment characteristics

(b) The forces exerted on the fluid mud flow are influenced by the fluid mud flow itself through damping of turbulence, and should therefore be simultaneously solved.

This implies that the transport of fluid mud cannot be accurately predicted by applying a complex hydrodynamic model in combination with a separate fluid mud module.

Transport will only occur if the shear exceeds the yield strength of the HCBS layer. The yield strength of mud depends on its bulk density. For mud from the Sea Scheldt the following empirical relationship is derived from yield strength measurement:  $\tau_y = a (\Delta\rho)^b$ , with  $a = 4.5 \cdot 10^{-12}$  Pa and  $b = 5.7$  (de Wit, 1995). The resulting yield strength is then used to determine the stability of the fluid mud or HCBS layer (Figure 6.1). Typically, thicker and denser layers are more likely to be transported by gravity force, whereas thinner, less dense layers are more likely to be driven by interfacial shear. For example a HCBS layer with  $\Delta\rho = 1 \text{ kg/m}^3$  and thickness 0.1 m on a bed with slope 0.01 experiences a gravitational shear stress of only 0.01 Pa, which is less than a typical interfacial shear stress of 0.1 to 1 Pa. Such relatively thin and low-concentrated layers are therefore predominantly driven by interfacial shear. However, a fluid mud layer  $\Delta\rho = 100 \text{ kg/m}^3$  and thickness 1 m on a bed with slope 0.01 experiences a gravitational shear stress of 10 Pa, well above the typical interfacial shear stress. The dynamics of such relatively thick and high-concentrated layers are therefore often decoupled from the overlying water body.

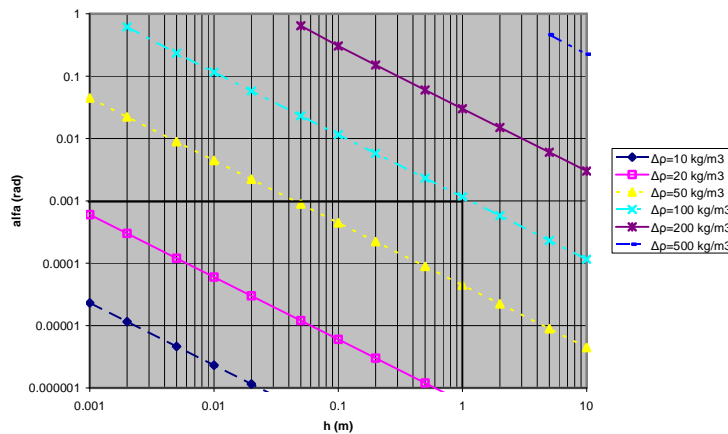


Figure 6.1 Stability criterion of mud layer with thickness  $h$  and excess density  $\Delta\rho$  on a bed slope  $\alpha$ . A mud layer with thickness 1 m and excess density  $100 \text{ kg/m}^3$  has a critical bed slope of 0.001 rad.

Process	Interfacial shear	Gravity
Mud layer	thin	thick
Sediment concentration	low	high
Current velocity	high	low
Angle of repose	low	high

### 6.3 Model setup

#### 6.3.1 Model physics

The transport of the fluid mud layers and the transport of suspended sediment is computed with the Slib3D code. The physical parameterizations of the Slib3D code are extensively described in Winterwerp et al. (submitted) and van Maren et al. (2007). Here we only give a very brief overview of the fundamental equations.

The settling velocity of mud particles increases through flocculation. The higher the sediment concentration  $c$ , the higher the collision frequency of individual particles, and therefore the settling velocity  $W_s$ . Flocs are broken down by turbulent shear and therefore the settling velocity decreases with increasing shear  $k$ . However, at low turbulent energy levels, the timescales and spatial scales for floc formation become so high that the settling velocities are low at very low turbulence levels. Hence, the settling velocity is maximal at high sediment concentrations and intermediate turbulence levels. This is parameterized with the flocculation module:

$$W_{s,0} = \left[ k_4 \frac{c^{1/2q}}{k^{3/8}} - k_2 \left( k_4 \frac{c^{1/2q}}{k^{3/8}} - D_0 \right) \exp \left\{ -\frac{k_3 k^{9/8} h^*}{n_f} \right\} \right]^{n_f - 1}$$

At higher concentrations, the settling of particles slows down because of hindered settling effects:

$$W_s = W_{s,0} \frac{(1 - \phi_*)^m (1 - \phi_p)}{(1 + 2.5\phi)}$$

Consolidation is modelled in the advection term of the balance equation for suspended sediment (see Winterwerp and van Kesteren, 2004):

$$\frac{\partial \phi_s}{\partial t} - \frac{\partial}{\partial z} (\Xi \phi_s) - \frac{\partial}{\partial z} \left( (D_s + \Gamma_T + \Gamma_c) \frac{\partial \phi_s}{\partial z} \right) = 0$$

with  $\Xi$  being a settling flux due to hindered settling and consolidation, and  $\Gamma_c$  diffusion due to consolidation. See Winterwerp et al. (submitted) for more details.

The shear stress is modelled with a continuous Bingham model:

$$\tau_{i,z} = \frac{a_y \partial u_i / \partial z}{1 + a_y \sqrt{(\partial u_j / \partial z)^2}} \tau_B + \mu \frac{\partial u_i}{\partial z}$$

in which viscosity  $\mu$  and the yield stress  $\tau_B$  are related to the relative sediment concentration  $\phi_p$  using fractal theory:

$$\mu_s = K_\mu \phi_p^n$$

$$\tau_B = K_y \phi_p^{\frac{2}{3-n_f}}$$

### 6.3.2 Simple slope application

The Slib3D code is first tested with a sloping rectangular basin with a length of 100 m, a width of 10 m, and an initial depth of 2 m. The slope, sediment concentration and model settings are variable. The grid cell size in the horizontal direction is 1 m, and consists of 40 layers in the vertical direction. The model is not forced at the boundaries: all flow dynamics are generated by sediment-induced density currents.

### 6.3.3 Schematized harbour basin

The simplified harbour application is a 500 m wide and 1 km long dock attached to a 50 km long estuary of uniform width of 500 m (Figure 6.2 and Figure 6.3). The grid cell size increases from 50 m in the dock to 1 km at the landward end. The vertical grid consists of 40 sigma layers. The hydrodynamic grid is composed of logarithmically upward increasing grid cell size, while the sediment concentration is computed on a general sigma grid that fluctuates with the sediment concentration gradient (see the previous section). The bed level increases from 10 m on the seaward side to 2.7 m on the landward side (Figure 6.4). The bed level in the harbour dock is 12 m, with a 1:200 slope between the dock and the estuary.

A fluid mud layer is deposited on the estuary bed at the location coloured orange in Figure 6.3, with a thickness of 15 cm and of 1 m, and with a concentration of 10 g/l and 100 g/l.

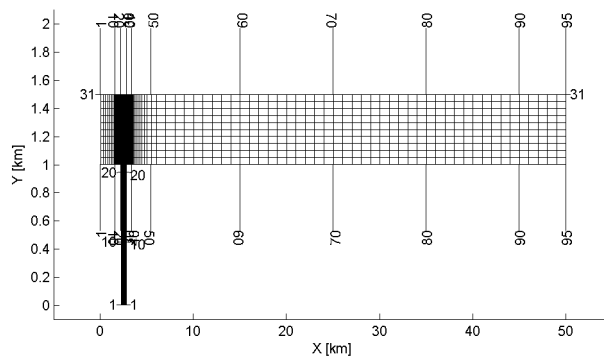


Figure 6.2 Grid layout of the simplified harbour application

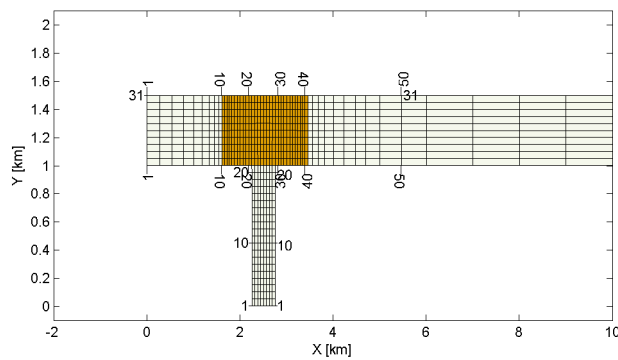


Figure 6.3 Detail of the simplified harbour application, with the location of the initial fluid mud patch coloured orange.

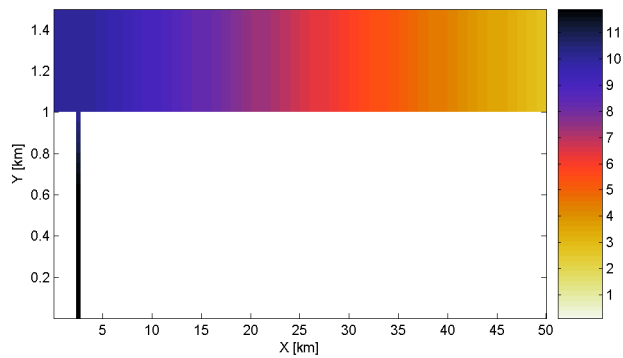


Figure 6.4 Bathymetry of the simplified harbour application

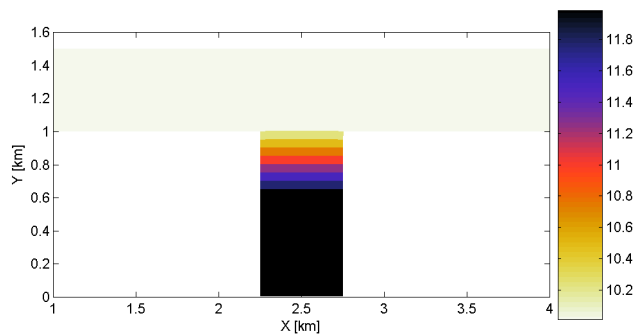


Figure 6.5 Detail of the bathymetry of the simplified harbour application

The model is driven with three types of boundary conditions. Case 1 is stationary: the water level is constant, and the discharge is zero (see Table 6.1). Flow dynamics are purely generated by sediment-induced density currents. Case 2 is a tropic forcing, consisting of an S2 amplitude of 1 m (waterlevel between -1 and +1 m, with a 12 hour period). A freshwater discharge of 500 m<sup>3</sup>/s is prescribed at the upstream boundary. Case 3 is case 2 including salinity. The upstream discharge is 0 ppt while the seaward boundary is 10 ppt. The water levels and salinity distribution is in equilibrium at the start of the simulation, but the currents are reset to 0 at T=0. The flow velocity is set to zero to prevent initial flow velocities into and out of the dock to dominate the initial sediment fluxes into the dock.

Table 6.1 Model forcing for case 1, 2, and 3.

Boundary condition	Case 1	Case 2	Case 3
Water level (downstream)	0	S2, A = 1 m	S2, A = 1 m
Discharge (upstream)	0	500 m <sup>3</sup> /s	500 m <sup>3</sup> /s
Salinity downstream	-	-	10
Salinity upstream	-	-	0

#### 6.3.4 Sediment settings

We start out with a basic setting given in Table 6.2 and Figure 6.6. These settings are based on actual physics, and optimised with experience gained with the model.

Table 6.2 Basic sediment parameter settings

General	Reference concentration	$c_{gel}$ [kg/m <sup>3</sup> ]	60
Flocculation	FlcNf	$n_f$ [-]	2.15
	FlcK2	$k_2$ [-]	1.
	FlcK3	$k_3$ [-]	1830
	FlcK4	$k_4$ [-]	0.00098
	FlcD0	$D_0$ [m]	1.e-03
	FlcD	$r$ [-]	0.44
Consolidation	FlcNf_cons	$n_f$ [-]	2.70
	cons_kk	$K_k$ [m/s]	1e-16
	cons_ksig	$K_p$ [Pa]	5e4
	cons_eta	$\eta$ [s/m]	1.0e5
Rheology	bin_cvisco	$K_\mu$ [Pa]	5000
	bin_cyield	$K_y$ [Pa.s]	5.0e8
	bin_cnvisco	$n$ [-]	4
	bin_abingh	$a_y$ [-]	1

The effect of the yield stress and viscosity is verified through a sensitivity analysis. A ten times higher/lower yield stress and viscosity (relative to the settings in Figure 6.6) is applied in the slope model.

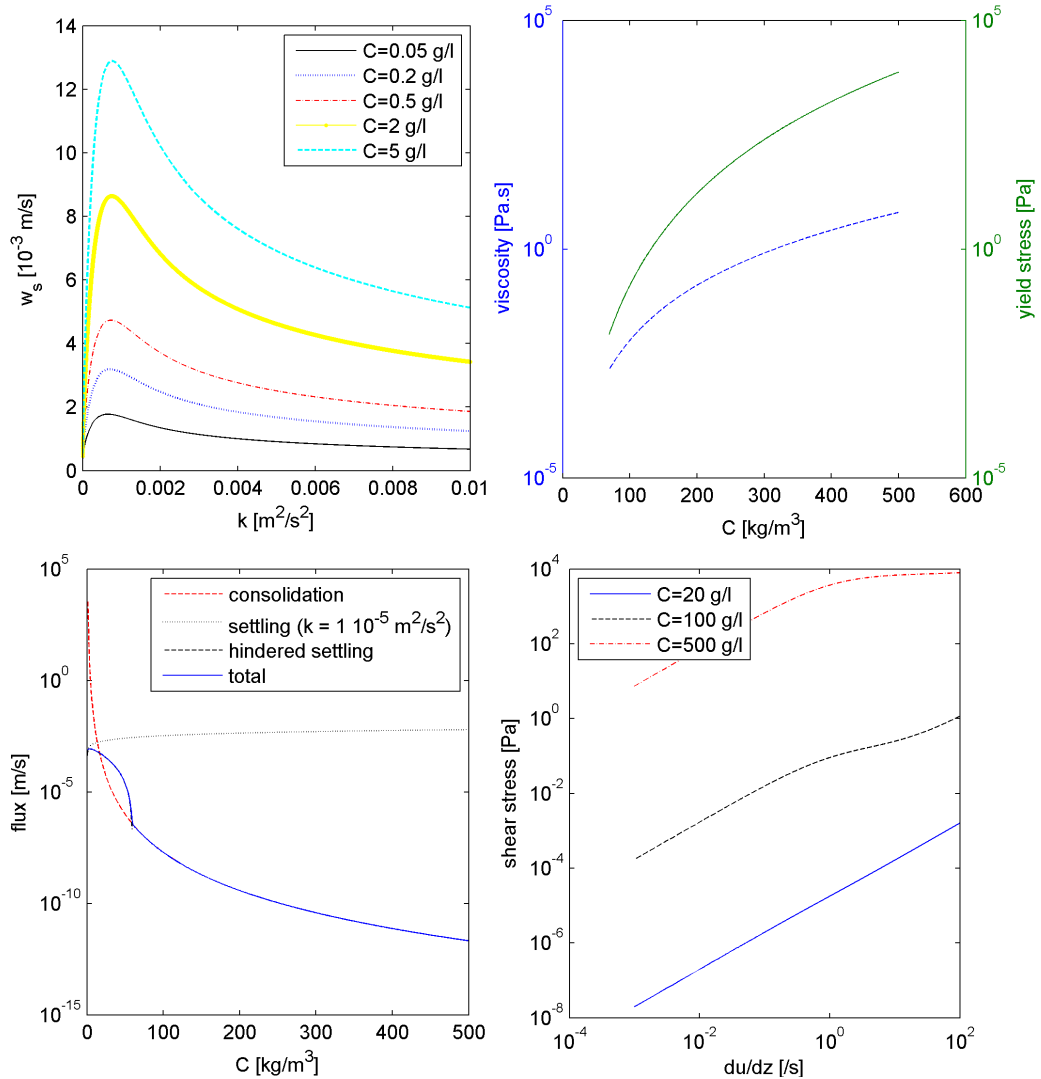


Figure 6.6 Reference sediment parameter settings. Top left: Relation between settling velocity  $w_s$ , turbulent kinetic energy  $k$ , and sediment concentration  $C$ , based on measurements and flocculation model settings of Winterwerp et al (2006). Top right: viscosity and yield strength as a function of sediment concentration  $C$ . Lower left: Settling function with and without hindered settling (using  $k = 1 \cdot 10^{-5} m^2/s^2$ ), by consolidation, and by (hindered) settling and consolidation combined. Lower right: shear stress as a function of sediment concentration  $C$  and velocity shear  $du/dz$ .

## 6.4 Simple slope model

### 6.4.1 Introduction

The aim of this work is to model fluid mud flows into harbour basins which takes place at relatively short timescales (hours - days). The timescales associated with consolidation are considerably longer (days to months), and therefore the focus here is on the rheology model settings, and not on the consolidation model settings. The settings applied in the consolidation module result in a relatively slow consolidation rate, so that the results are not substantially influenced by the consolidation model settings.

## 6.4.2 Results

Using the reference test case, using a sediment patch 12 cm thick on average (varying between 8 cm at 2 m water depth to 16 cm at 4 m water depth because of the sigma grid) with a concentration of 300 g/l, a downward sloping fluid mud layer develops with a flow velocity up to 0.3 m/s. Highest flow velocities occur above of the maximum sediment concentration peak (Figure 6.7). A thick sediment deposit forms downstream of the slope, slowing down the fluid mud layer.

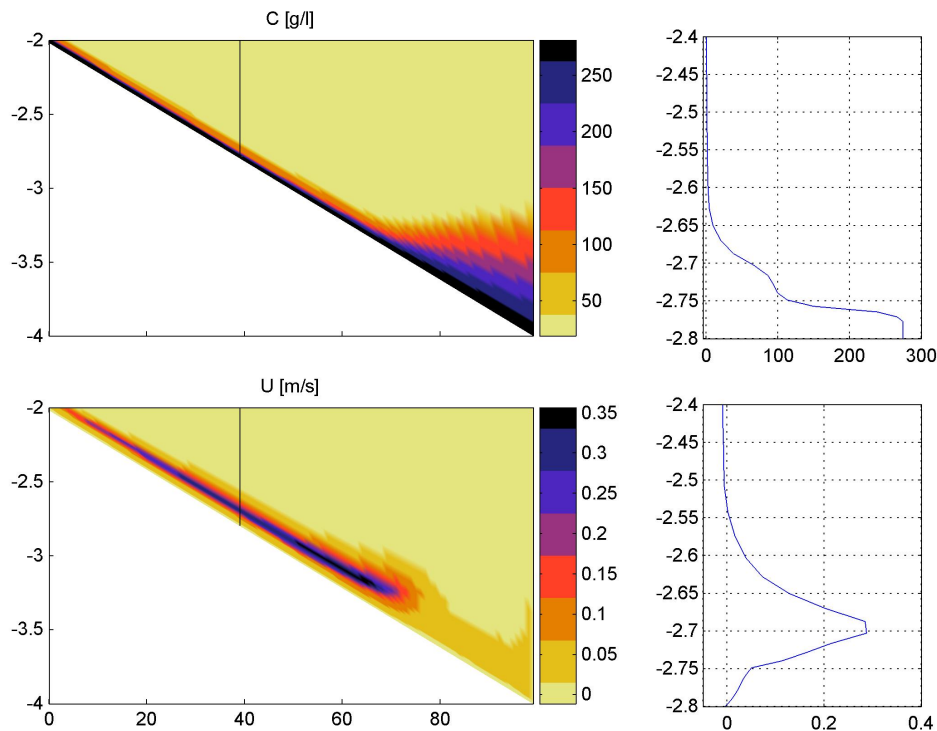


Figure 6.7 Sediment concentration (top,  $\text{kg/m}^3$ ) and flow velocity (bottom, m/s, positive flow velocity is directed downstream) after 10 minutes, using the reference parameter settings, an initial concentration of  $300 \text{ kg/m}^3$ , a mud layer thickness between 8 cm (left) to 16 cm (right), and a slope of 1:50. The location of the profiles on the right side are depicted with a black line on the contour image on the left.

The flow velocity in the fluid mud layer increases with sediment concentration (Figure 6.7 to Figure 6.9) from 0.15 ( $10 \text{ kg/m}^3$ ) to 0.25 m/s ( $50 \text{ kg/m}^3$ ) to 0.3 m/s ( $300 \text{ kg/m}^3$ ). This increase in flow velocity with the sediment concentration results from a balance between increasing horizontal pressure gradients (resulting from the larger sediment load) on the one hand, and the increased yield strength on the other hand. Large values for  $K_y$  or  $K_\mu$  increase the strength of the mud layers, and therefore this increase of flow velocity with sediment concentration depends on the settings for  $K_y$  or  $K_\mu$ . Using a ten times lower (Figure 6.10) or ten times higher (Figure 6.11) value for  $K_y$  results in slightly higher and lower flow velocities, respectively. The minor effect of the consolidation model settings on such short timescales is demonstrated by Figure 6.7 and Figure 6.12. The consolidation coefficient  $K_k$  is 3 orders of magnitude higher in Figure 6.12 (resulting in more rapid porewater expulsion and hence consolidation rates), but the flow velocity and sediment concentration are only marginally affected. A

decreasing bed level slope decreases the flow velocity in the fluid mud layer, in line with expectations (compare Figure 6.13 with Figure 6.7): a doubling of the slope results in an increase in flow velocity of close to 50% (0.17 m/s against 0.25 m/s).

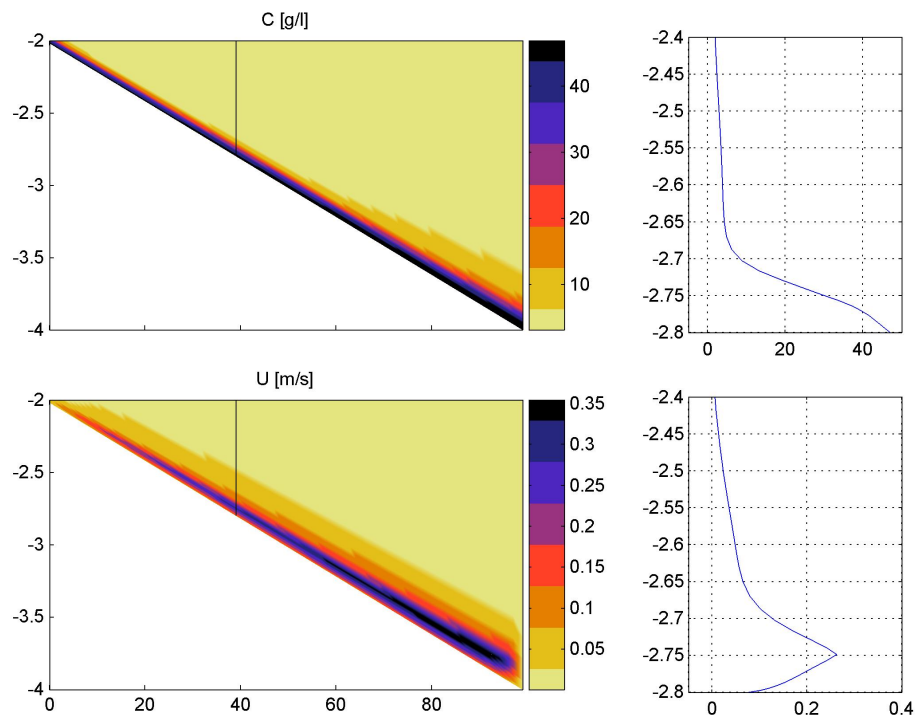


Figure 6.8 As in Figure 6.7 but with an initial sediment concentration of 50 g/l

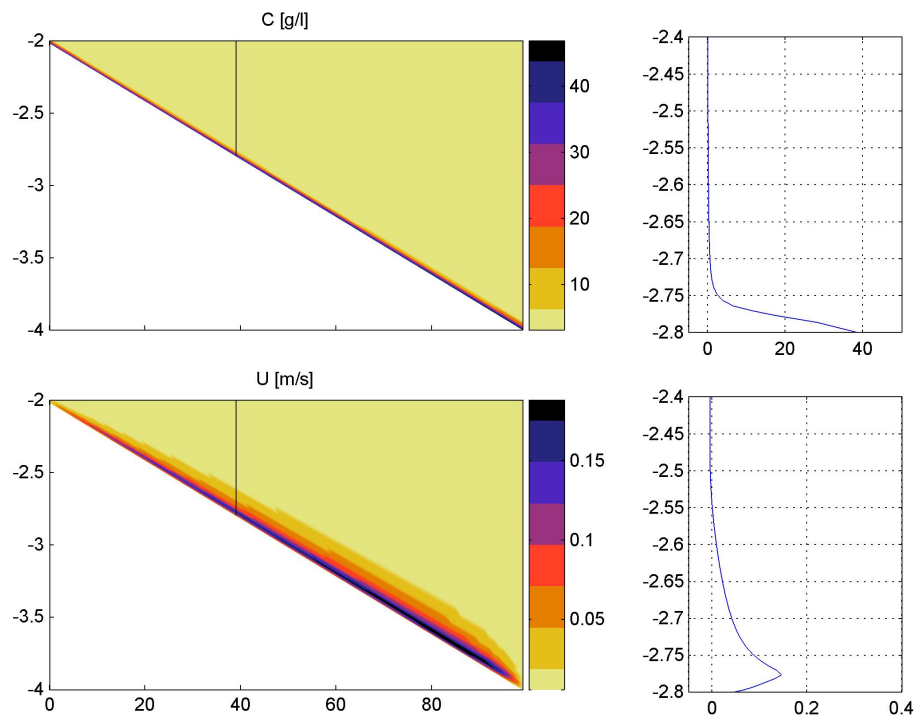


Figure 6.9 As in Figure 6.7 but with an initial sediment concentration of 10 g/l

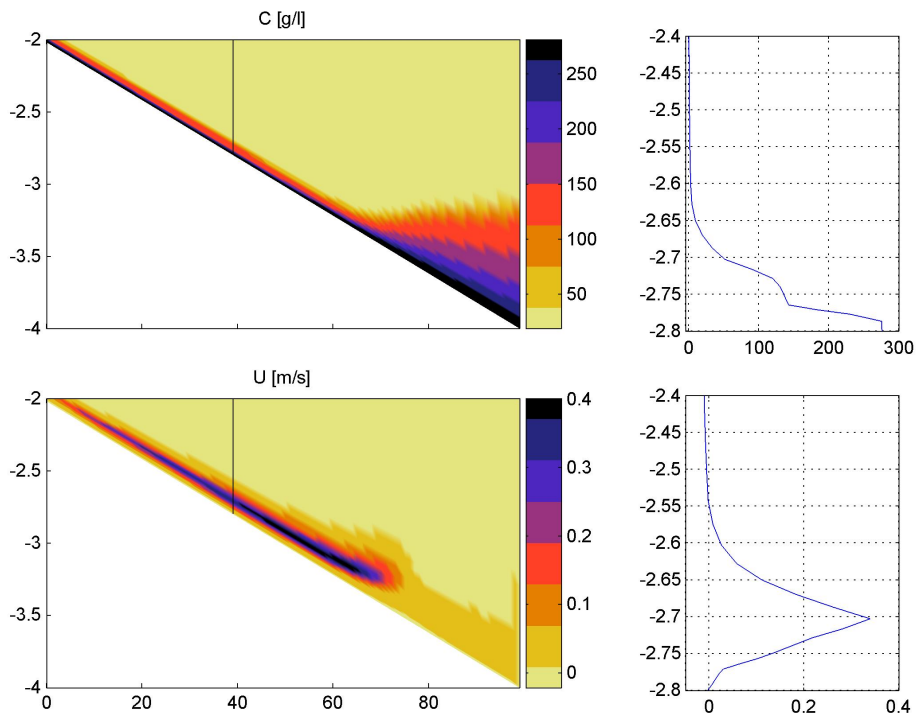


Figure 6.10 As in Figure 6.7 but with  $K_y = 5 \cdot 10^7$  instead of  $5 \cdot 10^8$

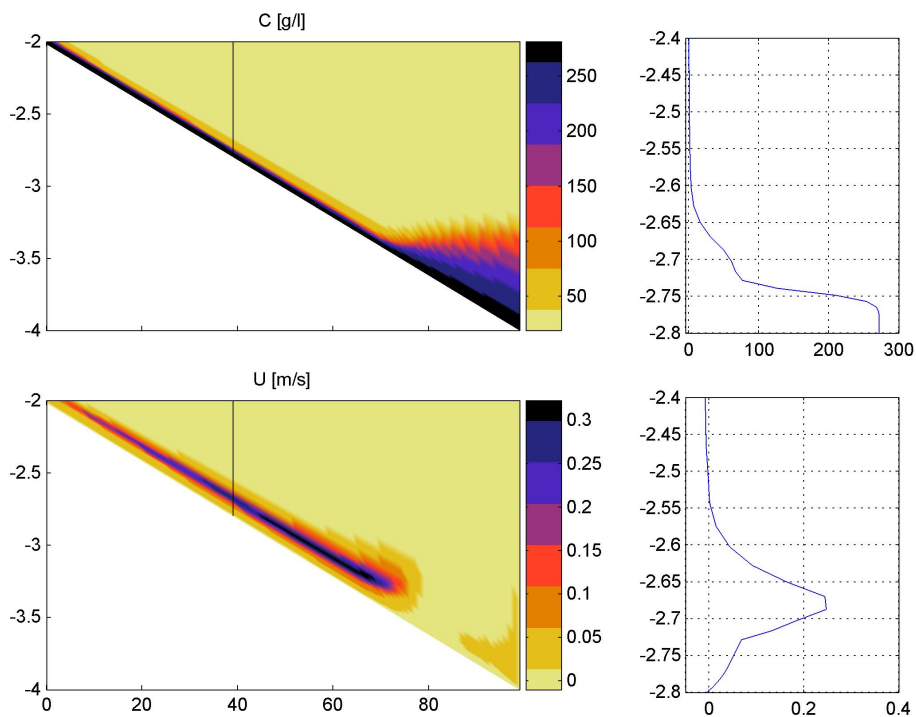


Figure 6.11 As in Figure 6.7 but with  $K_y = 5 \cdot 10^9$  instead of  $5 \cdot 10^8$

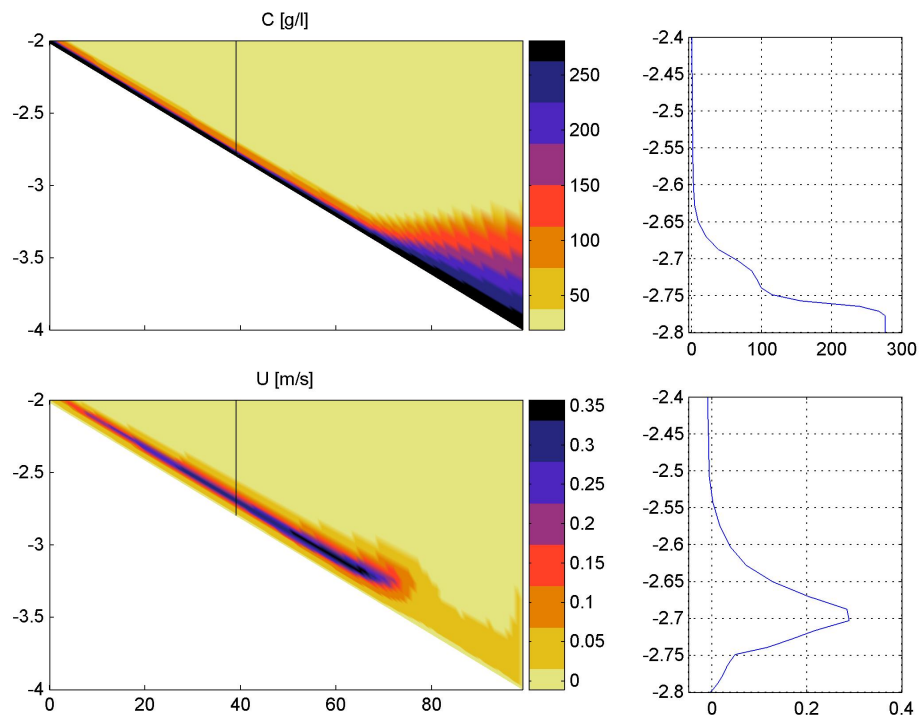


Figure 6.12 As in Figure 6.7 but with more rapid consolidation ( $K_k = 1 \cdot 10^{13}$  instead of  $1 \cdot 10^{16}$ )

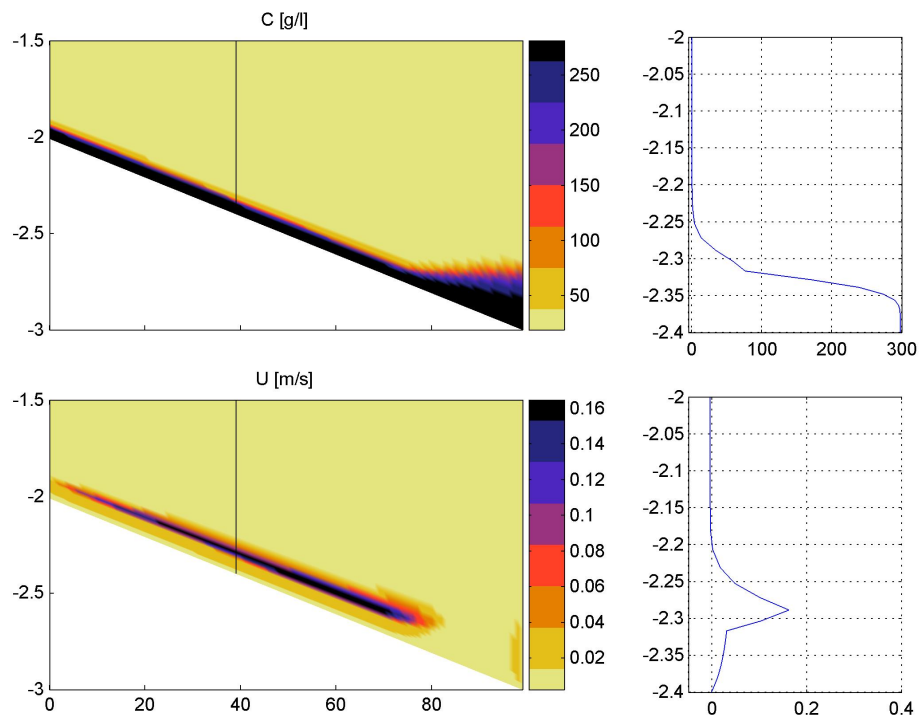


Figure 6.13 As in Figure 6.7 but with a slope of 1:100

### 6.4.3 Discussion

In order to evaluate the accuracy of the model results, they need to be compared with field experiments. This poses a problem because fluid mud flow measurements are only done in confined laboratory flumes, which are difficult to compare with the model because of scale effects. Very few, or possibly no, measurements exist of fluid mud flows in actual field conditions. Some indirect observations exist of turbidity currents, but these generally act on a larger scale than fluid mud flows. Therefore we compare the model results in a semi-qualitative sense with observations. Some typical profiles of sediment gravity flows have been compiled by Amy et al. (2005): see Figure 6.14.

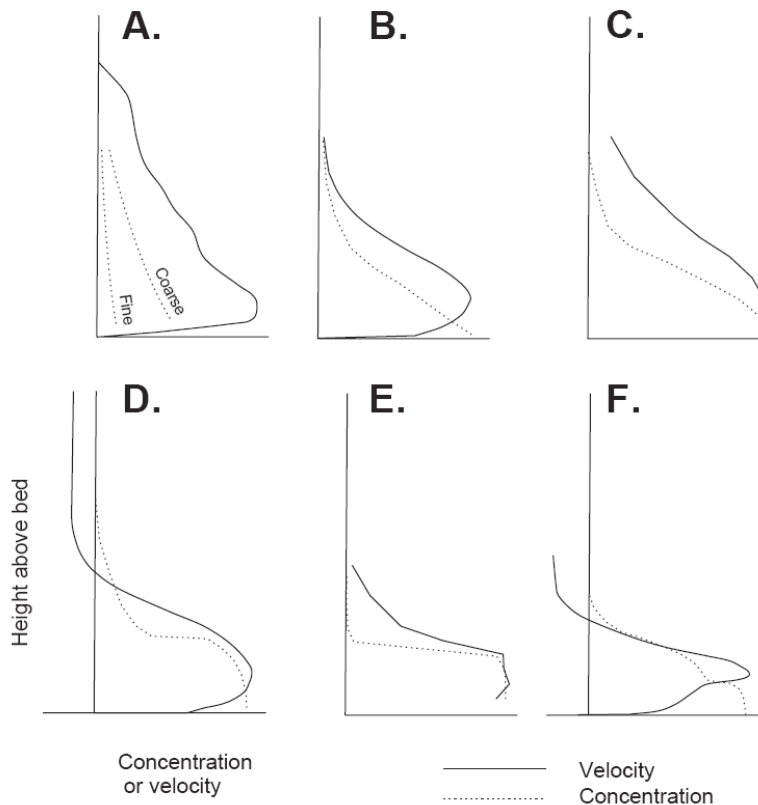


Figure 6.14 Measured concentration and velocity profiles of laboratory sediment gravity flows, from Amy et al. (2005). (A) Continuous concentration profile; strongly depositional subcritical turbidity current (Garcia, 1994). (B) Nearly continuous concentration profile (Altinakar et al., 1996). (C) Nearly continuous concentration profile; low-concentration fluid mudflow (van Kessel and Kranenburg, 1996). (D) Two-layer model with a stepped concentration profile above the velocity maximum (Middleton, 1966, 1993). (E) Stepped concentration and velocity profile; high-concentration fluid mudflow (van Kessel and Kranenburg, 1996). (F) Multi-stepped concentration profile of a high-concentration turbidity current Postma et al., 1988).

The modeled low-concentration gravity flows reasonably resemble Amy's type B and C gravity flows, while the modeled high-concentration gravity flows show good agreement with the multi-stepped profile (type F). An important difference between the modeled high-concentration gravity flows and observed gravity flows is that the observed type D and E are not reproduced by the model. The concentration profiles result from low mixing rates between the fluid mud and overlying water while the flow velocity profile is dominated by plug flow, typical for Bingham flow behaviour (van Kessel and Kranenburg, 1996). Possibly, this difference may be caused by the above-mentioned scale effects: the flow in flumes becomes laminar at lower sediment concentrations than in field conditions. Therefore it is concluded that the reference model settings (resulting

in the profiles shown in Figure 6.7 to Figure 6.9) sufficiently reproduce the flow in a fluid mud layer. These settings will therefore be applied in a slightly more realistic harbour setting.

## 6.5 Schematized harbour basin

### 6.5.1 Scenarios

The model is forced with three types of hydrodynamic scenarios: sediment-induced density currents, sediment-induced density currents and tidal currents, and tidal currents in combination with salinity- and sediment-induced density currents. Each of these scenarios are run for a thick mud patch (1 m thick), a thin mud patch (15 cm thick), at a low concentration ( $10 \text{ kg/m}^3$ ) and a high concentration ( $150 \text{ kg/m}^3$ ), using the reference sediment parameter settings, resulting in 12 simulations. The influx of sediment into the dock is evaluated at a transect halfway the slope between the dock and the estuary.

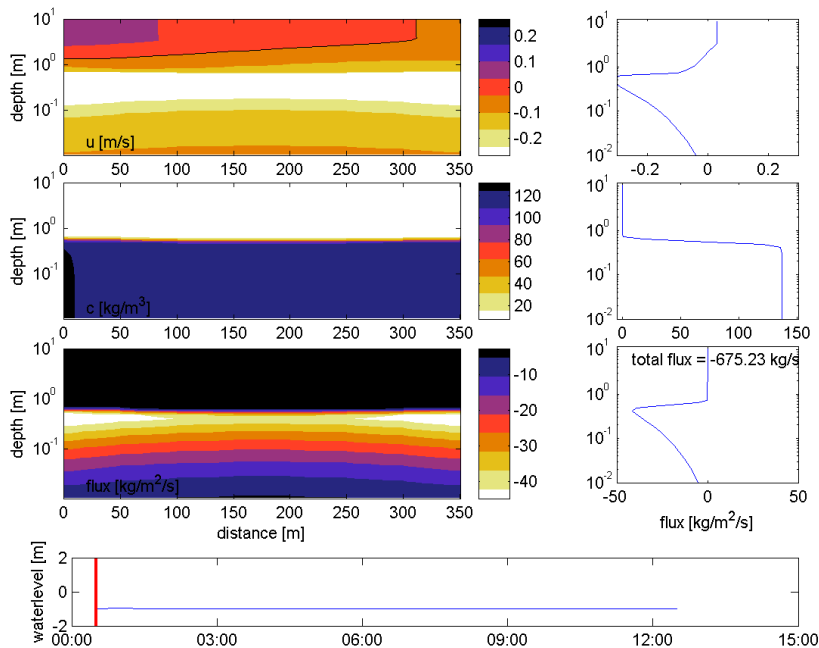


Figure 6.15 Flow velocity (top), sediment concentration (second panel from above), and sediment flux (third panel from above) after one hour simulation time, using the reference sediment parameter setting, 1 m of sediment at a concentration of  $150 \text{ kg/m}^3$ , and forced by sediment-induced density currents only. The lower panel is the water level in the first 13 hours (constant because there is no tidal forcing). The left panels are contours over the dock entrance, while the right-hand panels are averaged over the width of the dock. Note the logarithmic vertical scale.

We start our analysis of fluid mud flows with a 1 m thick, high-concentration layer without tidal forcing or salinity-induced currents. Within an hour, the sediment patch flows into the dock at a velocity up to 0.3 m/s and a sediment concentration close to  $150 \text{ kg/m}^3$  (Figure 6.15). The flow velocity rapidly decreases, and inflow ceases after two days (Figure 6.16).

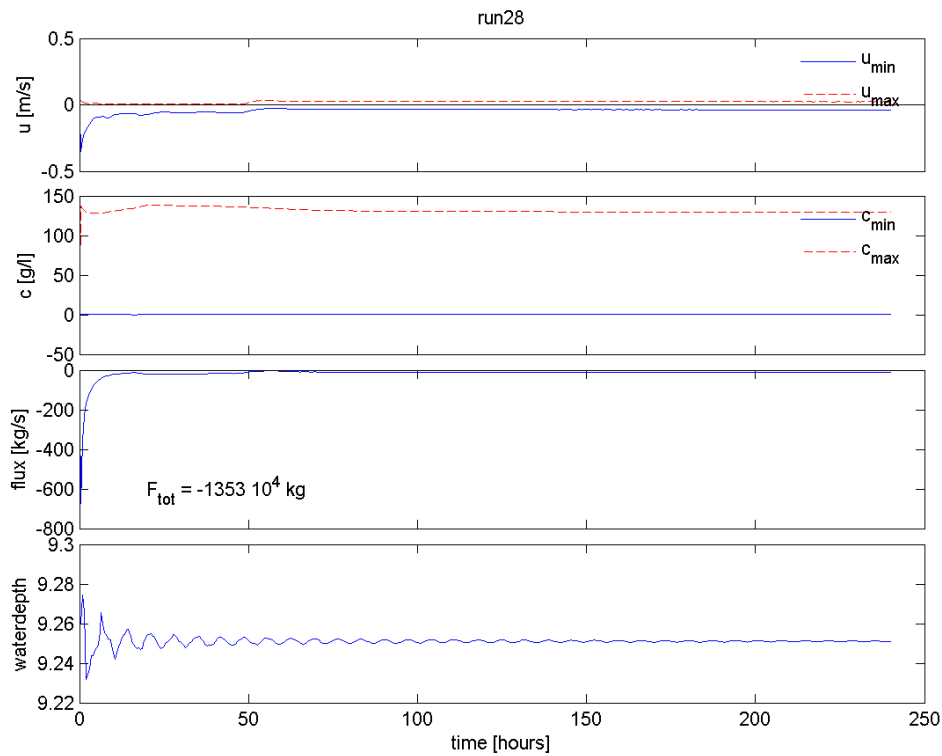


Figure 6.16 Flow velocity  $u$ , sediment concentration  $c$ , sediment flux  $F$  (all averaged over the dock width), and water level, for reference sediment parameter settings, one meter sediment of 150 g/l, and only forced by sediment-induced density currents (same simulation as Figure 6.15).

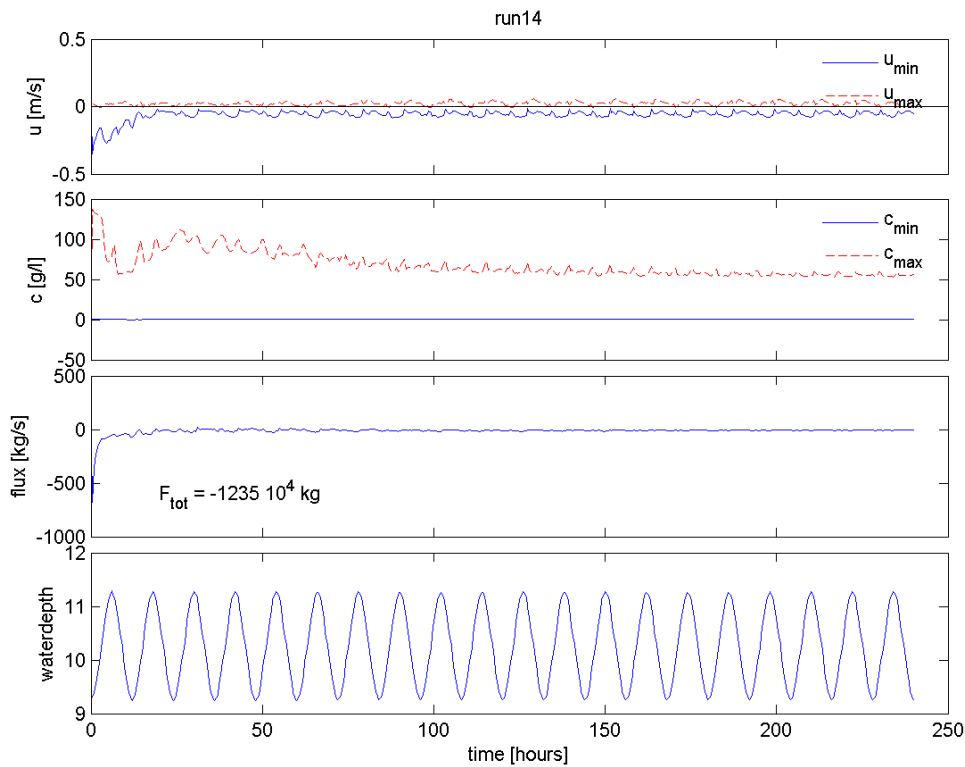


Figure 6.17 Flow velocity  $u$ , sediment concentration  $c$ , sediment flux  $F$  (all averaged over the dock width), and water level, for reference sediment parameter settings, one meter sediment of 150 g/l, forced by sediment-induced density currents and tides.

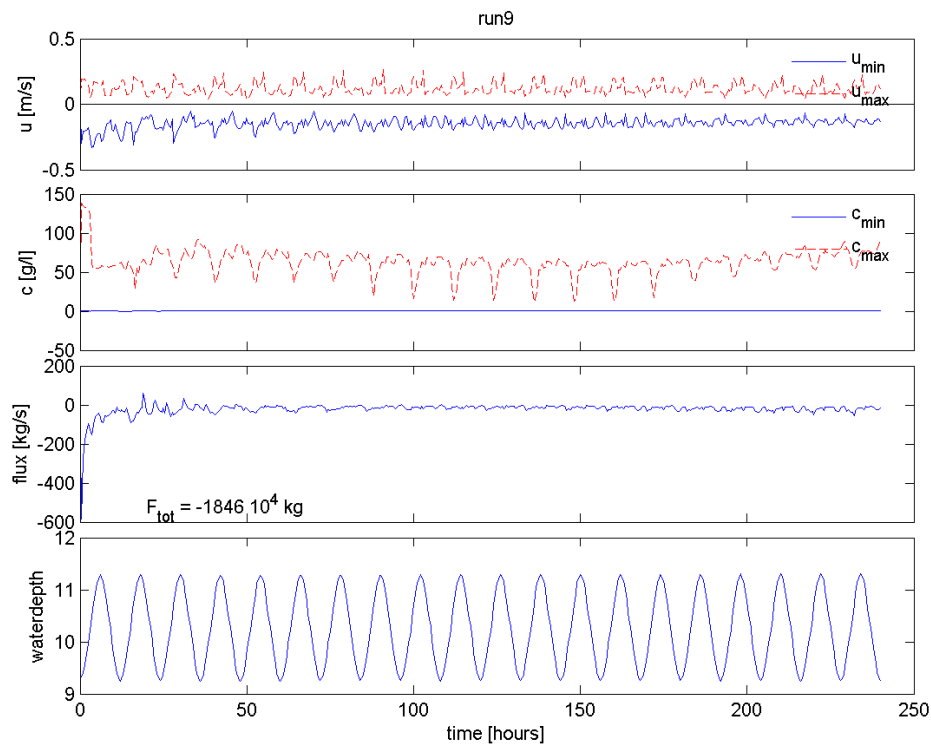


Figure 6.18 Flow velocity  $u$ , sediment concentration  $c$ , sediment flux  $F$  (all averaged over the dock width), and water level, for reference sediment parameter settings, one meter sediment of 150 g/l, forced by sediment-induced and salinity-induced density currents, and tides.

This pattern is more or less the same for the different hydrodynamic forcing (Figure 6.17 and Figure 6.18): most sediment enters the dock in the first day. The relative importance of salinity-induced currents and tidal currents increases with a decreasing amount of sediment in the initial sediment patch. This is illustrated with the sediment influx with resulting from sediment-induced forcing (Figure 6.19) and tide, salinity, and sediment forcing (Figure 6.20) in combination with a 15 cm thick, low-concentration (10 g/l) sediment patch. In the first, the main sediment influx is in the first 2 days, whereas sediment fluxes in the second reach a quasi steady state. After 10 days, the sediment flux is nearly equal to the initial sediment influx. This suggest that in this case, fluid mud flows do not substantially contribute to the sediment exchange. This is further supported by a snapshot of sediment exchange through the dock entrance during a period of sediment influx. The flow velocity is primarily forced by salinity (compare the flow velocity profile (top right) at low concentration and small thickness (Figure 6.21) with a thick high-concentration layer (Figure 6.15 for sediment-induced currents only, and Figure 6.22 for simulations with salinity and tide-induced currents as well).

The low-concentration, thick layer of sediment contains nearly the same amount of sediment as a high-concentration, thin layer of sediment (differing a factor 2). Comparing the sediment flux and flow velocity profiles of both these settings (Figure 6.23 and Figure 6.24), it seems that a thin layer with a high sediment concentration influences the flow dynamics, and thereby the sediment fluxes, more profoundly than a thick, low-concentration layer.

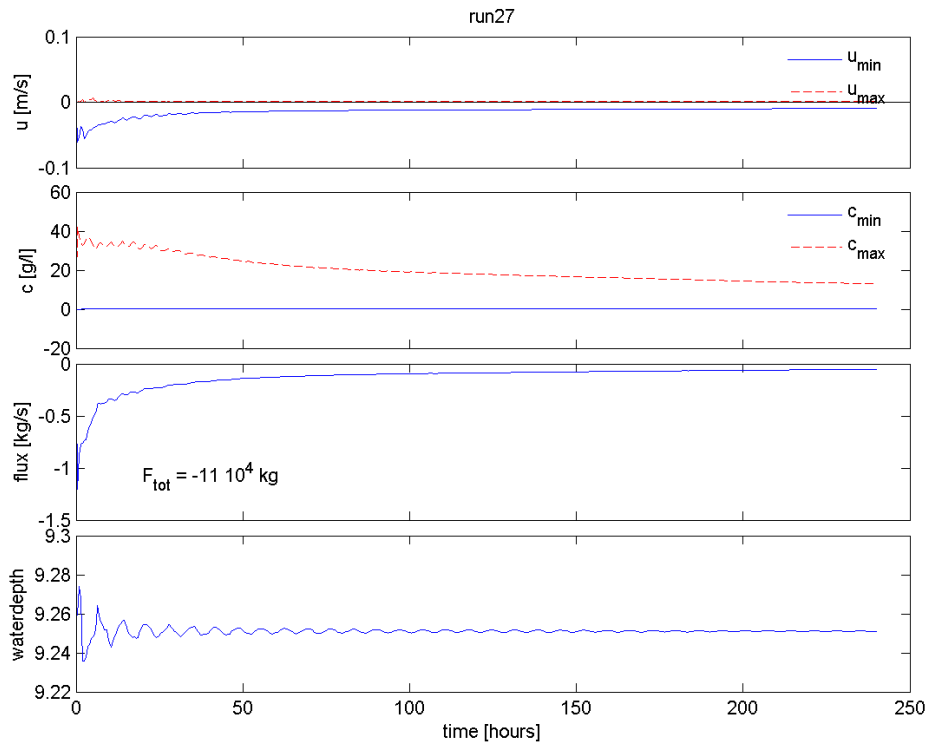


Figure 6.19 Flow velocity  $u$ , sediment concentration  $c$ , sediment flux  $F$  (all averaged over the dock width), and water level, for reference sediment parameter settings, 15 cm sediment of 10 g/l, and only forced by sediment-induced density currents

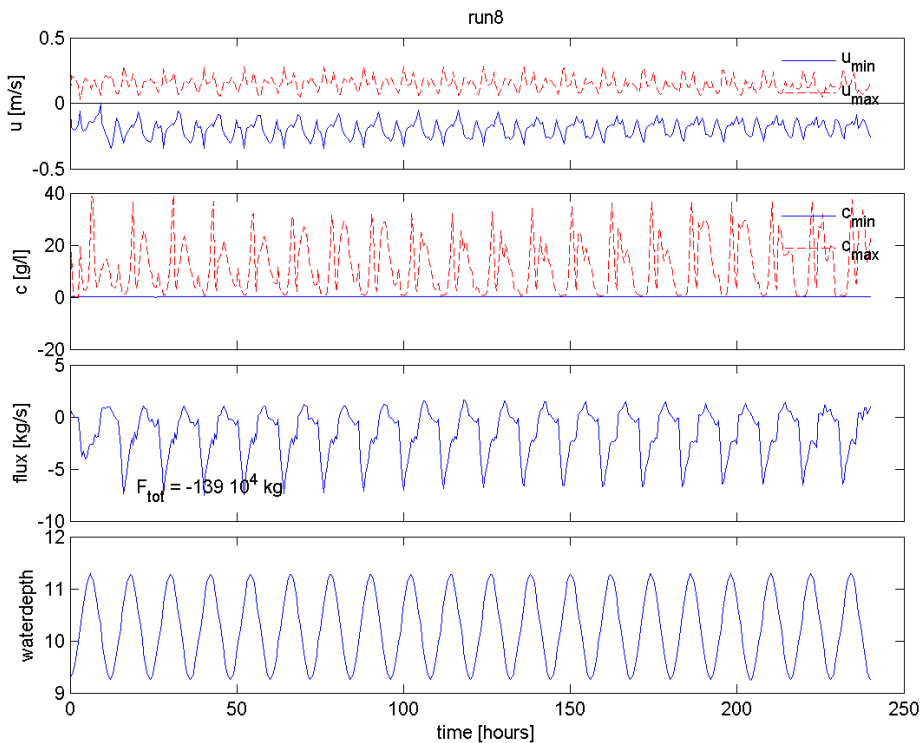


Figure 6.20 Flow velocity  $u$ , sediment concentration  $c$ , sediment flux  $F$  (all averaged over the dock width), and water level, for reference sediment parameter settings, 15 cm of sediment of 10 g/l, forced by sediment-induced and salinity-induced density currents, and tides.

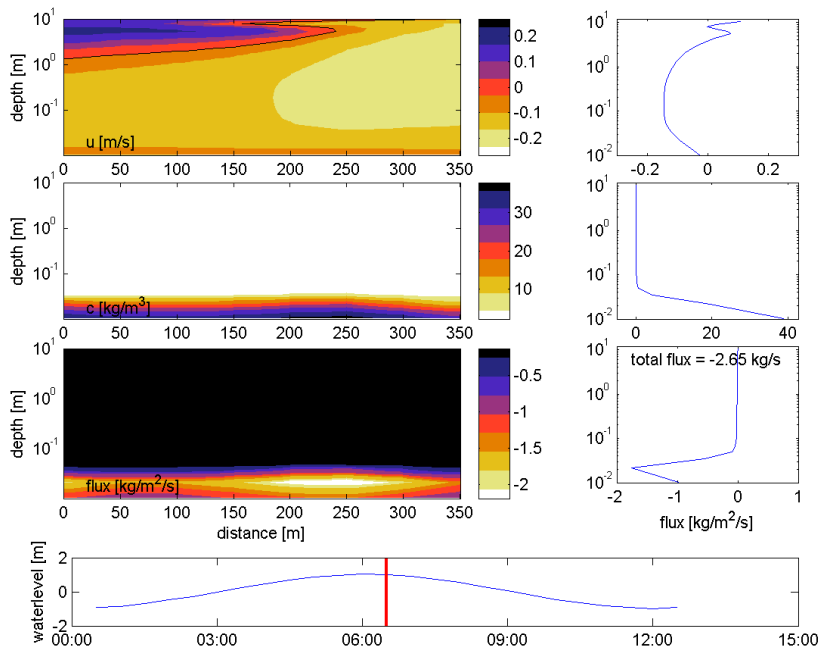


Figure 6.21 Flow velocity (top), sediment concentration (second panel from above), and sediment flux (third panel from above) after one hour simulation time, using the reference sediment parameter setting, 15 cm of sediment at a concentration of  $10 \text{ kg/m}^3$ , and forced by salinity and sediment-induced density currents and tides. The lower panel is the water level in the first 13 hours. The left panels are contours over the dock entrance, while the right-hand panels are averaged over the width of the dock. Note the logarithmic vertical scale.

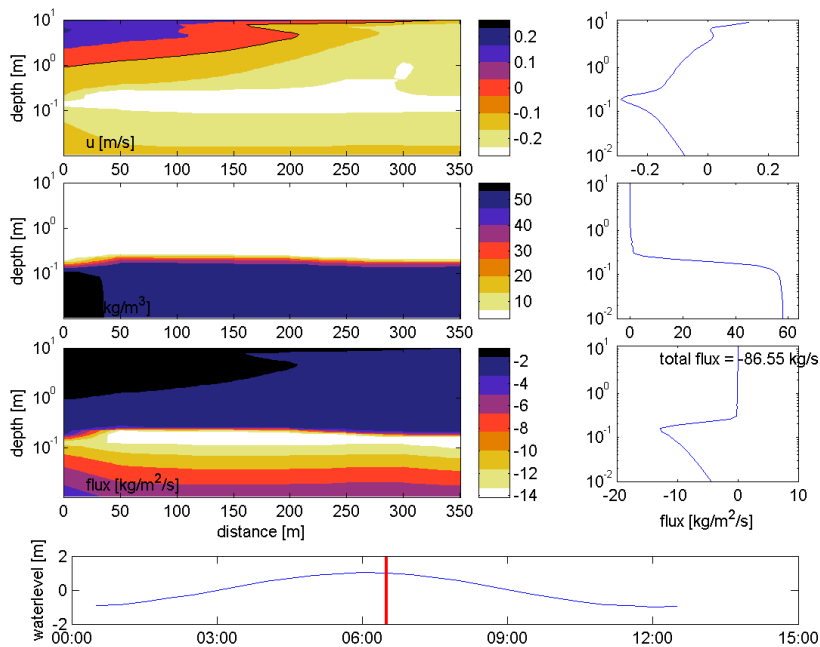


Figure 6.22 As Figure 6.21 but with 1 m of sediment at a concentration of  $150 \text{ kg/m}^3$ .

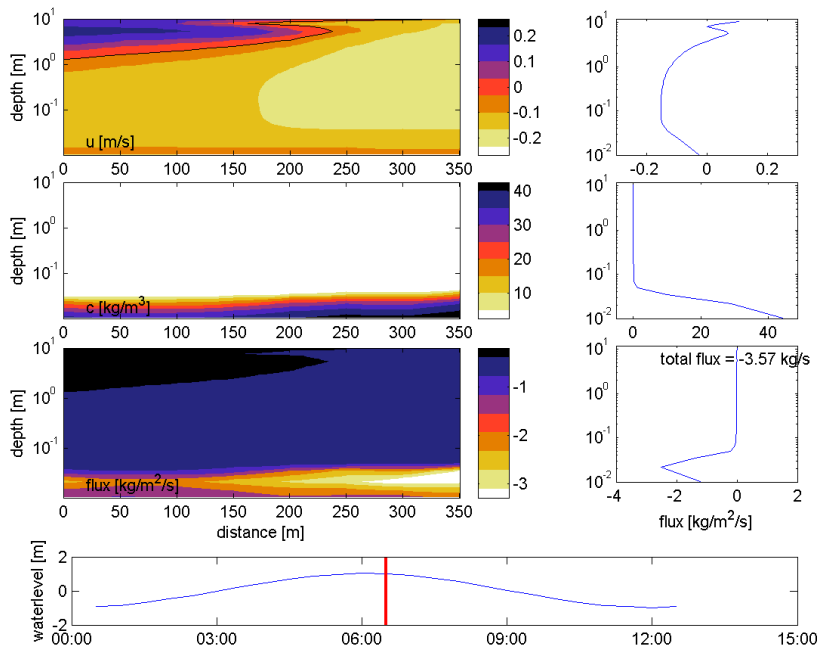


Figure 6.23 As Figure 6.21 but with 1 m of sediment at a concentration of 10 kg/m<sup>3</sup>.

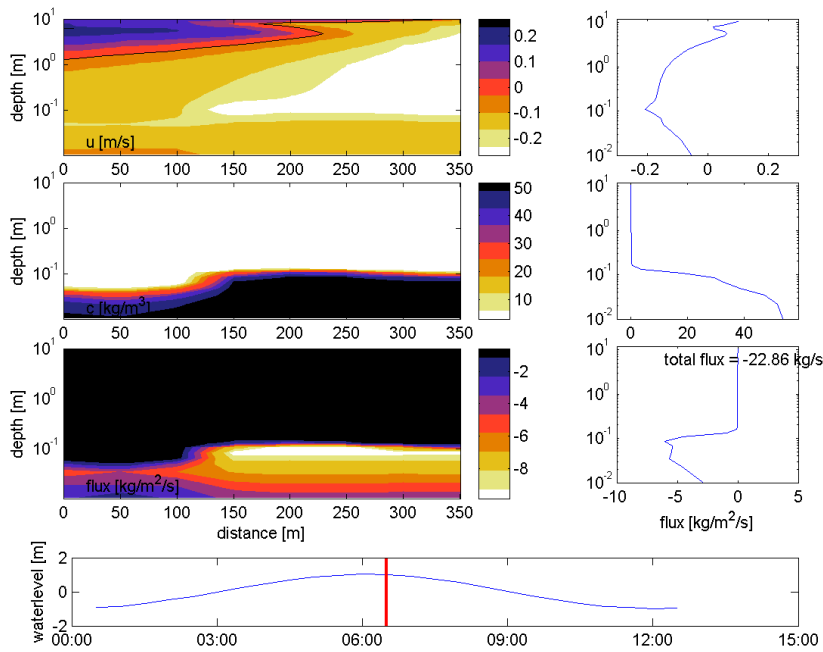


Figure 6.24 As Figure 6.21 but with 15 cm of sediment at a concentration of 150 kg/m<sup>3</sup>.

## 6.5.2 Budgets

In order to evaluate the effectiveness of the different hydrodynamic forcing on the transport of sediment into the dock, we compute how much of the initially available amount of sediment is transported into the dock. The relative contribution of tides and salinity-induced density currents is highest for a thin, low-concentration sediment layer. In that case, nearly all available sediment is transported into the dock (see Table 6.3 and Table 6.4). Probably, all sediment will also be eventually resuspended and transported into the dock for all other case 3 simulations, but the timescales considered here are too short to verify that. At the timescales simulated here, the transport of a thick, high-concentration layer is dominated by sediment-induced density currents: 9% of all the sediment flows into the dock when only sediment-induced currents are modelled while only an additional 3.2% flows into the dock when tides and salinity-induced density-driven flow are additionally modelled. The thin high-concentration layer and the thick low-concentration layer show behaviour in-between the extremes.

Table 6.3 Absolute sediment fluxes for the 12 scenarios

C (g/l)	H (m)	S (10 <sup>6</sup> kg)	Sediment flux in 10 <sup>4</sup> kg		
			case 1	case 2	case 3
10	1	1.5	54	113	149
10	0.15	10	11	80	139
150	1	22.5	1353	1235	1846
150	0.15	150	137	149	188

Table 6.4 Relative sediment fluxes for the 12 scenarios

C (g/l)	H (m)	S (10 <sup>6</sup> kg)	Sediment flux in % of total		
			case 1	case 2	case 3
10	1	10	5.4	11.3	14.9
10	0.15	1.5	7.3	53.3	92.7
150	1	150	9.0	8.2	12.3
150	0.15	22.5	6.1	6.6	8.4

## 6.6 Discussion

### 6.6.1 Transport mechanisms

The model results indicate that the fluid mud layer only substantially contributes to fluid mud transport in case of a thick, highly concentrated layer. A thin, low-concentrated layer is mainly transported by the ambient flow without an appreciable flow velocity gradient, and is therefore not considered a dynamic fluid mud layer. The thin, highly concentrated layer and the thick, low-concentrated layer have flow dynamics in-between these two extremes. The question then is to what extent the fluid mud layer is forced by gravity, by pressure gradients, or by interfacial shear. Shear stress generated by gravity amounts to  $\tau_g = \Delta\rho gh \sin\alpha$ , a horizontal pressure gradient  $dp/dx$  generates a shear stress  $\tau_p = h (dp/dx)$ , while the interfacial shear  $\tau_i$  generated by the velocity difference between the two layers is equal to  $\tau_i = f_i \rho (u_1 - u_2)^2$ .

Of these,  $\tau_i$  is independent of the initial layer thickness and only moderately dependant on the velocity gradient. For scenario 1 (only sediment-induced forcing),  $u_1-u_2$  is equal to 0. With tide-induced forcing, the maximum difference is 0.05 (difference between the lower layer and the bed while it peaks at 0.2 m/s including salinity-induced currents. The density  $\rho$  is taken a  $1000 \text{ kg/m}^3$ , and the friction factor  $f_i$  is estimated at 0.05 (typical value for the Darcy-Weissbach friction factor). This results in values of 0.5 Pa for scenario 2 and 2 Pa for scenario 3. Strictly, this value is 10% higher for highly concentrated flow in which the density is  $1100 \text{ kg/m}^3$ , but given the uncertainties in the friction factor estimate this difference is not accounted for here. The shear stresses generated by gravity and the horizontal pressure gradients do depend substantially on the thickness and the concentration of the fluid mud layer.

A sediment concentration of 10 g/l results in an excess density  $\Delta\rho$  of  $6.2 \text{ kg/m}^3$ , and 150 g/l in  $93.4 \text{ kg/m}^3$ . With a slope of 1:200, such as in the harbour simulation, the shear stresses generated by gravity vary from 0.05 to 4.6 Pa (Table 6.5). Hence, interfacial shear is expected to dominate transport in case of a thin layer and a thick, low-concentrated layer in case of salinity-driven density currents. With tidal currents only, the effect of interfacial shear and gravity currents is nearly equal. However, this is only partly in agreement with the modelled sediment fluxes. The tidal and salinity-induced density currents only marginally contribute to the transport of a highly concentrated fluid mud layer (thick as well as thin, see Table 6.4). It therefore seems that the interfacial shear stress is overestimated using  $f_i = 0.05$ . On the other hand, it may also be a model shortcoming. Unfortunately, this is difficult to asses due to the limited availability of field data on this subject.

Table 6.5 Shear stress generated by gravity (using a  $\alpha=1/200$ ) and horizontal pressure gradients (using  $x=400 \text{ m}$ )

Shear stress (Pa)	10 g/l		150 g/l	
	15 cm	100 cm	15 cm	100 cm
$\tau_g = \Delta\rho gh \sin\alpha$	0.05	0.3	0.7	4.6
$\tau_p = h (dp/dx)$	0.002	0.03	0.08	1.1

The value of the horizontal pressure gradients depends on the distance over which it is evaluated. In the harbour dock simulations, we start out with a patch of sediment of a certain thickness and concentration. The average excess pressure in this patch equals  $\Delta\rho gh/2$ . Initially, the shear stress generated by horizontal pressure gradients between this patch and immediately next to this patch approaches infinity as  $dx$  approaches zero. Therefore, the flow dynamics in the fluid mud layer are at first dominated by the horizontal pressure gradients. However, in order to compare the shear stress generated by the horizontal pressure gradients and by gravity, we assume  $dx$  to be 400 m (length of the slope between the estuary and the dock), and the  $dP$  to be the maximum initial pressure difference. This results in shear stresses varying between 0.002 and 1.1 Pa. Overall, they are nearly an order of magnitude lower than gravity-driven shear stresses. Therefore it can be concluded that although initially, the flow dynamics in the fluid mud layer are dominated by pressure gradients, this it becomes rapidly dominated by gravity. In the model results, this is probably exemplified by the transition from  $u > 0.3 \text{ m/s}$  to  $u \approx 0.1 \text{ m/s}$  after several hours (see, for example, Figure 6.16).

### 6.6.2 Implications for harbour siltation

The relative importance of fluid mud flows to harbour siltation has so far been very poorly quantified with field observations. It is therefore not possible to quantitatively validate the model applied here. However, the model results seem reasonable in a qualitative sense. Assuming that the model reproduces the actual physics sufficiently, we can extrapolate these results to real-world cases.

Fluid mud layers can be formed when siltation rates of fine sediment exceeds the consolidation rate of the bed. This generally happens during slack tide in turbid estuaries. The fluid mud layers formed in this way will be relatively thin, with concentrations of several tens of g/l. From the model results presented here, it seems that these layers will not propagate into harbour dock through flow dynamics decoupled from the ambient flow. The high concentrations do, of course, contribute to harbour siltation, through advection by the ambient currents.

Alternatively, fluid mud layers may be formed in a turbidity maximum with very high sediment concentrations, which are only occasionally stirred up (by e.g. spring tidal currents, or passing ships). This generates a very thick, relatively low-concentrated fluid mud layer (such as the Ems in Germany, or the Loire in France). These may substantially contribute to harbour siltation.

Highly-concentrated fluid mud layers primarily exist in consolidating harbour basins which are at rest, through liquefaction by waves, or through water injection dredging. Since consolidating fluid muds in harbour basins are not expected to generate migrating density currents, only wave-generated resuspension and water injection dredging will probably result in highly concentrated, migrating fluid mud layers.

## 6.7 Conclusions

We have developed a fine sediment transport models that simulates the consolidation and transport of fluid muds using a flocculation, consolidation, and rheology module. The flocculation module has already been extensively tested (see e.g. Winterwerp et al, 2006), but the consolidation and rheology module had not. The interest in this study was on harbour siltation processes on relatively short timescales, and therefore we have focussed on the rheology module. The model reasonably reproduces sediment-induced density currents on a slope and in a simplified harbour basin geometry. The transport of the highly concentrated fluid mud layer is initially generated by horizontal pressure gradients, in a later stage by gravity flow. At high concentrations the transport of the fluid mud layer is generated by gravity flows (although initially also by horizontal pressure gradients). As a result, salinity-induced density currents and tidal exchange flows do only partly contribute to the overall sediment influx. At low concentrations, sediment is mainly transported into the dock through advection by ambient currents (especially salinity-induced density driven currents). Interfacial shear seemed to be of lesser importance, but this may also be a model deficiency.



## 7 References

- Altinakar, M.S., Graf, W.H., Hopfinger, E.J. (1996). Flow structure in turbidity currents. *Journal of Hydraulic Research* 34, 713–718.
- Alves, J.H. and M.L. Banner (2003). Performance of a saturation-based dissipation-rate source term in modelling the fetch-limited evolution of wind waves. *J. Phys. Oceanogr.*, **33**: 1274-1298.
- Amy, L. A., J. Peakall and P.J. Talling (2005). Density- and viscosity stratified gravity currents: Insight from laboratory experiments and implications for submarine flow deposits, *Sedimentary Geology* 179, pp. 5–29.
- Battjes, J.A. and J.P.F.M. Janssen (1978). Energy loss and set-up due to breaking of random waves, *Proc. 16<sup>th</sup> Int. Conf. Coastal Engineering*, ASCE, 569-587.
- Bruens, A., T. van Kessel, J. de Kok, P. de Grave (2007). Resultaten Voortschrijdend Onderzoeksprogramma Slib 2007. Delft Hydraulics report Z4374, 79 p.
- Caires, S., J. Groeneweg, and A. Sterl (2006). Changes in North Sea extreme waves, *Proc. of the 9th int. workshop on wave hindcasting and forecasting*, JCOMM Tech. Rep. No. 34 / WMO-TD. No. 1368.
- Caires, S., J. Groeneweg, and A. Sterl (2008). Path and futures changes in the North Sea extreme waves, *Proc. 31<sup>th</sup> Int. Conf. Coastal Engineering*, ASCE.
- Cavaleri, L. and P. Malanotte-Rizzoli (1981). Wind wave prediction in shallow water: Theory and applications. *J. Geophys. Res.*, **86**, No. C11, 10,961-10,973
- Collins, J.I. (1972). Prediction of shallow water spectra, *J. Geophys. Res.*, **77**, no. 15, 2693-2707.
- Creutzberg, F., and H. Postma (1979). An experimental approach to the distribution of mud in the southern North Sea.--Neth. J. Sea Res. 13 (1): 99-116.
- De Nijs, M.A.J., J. C. Winterwerp, and J. D. Pietrzak., On harbour siltation in the fresh-salt water mixing region. *Continental Shelf Research* (2008), doi:10.1016/j.csr.2008.01.019.
- De Wit, P. J. (1995). Liquefaction of cohesive sediments caused by waves. PhD thesis, Delft University, 197 p.
- Dellapenna, T. M., S. A. Kuehl and L. C. Schaffner (1998). Sea-bed Mixing and Particle Residence Times in Biologically and Physically Dominated Estuarine Systems: a Comparison of Lower Chesapeake Bay and the York River Subestuary. *Estuarine, Coastal and Shelf Science* 46, 777–795
- Dellapenna, T. M., S. A. Kuehl, L. C. Schaffner (2003). Ephemeral deposition, seabed mixing and fine-scale strata formation in the York River estuary, Chesapeake Bay. *Estuarine, Coastal and Shelf Science* 58, p. 621–643
- Eldeberky, Y. (1996). Nonlinear transformation of wave spectra in the nearshore zone, *Ph.D. thesis*, Delft University of Technology, Department of Civil Engineering, The Netherlands
- Forster, S., R. N. Glud, J. K. Gundersen and M. Huettel (1999). In situ Study of Bromide Tracer and Oxygen Flux in Coastal Sediments. *Estuarine, Coastal and Shelf Science* 49, p. 813–827.
- Garcia, M.H. (1994). Depositional turbidity currents laden with poorly sorted sediment. *Journal of Hydraulic Engineering* 120, 1240– 1263.

- Gibbes, B., C. Robinson, H. Carey, L. Li, D. Lockington (2008a). Tidally driven pore water exchange in offshore intertidal sandbanks: Part I. Field measurements. *Est. Coast. Shelf Science* 79, p. 121-132
- Gibbes, B., C. Robinson, L. Li, D. Lockington, H. Li (2008b). Tidally driven pore water exchange in offshore intertidal sandbanks: Part II. Numerical simulations. *Est. Coast. Shelf Science* 80, p. 472-482.
- Harris, C.K. and P.L. Wiberg (1996). Approaches to quantifying long-term continental shelf sediment transport with an example from the Northern California STRESS mid-shelf site. *Cont. Shelf Res.*, Vol 17, No 11, pp 1389-1418.
- Hasselmann, K. (1974). On the spectral dissipation of ocean waves due to whitecapping, *Bound.-layer Meteor.*, 6, 1-2, 107-127
- Hasselmann, K., T.P. Barnett, E. Bouws, H. Carlson, D.E. Cartwright, K. Enke, J.A. Ewing, H. Gienapp, D.E. Hasselmann, P. Kruseman, A. Meerburg, P. Müller, D.J. Olbers, K. Richter, W. Sell and H. Walden (1973). Measurements of wind-wave growth and swell decay during the Joint North Sea Wave Project (JONSWAP), *Dtsch. Hydrogr. Z. Suppl.*, 12, A8.
- Hasselmann, S. and Hasselmann, K. (1985). Computations and parameterizations of the nonlinear energy transfer in a gravity-wave spectrum. Part I: A new method for efficient computations of the exact nonlinear transfer integral, *Journal of Physical Oceanography*, 15, no. 11, pp. 1369-1377.
- Heberta, A. B., F. J. Sansone, G. R. Pawlak (2007). Tracer dispersal in sandy sediment porewater under enhanced physical forcing. *Continental Shelf Research* 27 2278–2287.
- Houwing, E.J. (1999). Determination of the critical erosion threshold of cohesive sediments on intertidal mudflats along the Dutch Wadden Sea coast. *Estuar. Coast. Shelf Sci.* 49, 545–555.
- Huettel, M. and Webster, I. T. (2001). Porewater flow in permeable sediment. In Boudreau, B. P., and B.B. Jorgensen (eds): *The benthic boundary layer*. Oxford University Press, New York, p. 144-179.
- Huettel, M., and Gust (1992). Impact of bioroughness on interfacial solute exchange in permeable sediments. *Marine Ecology Progress Series* vol 89, p. 253-267.
- Huettel, M., W. Ziebis, and S. Forster (1996). Flow-induced uptake of particulate matter in permeable sediments. *Limnol. Oceanogr.*, 41(2), p. 309-322
- Huettel, M., W. Ziebis, S. Forster, and G. W. Luther (1998). Advective transport affecting metal and nutrient distributions and interfacial fluxes in permeable sediments. *Geochimica et Cosmochimica Acta*, Vol. 62, No. 4, pp. 613–631.
- Jacobs, W., W.G.M. van Kesteren and J.C. Winterwerp (2005). Strength of sediment mixtures as a function of sand content and clay mineralogy. INTERCOH.
- Jacobs, Walter (2006). Eco-morphology of estuaries and tidal lagoons: literature review and experiments on sand-mud mixtures, TU-report No. 1-06.
- Janssen, P.A.E.M. (1991). Quasi-linear theory of wind-wave generation applied to wave forecasting, *J. Phys. Oceanogr.*, 21, 1631-1642.
- Janssen, P.A.E.M., D. Doyle, J. Bidlot, B. Hansen, L. Isaksen and P. Viterbo (2002). Impact and feedback of ocean waves on the atmosphere. *Advances in Fluid Mechanics, Atmosphere-Ocean Interactions*, I, WIT press, Ed. W. Perrie. 155-197.
- Janssen, P.A.E.M., P. Lionello and L. Zambresky (1989). On the interaction of wind and waves. *Philos. Trans. Roy. Soc. London*, A329, 289-301.

- Kleinhans M.G., O. Montfort, P.J.T. Dankers, L.C. van Rijn, W. Bonne (2005). Mud dynamics on the shoreface and upper shelf, Noordwijk, the Netherlands. In L.C. van Rijn, R.L. Soulsby, P. Hoekstra, and A.G. Davies: Sandpit, sand transport and morphology of offshore mining pits. Aqua Publications, the Netherlands, p. Z.1-Z.15.
- Komen, G.J., Cavaleri, L., Donelan, M., Hasselmann, K., Hasselmann, S. and P.A.E.M. Janssen (1994). *Dynamics and Modelling of Ocean Waves*, Cambridge University Press, 532 p.
- Komen, G.J., S. Hasselmann, and K. Hasselmann (1984). On the existence of a fully developed windsea spectrum, *J. Phys. Oceanogr.*, **14**, 1271-1285
- Krishnappan, B.G. and P. Engel (2006). Entrapment of fines in coarse sediment beds. Proc. River Flows 2006. Feirreira, Alves, Leal and Cardoso (Eds). Taylor and Francis Group London, ISBN 0-415-40815-6. pp. 817–824.
- Laane, R.W.P.M., H.L.A. Sonneveldt, A.J. Van der Weyden, J.P.G. Loch, G. Groeneveld (1999). Trends in the spatial and temporal distribution of metals (Cd, Cu, Zn and Pb) and organic compounds (PCBs and PAHs) in Dutch coastal zone sediments from 1981 to 1996: a model case study for Cd and PCBs. *Journal of Sea Research* 41, p. 1–17
- Lee, H II and R. C. Swartz (1980). Biological processes affecting the distribution of pollutants in marine sediments, part II: Biodeposition and Bioturbation. In: Baker, R.A. (ed): Contaminants and sediments Vol. 2: analysis, chemistry and biology. Ann Harbor Science Publishers Inc., Michigan, U.S.
- Madsen, O.S., Y.-K. Poon and H.C. Graber (1988). Spectral wave attenuation by bottom friction: Theory, *Proc. 21<sup>st</sup> Int. Conf. Coastal Engineering*, ASCE, 492-504
- Marinelli, R.L., R. A. Jahnke, D. B. Craven, J. R. Nelson, and J. E. Eckman (1998). Sediment nutrient dynamics on the South Atlantic Bight continental shelf. *Limnol. Oceanogr.* 45 (3), p. 550-557.
- Mastbergen, D.R. and van den Berg, J.H. (2003) Breaching in fine sands and the generation of sustained turbidity currents in submarine canyons. *Sedimentology* 50, 625–637.
- Middleton, G.V. (1966). Experiments on density and turbidity currents: II. Uniform flow of density currents. *Canadian Journal of Earth Sciences* 3, 627–637.
- Middleton, G.V. (1993). Sediment deposition from turbidity currents. *Annual Review of Earth and Planetary Sciences* 21, 89– 114.
- Mitchell, J.K. (1976). *Fundamentals of Soil Behaviour*. University of California, Wiley, Berkeley.
- Mitchener, H. and Torfs, H. (1996). Erosion of sand – mud mixtures. *Coastal Eng.* 29, 1–25.
- Obhrai, C., P. Nielsen, C.E. Vincent (1999). Influence of infiltration on suspended sediment under waves. *Coastal Engineering* 45 111– 123.
- Paarlberg, A.J., M.A.F. Knaapen, M.B. de Vries, S.J.M.H. Hulscher, Z.B. Wang. Biological influences on morphology and bed composition of an intertidal flat. *Estuarine, Coastal and Shelf Science* 64, p. 577-590
- Panagiotopoulos, I., Voulgaris, I.G. and Collins, M.B. (1997). The influence of clay on the threshold of movement on fine sandy beds. *Coastal Eng.* 32, 19–43.
- Pierson, W.J. and L. Moskowitz (1964). A proposed spectral form for fully developed wind seas based on the similarity theory of S.A. Kitaigorodskii, *J. Geophys. Res.*, **69**, 24, 5181-5190.

- Precht, E., Huettel, M. (2004). Rapid wave-driven advective pore water exchange in a permeable coastal sediment. *Journal of Sea Research* 51, 93–107.
- Prooijen, B. van, T. van Kessel, M. van Ledden (2007). Modelling of fine sediment in a sandy environment – the coastal zone of the Netherlands, submitted to: IAHR 2007 Conference.
- Prooijen, B., J.C. Winterwerp, A stochastic formulation for erosion of cohesive sediments, submitted to *Journal of Geophysical Research*.
- Raudviki, A.J. (1990) *Loose Boundary Hydraulics*, 3<sup>rd</sup> edn. Pergamon Press, Oxford.
- Reimers, C. E. H. A. Stecher, G. L. Taghon, C. M. Fuller, M. Huettel, A. Rusch, N. Ryckelynck, C. Wild (2004). In situ measurements of advective solute transport in permeable shelf sands. *Continental Shelf Research* 24 p. 183–201.
- Riedl, R. J., N. Huang, and R. Machan (1972). The subtidal pump: a mechanism of interstitial water exchange by wave action. *Marine Biology* 13, p. 210 – 221.
- Ris, R.C. (1997): *Spectral Modelling of Wind Waves in Coastal Areas* (Ph.D. Dissertation Delft University of Technology), Communications on Hydraulic and Geotechnical Engineering, Report No. 97-4, Delft.
- Ris, R.C., N. Booij and L.H. Holthuijsen (1999): A third-generation wave model for coastal regions, Part II: Verification, *J. Geophys. Res.*, **104**, C4, 7667– 7681.
- Roelvink, J.A., T. van der Kaaij and B.G. Ruesink. (2001). Calibration and verification of large-scale 2D/3D flow models Phase 1. ONL Coast and Sea studies, Project 2: Hydrodynamics and morphology. Report no. Z3029.10. 131 pp.
- Rogers, W.E., Hwang, P.A., Wang, D.W., Kaihatu, J.M. (2000): Analysis of SWAN model with in situ and remotely sensed data from SandyDuck'97. *Proc. 27<sup>th</sup> Int. Conf. on Coastal Engineering*, Sydney, Australia, ASCE, 812-825.
- Rogers, W.E., P.A. Hwang and D.W. Wang (2003): Investigation of wave growth and decay in the SWAN model: three regional-scale applications. *J. Phys. Oceanogr.*, **33**: 366-389.
- Rusch, A., M. Huettel and S. Forster (2000). Particulate Organic Matter in Permeable Marine Sands—Dynamics in Time and Depth. *Estuarine, Coastal and Shelf Science* 51, p. 399–414.
- Rutgers van der Loeff, M. M. (1980). Nutrients in the interstitial waters of the Southern bight of the North Sea. *Netherlands journal of sea research* 14 (2), p. 144-171.
- Rutgers van der Loeff (1981). Wave effects on sediment water exchange in a submerged sand bed. *Netherlands journal of sea research* 15 (1): 100-112.
- Sanford, L. P. (2008). Modeling a dynamically varying mixed sediment bed with erosion, deposition, bioturbation, consolidation, and armoring. *Computers & Geosciences* 34, p. 1263–1283
- Suijlen, J.M. and Duin, R.N.M. (2001). Variability of near-surface total suspended matter concentrations in the Dutch coastal zone of the North Sea. Climatological study on the suspended matter concentrations in Dutch coastal zone of the North Sea. Climatological study on the suspended matter concentrations in the North Sea. Report RIKZ/OS/2001.150X.
- Thibodeaux, L. J. and J. D. Boyle (1987). Bedform-generated convective transport in bottom sediment. *Nature*, Vol. 325, p. 341-343.
- Torfs, H. (1995). Erosion of mud/sand mixtures. PhD thesis, Katholieke Universiteit Leuven, Leuven.
- Turner, I.L., and G. Masselink (1998). Swash infiltration-exfiltration and sediment transport. *J. Geoph. Res.*, Vol 103 (C13),p. 30.813–30.824

- Van der Westhuysen, A. J., M. Zijlema and J. A. Battjes (2007): Nonlinear saturation-based whitecapping dissipation in SWAN for deep and shallow water. *Coastal Engng*, **54**, 151-170..
- van Heteren, S., P. Kiden, and J.M.M. Hettelaar (2007). Inventarisatie slibgehalte Noordzeebodem tussen Cadzand en Den Helder. TNO-rapport 2007-U-R0584/C
- Van Kessel, T. (2008). Projectplan Instrumentarium effectvoorspelling slib. Deltares Report Z4773, 11 p.
- Van Kessel, T. and Brière, C. (2006). Modelling of seasonal SPM variations in the Dutch coastal zone. Delft Hydraulics report Z4150, 41 p.
- Van Kessel, T. (2002). Modelling of sand-mud mixtures. Steps towards implementation into standard version Delft3D, Report Z2840, WL | Delft Hydraulics.
- van Kessel, T., G. de Boer, and P. Boderie (2008). Calibration suspended sediment model Markermeer. Deltares report Q4612.
- van Kessel, T., J. C. Winterwerp, B. van Prooijen, M. van Ledden, and W. Borst (subm.). Modelling the seasonal dynamics of SPM with a simple algorithm for the buffering of fines in a sandy bed. submitted to Cont. Shelf Res.
- van Kessel, T., Kranenburg, C. (1996). Gravity current of fluid mud on sloping bed. *Journal of Hydraulic Engineering* 122, 711– 717.
- van Ledden, M. (2003). Sand-mud segregation in estuaries and tidal basins. PhD thesis, Delft University of Technology, 221 p.
- van Ledden, M., van Kesteren, W.G.M. and Winterwerp, J.C. (2004) A conceptual framework for the erosion behaviour of sand-mud mixtures. *Cont. Shelf Res.* 24, 1–11.
- Van Maren, D. S. , Winterwerp, J.C., and Uittenboogaard, R. E. (2007). New developments in the mud transport module of Delft3D, report II: Implementation, sensitivity analysis, calibration and validation. Delft Hydraulics report Z3824.55, 324 p.
- Van Maren, D.S., A. de Swaaf, and T. van Kessel (2008). VOP slib: werkplan 2009. Deltares report Z4773.90, 11 p.
- Van Rijn, L. C. (2007). Unified view of sediment transport by currents and waves, Part I, II, III and IV, *Journal of Hydraulic Engineering*, ASCE, Vol. 133, No. 6 and 7.
- Van Rijn, L.C. (1993). Principles of Sediment Transport in Rivers, Estuaries and Coastal Seas., University of Utrecht and Delft Hydraulics, AQUA Publications.
- Webster, I. T. (2003). Wave Enhancement of Diffusivities within surficial sediments. *Environmental fluid mechanics* 3, p. 269-288.
- Wilson, A.M., M. Huettel, S. Klein (2008). Grain size and depositional environment as predictors of permeability in coastal marine sands. *Estuarine, Coastal and Shelf Science* 80, p. 193–199.
- Winterwerp, J. C. (2005). Reducing harbor sedimentation, I: Methodology. *Journal of Waterway, Port, Coastal and Ocean Engineering*, Nov. 2005, p 258-266.
- Winterwerp, J. C., A.J. Manning, C. Martens, T. de Mulder, J. Vanlede (2006). A heuristic formula for turbulence-induced flocculation of cohesive sediment. *Estuarine, coastal and shelf Science* 68, p 195-207.
- Winterwerp, J.C., Uittenbogaard, R.E., van Maren, D.S., Vanlede, J. (submitted). An integral model for high-concentrated mud suspensions in estuaries part 1: model setup. *Intercoho 2007 proceedings*.

Winterwerp, J.C., van Kessel, T. (2003). Siltation by sediment-induced density currents. *Ocean Dynamics* 53, 186–196.

Yan, L. (1987): An improved wind input source term for third generation ocean wave modelling, Sci. Rep. WR 87-8, KNMI, De Bilt, 20 p.

## A Sand-mud interaction in Delft3D-WAQ

De procesformuleringen zijn eerder beschreven in Van Ledden (2003) en Van Kessel (2002). In dit project zijn alleen de erosieformuleringen voor slib aangepast. De erosie van zand is niet beschouwd, omdat deze binnen WAQ slechts op een zeer schematische wijze kan worden meegenomen. Het transport van zand zal in de toekomst worden ontleend aan de daarvoor te ontwikkelde modules binnen WAQ, welke zijn overgezet vanuit Delft3D.

De invloed van het slibgehalte op erosie vindt plaats door een aanpassing van de kritieke schuifspanning voor erosie en van de erosieparameter  $M$ . Daarbij is, conform de aanpak van Van Ledden, een niet-cohesief en een cohesief regime onderscheiden.

### A.1 Definities

Indien het slibgehalte  $p_m$  (Eng: mud content; %<63  $\mu\text{m}$ ) van de bodem kleiner is dan een kritieke waarde  $p_{m,cr}$  is sprake van niet-cohesief gedrag. De definitie van het slibgehalte  $p_m$  (mud content) is volgens Van Ledden het massa-percentage van het totale monster met een korreldiameter kleiner dan 63  $\mu\text{m}$ . In deze notitie wordt het slibgehalte niet uitgedrukt als percentage maar als fractie:

$$p_m = \frac{M_{slib}}{M_{totaal}}$$

Een andere definitie voor de slibfractie is:

$$f_m = \frac{M_{slib}}{M_{zand}}$$

De relatie tussen beide is:  $f_{slib} = \frac{p_m}{1 - p_m}$

**A.2 Niet-cohesief regime (zand gedomineerd):  $p_m < p_{m,cr}$** **A.2.1 Erosiesnelheid en erosieparameter**

Door Van Ledden (2003) wordt de erosiesnelheid van slib,  $E_m$  [m/s], gegeven door:

$$E_m = f_m E_{zand} = \frac{p_m}{1-p_m} E_{zand} = \frac{p_m}{1-p_m} M_{nc} T_{nc}^{\alpha_{b2}-0.9} \quad \text{voor } p_m \leq p_{m,cr}$$

$$M_{nc} = \frac{\alpha_{b1}}{3} \frac{\sqrt{\Delta g d_{50}}}{D_*^{0.9}}$$

$$T_{nc} = \frac{\tau_b}{\tau_{e,nc}} - 1 \quad \text{voor } \tau_b > \tau_{e,nc}$$

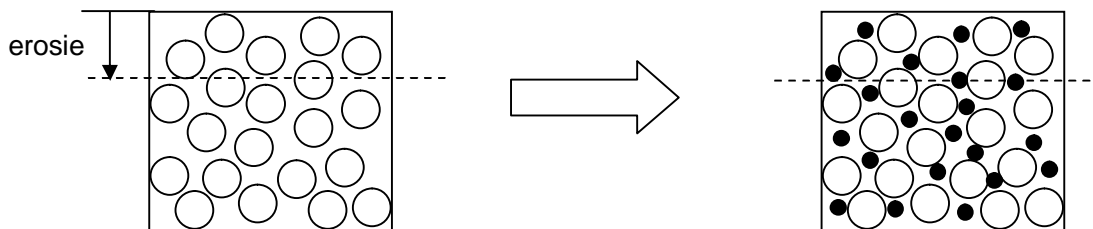
$$T_{nc} = 0 \quad \text{voor } \tau_b \leq \tau_{e,nc}$$

$$D_* = d_{50} \left( \frac{\Delta g}{\nu^2} \right)^{1/3}$$

$$\Delta = \frac{\rho_s - \rho_w}{\rho_w}$$
(A.1)

waarin  $\rho_s$  en  $\rho_w$  de sediment- en waterdichtheid [kg/m<sup>3</sup>],  $g$  de gravitatieversnelling [m/s<sup>2</sup>],  $d_{50}$  de mediane zandkorreldiameter [m],  $T_{nc}$  de schuifspanningsparameter [-] (zie verder) en  $\nu$  de kinematische viscositeit [m<sup>2</sup>/s]. Hierbij is verondersteld, dat de aanwezigheid van slib in de poriën van het zandpakket de erosieparameter  $M_{nc}$  van het zand niet beïnvloedt en dat het slib met het zand proportioneel wordt 'mee geërodeerd', zie de schets hieronder<sup>1</sup>.

Zonder slib Met slib



In dat geval geldt:  $E_{slib} = \frac{M_{slib}}{M_{zand}} E_{zand} = f_m E_{zand} = \frac{p_m}{1-p_m} E_{zand}$

De erosieparameter  $M_{nc}$  is constant voor  $p_m < p_{m,cr}$  en de erosiesnelheid van het slib wordt alleen bepaald door het slibgehalte  $p_m$  en de bodemschuifspanningsparameter  $T$ . De constanten  $\alpha_{b1}$  en  $\alpha_{b2}$  zijn door Van Ledden (2003) als volgt gedefinieerd:

<sup>1</sup> Er is wel een invloed van het slib op de kritieke erosieschuifspanning, zie hierna.

$$T_{nc} < 3: \alpha_{b1} = 0.053 \quad \alpha_{b2} = 2.1;$$

$$T_{nc} > 3: \alpha_{b1} = 0.1 \quad \alpha_{b2} = 1.5.$$

In Van Kessel (2002) wordt voor vgl. (A.1) voorgesteld:

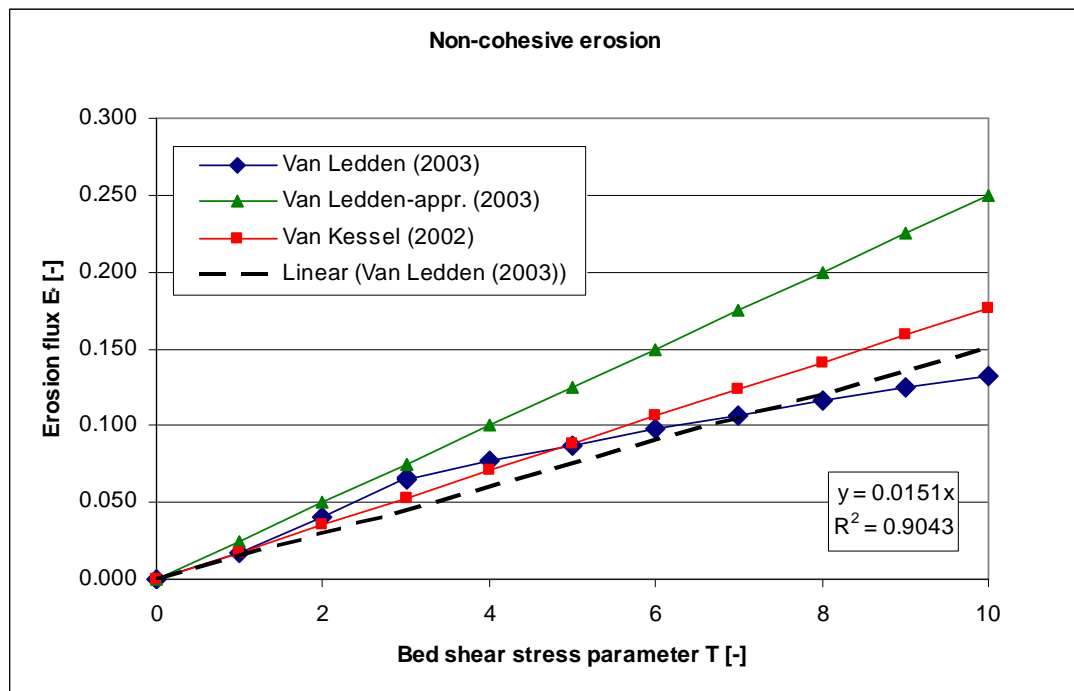
$$T_{nc} > 0: \alpha_{b1} = 0.053 \quad \alpha_{b2} - 0.9 = 1.$$

Hierdoor wordt de macht van de schuifspanningsparameter  $T_{nc}$  gelijk aan 1.

De vergelijking  $E_m^* = \frac{E_m}{\frac{p_m}{1-p_m} \frac{\sqrt{\Delta g d_{50}}}{D_*^{0.9}}} = \frac{\alpha_{b1}}{3} T_{nc}^{\alpha_{b2}-0.9}$  is weergegeven in onderstaande

figuur, zowel volgens Van Ledden (2002) als volgens Van Kessel (2002). De laatste blijkt in het gegeven bereik  $0 < T_{nc} < 10$  goed de vergelijking volgens Van Ledden te benaderen.

De erosieparameter  $M_{nc}$  wordt direct als invoerparameter opgegeven en niet uitgerekend als functie van de sediment- en vloeistof parameters. Dit zal (later) in de morfologiemodules van WAQ worden gedaan.



#### Opmerkingen:

- Het slibgehalte is gedefinieerd als:  $p_m = \frac{M_{slib}}{M_{zand} + M_{slib}}$
- In Van Kessel (2002) wordt voor de slibfractie eveneens  $p_m$  gebruikt. Deze is echter voor *het niet-cohesieve regime* impliciet gedefinieerd als  $p_m = \frac{M_{slib}}{M_{zand}}$ , waardoor geschreven wordt:  $E_{slib} = p_m E_{zand}$ . Dit betekent, dat  $p_m$  in Van Kessel

(2002) in het niet-cohesieve regime dezelfde betekenis heeft als  $f_m$  in dit rapport.

- De erosiesnelheid en erosieparameter hebben beiden als dimensie m/s!
- Van Ledden geeft op blz. 63  $\alpha_{b1} = 0,075$  en  $\alpha_{b2} = 1,9$  als gemiddelden van resp. 0,053 en 0,1 en van 1,5 en 2,1. Dit geeft de groene lijn in bovenstaande figuur en leidt dus tot een overschatting. De 'best-fit' voor  $0 < T < 10$  (dit is het bereik voor  $T$  voor de proeven voor de pick-up functie van Van Rijn (1993, Fig. 7.2.8) leidt tot  $\alpha_{b1} = 0,045$  en  $\alpha_{b2} = 1,9$ .

#### A.2.2 Kritieke erosieschuifspanning ( $p_m < p_{m,cr}$ )

De kritieke bodemschuifspanning voor erosie  $\tau_{e,nc}$  wordt gegeven door (Van Ledden, 2003, en Van Kessel, 2002):

$$\tau_{e,nc} = \tau_{cr,s} (1 + p_m)^\beta \quad \text{voor } p_m \leq p_{m,cr} \quad (\text{A.2})$$

waarin  $\tau_{cr,s}$  de kritieke bodemschuifspanning voor zand [Pa],  $p_m$  het slibgehalte [-] en  $\beta$  een empirische constante [-]. Hierbij varieert  $\beta$  tussen 0.75 en 1.25.

#### Opmerkingen:

De berekening  $\tau_{cr,s}$  voor de 'initiation of motion' volgens Van Rijn (2007) verloopt als volgt:

$$\theta_{cr} = 0.115 (D_*)^{-0.5} \quad \text{voor } D_* < 4$$

$$\theta_{cr} = 0.14 (D_*)^{-0.64} \quad \text{voor } 4 \leq D_* < 10$$

$$\tau_{cr,s} = \theta_{cr} (\rho_s - \rho_w) g d_{50}$$

Voor het niet-cohesieve regime (in Van Rijn (2007) is dit het geval als de deeltjesgrootte in de bodem groter is dan  $62 \mu\text{m}$ ). Er geldt in dat geval  $\beta = 3$  in vergelijking (1.2).

In Van Rijn (1993) wordt de 'initiation of suspension' als volgt berekend:

$$\theta_{cr} = \frac{16w_s^2}{D_*^2 \Delta g d_{50}} \quad \text{voor } 1 < D_* < 10$$

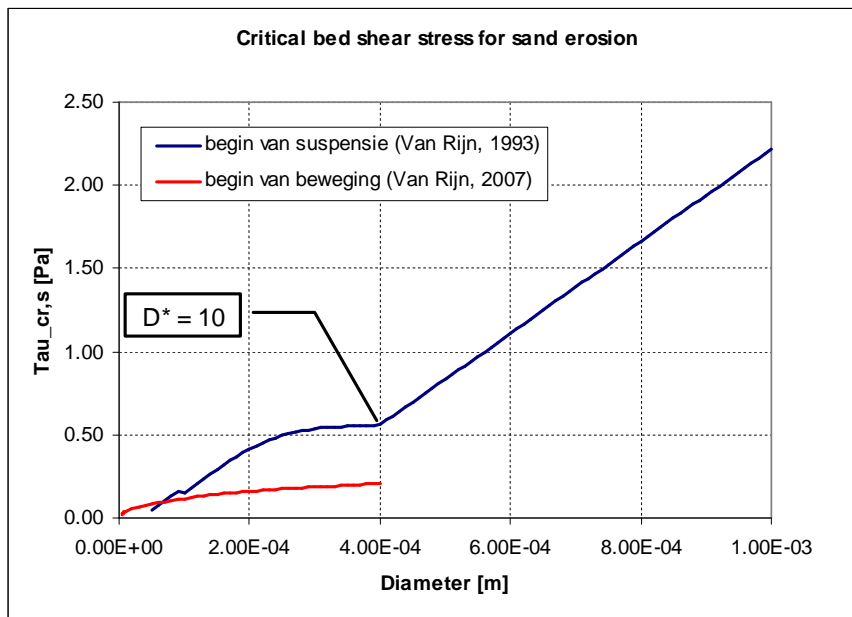
$$\theta_{cr} = \frac{0.16w_s^2}{\Delta g d_{50}} \quad \text{voor } D_* > 10$$

$$w_s = \frac{\Delta g d_s^2}{18\nu} \quad 1 < d_s < 100 \mu\text{m}$$

$$w_s = \frac{10\nu}{d_s} \left[ \left( 1 + \frac{0.01 \Delta g d_s^3}{\nu^2} \right)^{0.5} - 1 \right] \quad 100 < d_s < 1000 \mu\text{m}$$

In de vergelijkingen voor de valsnelheid is  $d_s$  de representatieve diameter voor het suspensiemateriaal. Bovenstaande geldt alleen voor stroming, d.w.z. niet voor de situatie met golven.

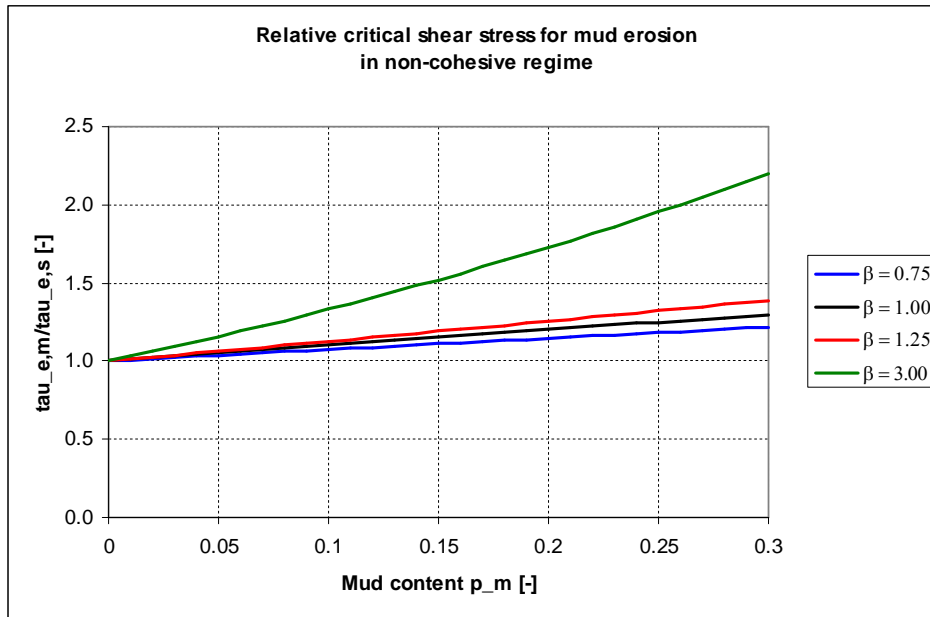
Waarden voor de kritieke schuifspanning voor 'initiation of suspension' zijn kleiner dan 2 Pa voor korreldiameters <1000  $\mu\text{m}$ . De variatie van  $\tau_{cr,s}$  met  $d_{50}$  is als volgt:



Karakteristieke bodemschuifspanningen voor het begin van beweging en het begin van suspensie zijn:

$d_{50}$ [ $\mu\text{m}$ ]	$\tau_{cr,s}$ [Pa]	
	begin van beweging	begin van suspensie
50	0.08	0.05
100	0.12	0.15
200	0.16	0.41
300	0.19	0.54
400	0.21	0.56
500		0.83
1000		2.21

Onderstaande figuur geeft de kritieke bodemschuifspanning voor erosie als functie van het slibgehalte voor  $\beta = 0.75-1.25$  (Van Ledden, 2003) en voor  $\beta = 3$  (Van Rijn, 2007).



### A.3 Cohesief regime (slib gedomineerd): $p_m > p_{m,cr}$

Indien het slibgehalte in de bodem groter is dan een kritieke waarde gedraagt de bodem zich cohesief. De bodem wordt homogeen beschouwd, waarbij de erosiefluxen van zand en slib proportioneel zijn met resp. het zand- en slibgehalte van de bodem (zie Van Kessel, 2002):

$$E_{zand} = (1 - p_m) M_c T_c$$

$$E_{slib} = p_m M_c T_c$$

$$\rightarrow E_{slib} = \frac{p_m}{1 - p_m} E_{zand}$$

$$T_c = \frac{\tau_b}{\tau_{e,c}} - 1 \quad \text{voor } \tau_b > \tau_{e,c}$$

$$T_c = 0 \quad \text{voor } \tau_b \leq \tau_{e,c}$$

waarin  $M_c$  de erosieparameter voor het cohesieve regime [m/s] en  $T_c$  de schuifspanningsparameter voor het cohesieve regime [-]

#### Opmerkingen:

- In Van Kessel (2002) is (kennelijk)  $p_m$  voor het cohesieve regime gedefinieerd als de massa van het slib t.o.v. de totale massa (zand+slib). Voor het niet-cohesieve regime is de gehanteerde definitie voor het slibgehalte de massa van het slib t.o.v. de massa van het zand. Bij de implementatie zal voor beide

regimes uitgegaan worden van de definitie  $p_m = \frac{M_{slib}}{M_{zand} + M_{slib}}$

- Alleen de erosiesnelheid voor slib is geïmplementeerd; de erosie voor zand zal worden bepaald in de toekomstige morfologiemodule van WAQ.

### A.3.1 Erosieparameter $M_c$ ( $p_m > p_{m,cr}$ )

Voor de bepaling van de erosieparameter  $M_c$  bij een slibgehalte  $p_m$  wordt lineair geïnterpoleerd tussen  $\log\left(\frac{M_{nc}}{1-p_{m,cr}}\right)$  en  $\log(M_e)$  (zie Van Ledden, 2003). In dat geval volgt, dat de erosiesnelheden voor  $p_m = p_{m,cr}$  zowel in het niet-cohesieve als het cohesieve regime gelijk zijn aan  $E = p_m \frac{M_{nc}}{1-p_m} T$  ( $T_{nc} = T_c = T$ ):

$$\log(M_c) = \frac{\log\left(\frac{M_{nc}}{1-p_{m,cr}}\right) - \log(M_e)}{1-p_{m,cr}} (1-p_m) + \log(M_e) \quad \text{voor } p_m > p_{m,cr}$$

#### Opmerkingen:

- De afname van de erosieparameter  $M_c$  met een toename van het slibgehalte  $p_m$  is wellicht niet realistisch. Entrainment van zand (grotere korreldiameter en dus grotere valsnelheid) zal kleiner zijn dan de entrainment van slib ofwel een toename van het slibgehalte zou dan tot een toename van de erosiesnelheid moeten leiden.
- $M_{nc}$  hangt af van de bodemschuifspanning, omdat  $\alpha_{b1}$  en  $\alpha_{b2}$  verschillend zijn voor  $0 < T < 3$  en  $T > 3$ . Dit zou betekenen, dat via de interpolatie  $M_c$  ook varieert met  $T$ . Van Ledden voorkomt dit, door beide constanten een vaste waarde te geven onafhankelijk van  $T$ . Deze aanpak wordt ook hier gevolgd, zie eerder met  $\alpha_{b1} = 0.053$  en  $\alpha_{b2} = 1.9$ .
- De erosiesnelheid van zand voor een cohesieve bodem kan niet groter zijn dan de erosiesnelheid van zand voor een volledig zandige bodem en moet dus kleiner zijn dan  $w_s C_a$ .

### A.3.2 Kritieke erosieschuifspanning ( $p_m > p_{m,cr}$ )

Indien de bodem volledig uit slib bestaat,  $p_m = 1$ , is de kritieke erosieschuifspanning voor het slib  $\tau_e$ . Voor  $p_m = p_{m,cr}$  is de kritieke erosieschuifspanning gelijk aan  $\tau_{cr,s}(1+p_{m,cr})^\beta$ . Tussen beide waarden wordt lineair geïnterpoleerd voor de bepaling van de kritieke erosieschuifspanning  $\tau_{e,c}$  bij een slibgehalte  $p_m$  volgens:

$$\tau_{e,c} = \left[ \frac{\tau_{cr,s}(1+p_{m,cr})^\beta - \tau_e}{1-p_{m,cr}} \right] (1-p_m) + \tau_e \quad \text{voor } p_m > p_{m,cr}$$

#### Opmerkingen:

- In Van Kessel (2002) staat abusievelijk vermeld in de teller van de term tussen vierkante haken  $\tau_{cr,s}(1+p_m)^\beta$  (d.i.  $p_m$  i.p.v.  $p_{m,cr}$ ).
- Van Rijn (2007) geeft de kritieke erosieschuifspanning voor bodems met een cohesief gedrag. De kritieke schuifspanning  $\tau_{e,c}$  wordt niet gegeven als functie van het slibgehalte maar van de mediane korrelgrootte van het bed:

$$\tau_{e,c} = \tau_{cr,s} \left( \frac{d_{sand}}{d_{50}} \right)^{\gamma-1} \quad \text{voor } 4 < d_{50} < 62 \mu m$$

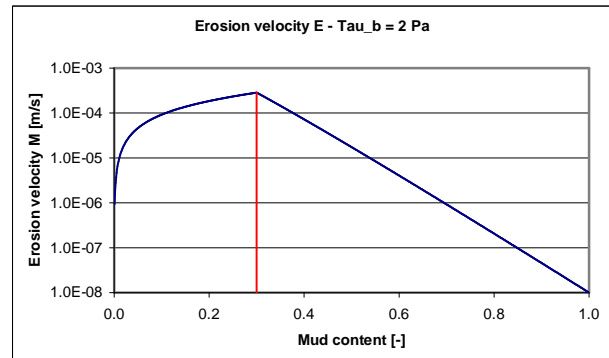
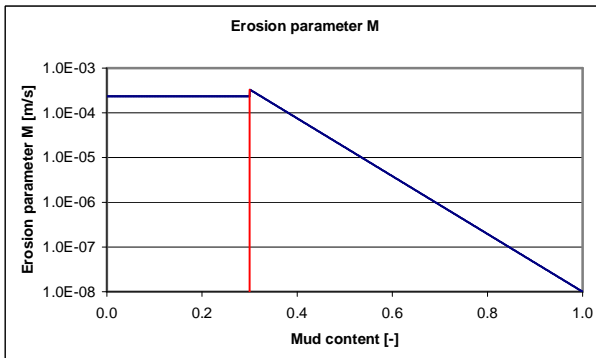
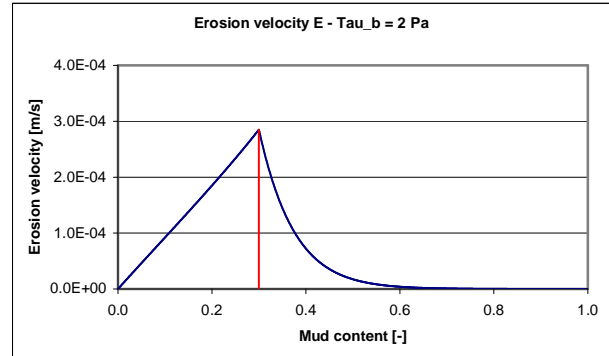
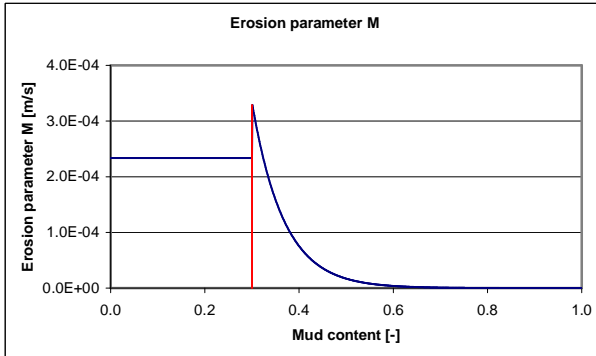
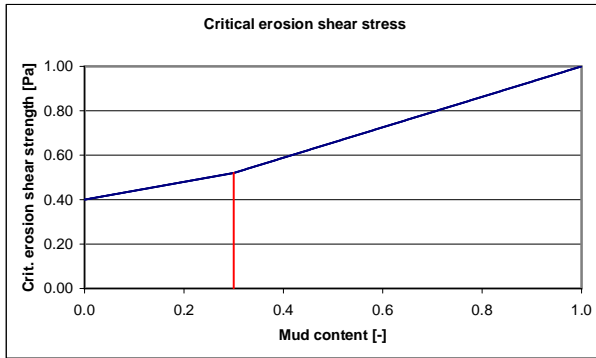
met  $\gamma$  een empirische constante ( $\gamma = 1.5-2$ ),  $d_{sand} = 62 \mu m$  en  $d_{50}$  de mediane korreldiameter van het bed. Op basis van bovenstaande zou voor  $\gamma = 2$  de kritieke erosieschuifspanning van een cohesieve bodem met een mediane

korreldiameter van  $4 \mu\text{m}$  dus een factor  $62/4 \approx 15$  groter zijn dan de kritieke erosieschuifspanning van (niet-cohesief) kwarts met een korreldiameter van  $4 \mu\text{m}$ . De kritieke erosieschuifspanning neemt dan toe van ongeveer  $0,1 \text{ Pa}$  voor een niet-cohesieve bodem met  $d_{50} = 62 \mu\text{m}$  ( $p_m = 0$ ) en  $0,2 \text{ Pa}$  voor een bodem met  $d_{50} = 62 \mu\text{m}$  ( $p_m = 0,3$ ;  $\beta = 3$ ) tot  $0,36 \text{ Pa}$  voor een cohesieve bodem met  $d_{50} = 4 \mu\text{m}$  ( $\gamma = 2$ ). Voor het geval  $\gamma = 1.5$  blijft de kritieke erosieschuifspanning op het niveau van  $0,1 \text{ Pa}$ .

#### A.4 Samenvatting

Onderstaand worden ter illustratie de veranderingen van de erosieparameter  $M_{nc}$  en  $M_c$  en de kritieke erosieschuifspanning  $\tau_{nc}$  en  $\tau_c$  gegeven als functie van het slibgehalte  $p_m$ . Hierbij is uitgegaan van de volgende waarden van de sedimentparameters:

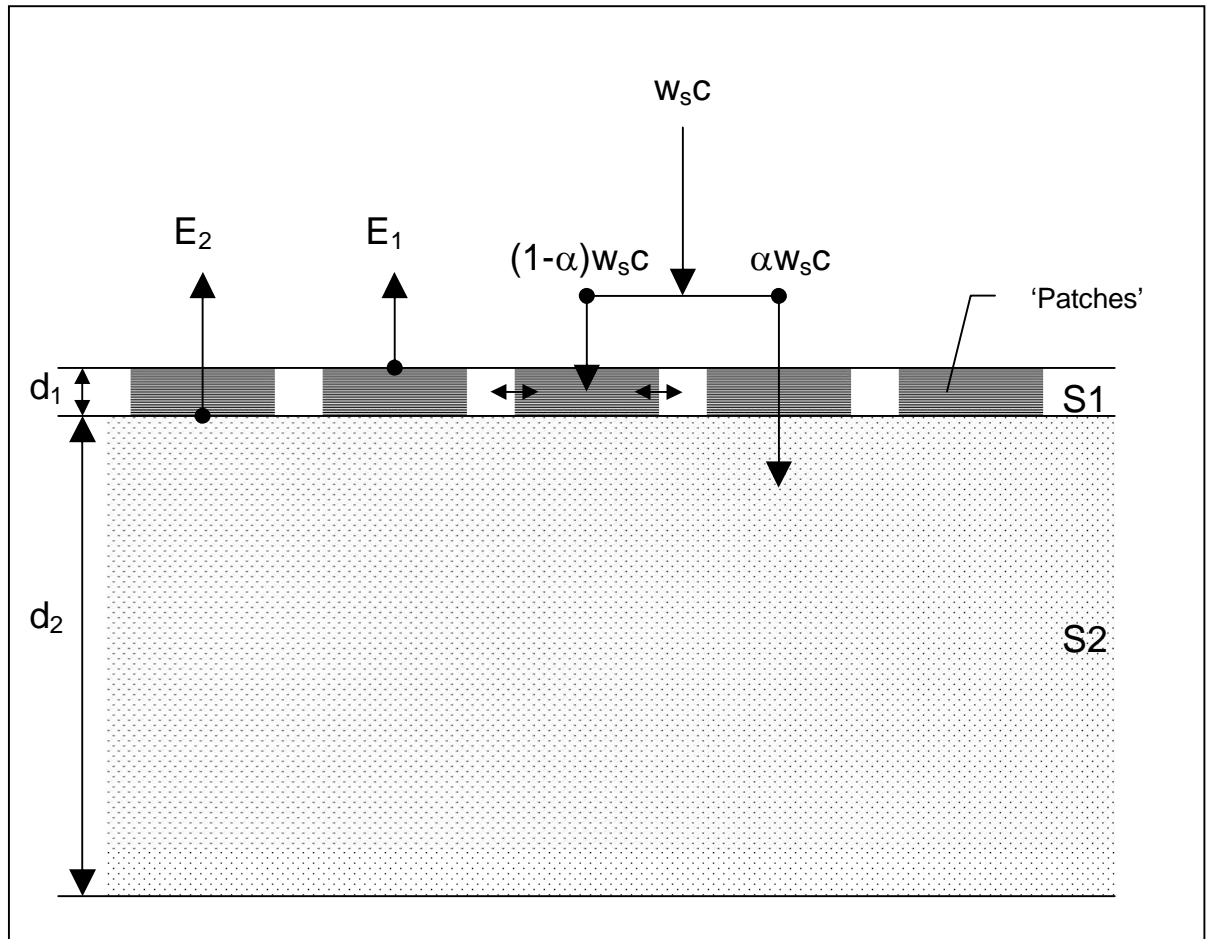
Parameter	Waarde	Dimensie
$p_{m,cr}$	0.3	-
$d_{50}$	200	$\mu\text{m}$
$\rho_s$	2650	$\text{kg/m}^3$
$\rho_w$	1000	$\text{kg/m}^3$
$\alpha_{b1}$	0.053	-
$\alpha_{b2}$	1.9	-
$\nu$	$1 \cdot 10^{-6}$	$\text{m}^2/\text{s}$
$\beta$	1	-
$\tau_{cr,s}$ ( $d = 200 \mu\text{m}$ )	0.4	Pa
$M_e$	$1 \cdot 10^{-8}$	m/s
$\tau_e$	0.5 à 1.0	Pa





## B Beschrijving Buffer model

Er worden twee lagen onderscheiden: een sliblaag S1 en een laag S2, welke een mengsel is van zand en slib, zie onderstaande figuur.



De figuur suggereert, dat laag S1 de onderliggende laag S2 volledig afdekt. In werkelijkheid zal bij een geringe massa slib in laag S1 (per  $m^2$ ) het slib in de vorm van 'patches' voorkomen. De 'patches' worden verondersteld zich ten gevolge van sedimentatie uit te breiden, totdat een aaneengesloten bovenlaag is ontstaan.

De sedimentatie- en erosieformuleringen zijn als volgt:

- Sedimentatieflux naar laag S1:  $(1-\alpha) w_s c$
- Sedimentatieflux naar laag S2:  $\alpha w_s c$

De 'sedimentatieflux' naar laag S2 vindt ongeacht de 'bedekkingsgraad' van laag S1 plaats. Deze flux kan als fysische oorzaken hebben: consolidatie, bioturbatie en omwerking van de toplaag ten gevolge van de voortplanting van beddingvormen. Voor  $\alpha$  geldt:  $\alpha \ll 1$ . Er vindt geen buffering van slib in laag S2 meer plaats, indien de poriën van het zandskelet van laag S2 voor een groot deel zijn gevuld met slib. Als criterium wordt gebruikt:

$$\alpha = 0 \text{ indien } f_m = \frac{M_{\text{slib}}}{M_{\text{zand}}} = 1$$

**Opmerking:**

- Dit criterium is globaal. Het zou gebaseerd kunnen worden op de porositeit van een korrelskelet van zand. Bij een porositeit  $n$  zal bij volledige vulling van de poriën met slib de parameter  $f_m$  gelijk zijn aan  $n/(1-n)$ . Voor  $n = 0.5$  volgt inderdaad  $f_m = 1$ . Bij een porositeit van 0,4 volgt  $f_m = 0,67$ . Het is echter niet waarschijnlijk, dat de poriën volledig zullen worden gevuld met slib. Hierdoor zal  $f_m$  kleiner zijn dan 1. Bijvoorbeeld, indien de poriën voor de helft worden gevuld met slib volgt  $f_m = n/[2(1-n)]$ . Indien  $n = 0,4$  à  $0,5$  volgt  $f_m = 0,33$  à  $0,5$ . De kritieke waarde voor  $f_m$  kan door de gebruiker worden opgegeven.

De erosieflux  $E_1$  van laag S1 is als volgt:

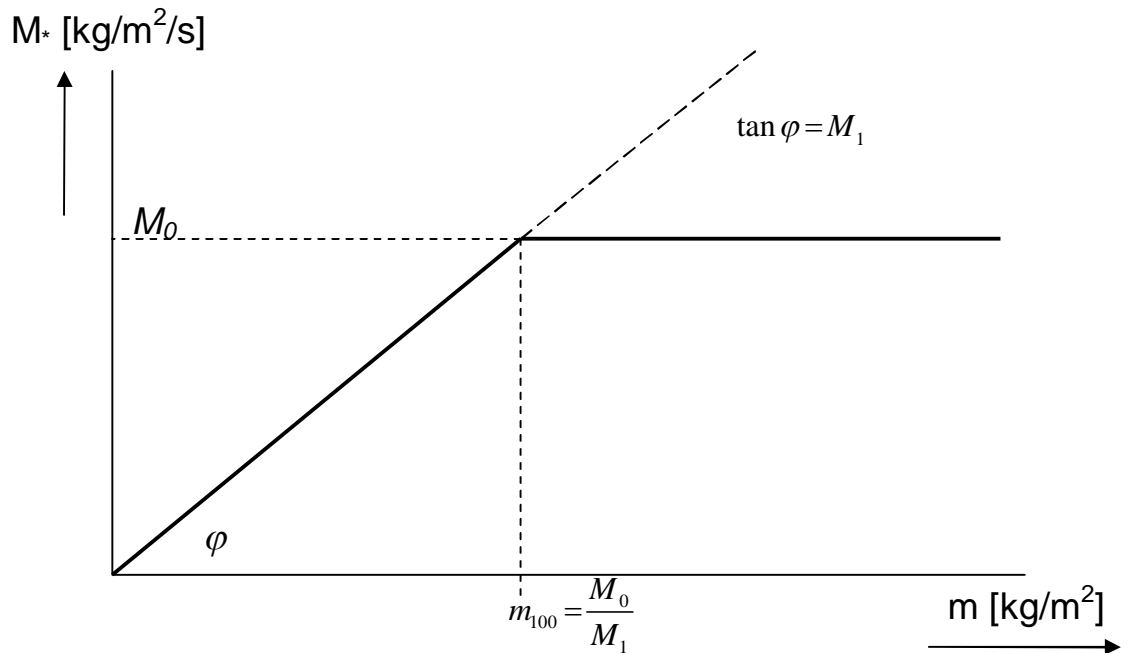
- Erosieflux van laag S1:  $E_1 = \min(E_0, E_1')$  ofwel  $M_* = \min(m(t)M_1, M_0)$  met:
  - $E_0 = M_0 \left( \frac{\tau_b}{\tau_{e,1}} - 1 \right)$ , d.i. de erosie van een *volledig afdekkende* sliblaag (in het Buffermodel bestaat laag S1 voor 100% uit slib);
  - $E_1' = m(t)M_1 \left( \frac{\tau_b}{\tau_{e,1}} - 1 \right)$ , d.i. de erosie van een *gedeeltelijk afdekkende* sliblaag.

Naar gelang de 'patches' in oppervlak toenemen neemt de slibmassa in laag S1 evenredig toe. De erosie is daardoor evenredig aan de slibmassa in laag S1. Op het moment  $t = t_{100\%}$  dat een volledig (=100%) afdekkende sliblaag is ontstaan geldt:  $m_{100\%} M_1 = M_0$ , zie onderstaande figuur. Voor  $m(t) < m_{100\%}$  is de erosie  $E_1'$  dan evenredig met  $m(t) = \frac{d_1(t)}{d_1^{100\%}} m_{100\%}$  waarbij  $d(t)$  de actuele dikte is van laag S1 en  $d_1^{100\%}$  de opgegeven

laagdikte voor de situatie dat sprake is van een volledig afdekkende sliblaag.  $d_1^{100\%}$  zal van dezelfde grootte-orde zijn als de hoogte van de bodenvormen. Voor  $m(t) > m_{100\%}$  is de erosie evenredig met  $M_0$ .

In plaats van gebruik te maken van de laagdikte kan ook worden uitgegaan van de

$$\text{slibmassa in laag S1: } m(t) = \frac{M_1(t)}{M_1^{100\%}} m_{100\%}$$



- Erosieflux van laag S2:  $E_2 = M_2 \left( \frac{\tau_b}{\tau_{e,2}} - 1 \right)$

De erosieflux  $E_2$  heeft betrekking op het slib in laag S2 (het zand erodeert niet). Momenteel wordt hiervoor de pick-up functie van Van Rijn (1993) gehanteerd. Er geldt dan:

$$E_2 = f_{slib} E_{pick\ up} \quad \text{met} \quad f_{slib} = \frac{M_{slib}}{M_{zand}}$$

$$E_{pick\ up} = 0.00033 \rho_s \sqrt{\left( \frac{\rho_s - \rho_w}{\rho_w} g d_{50} \right)} D_*^{0.3} T^{1.5} \quad [\text{kg/m}^2/\text{s}] \quad (\text{B.1})$$

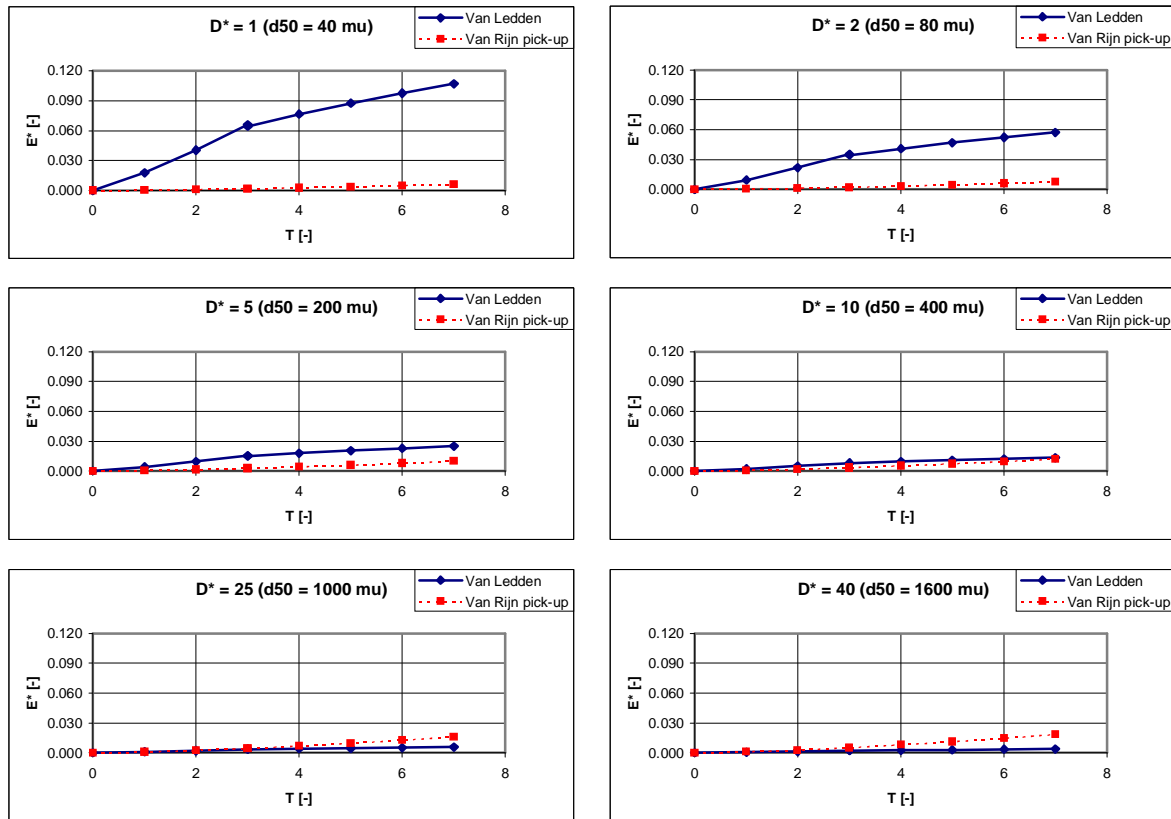
De erosiesnelheid voor zand (in m/s) in Vgl. (A.1) kan worden vergeleken met de erosiesnelheid volgens de pick-up functie van Van Rijn volgens Vgl. (B.1). Beiden worden als volgt geschreven:

$$\text{Van Ledden:} \quad \frac{E_{zand}}{\sqrt{\Delta g d_{50}}} = \frac{\alpha_{b1}}{3} D_*^{-0.9} T_{nc}^{\alpha_{b2}-0.9} \quad [-]$$

$$\text{Van Rijn:} \quad \frac{E_{pick\ up}}{\sqrt{(\Delta g d_{50})}} = 0.00033 D_*^{0.3} T^{1.5} \quad [-]$$

Het is opvallend, dat de erosiesnelheid volgens Van Ledden (eveneens gebaseerd op Van Rijn maar op basis van een beschouwing voor het bodemtransport) evenredig is met  $(d_{50})^{-0.4}$ , terwijl de erosiesnelheid volgens de pick-up functie evenredig is met  $(d_{50})^{0.8}$ . Onderstaande figuur toont beide vergelijkingen voor  $D_* = 1$  ( $d_{50} = 40 \mu\text{m}$ ), 2 ( $d_{50}$

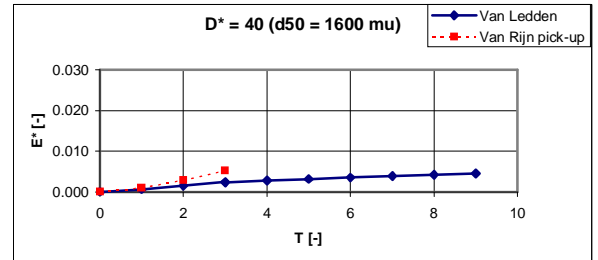
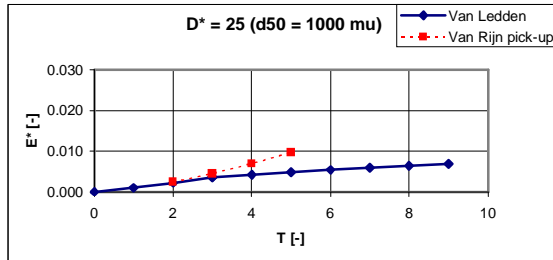
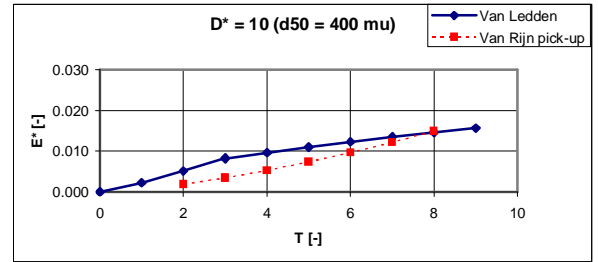
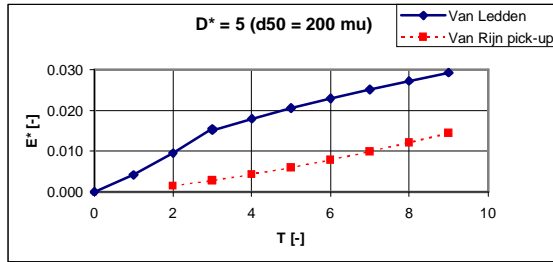
= 80  $\mu\text{m}$ ), 5 ( $d_{50} = 200 \mu\text{m}$ ), 10 ( $d_{50} = 400 \mu\text{m}$ ) en 25 ( $d_{50} = 1000 \mu\text{m}$ ). Uit de figuur volgt, dat de erosiesnelheid zoals gebruikt door Van Ledden vooral voor fijn zand (< 200-300  $\mu\text{m}$ ) vele malen groter is dan de erosiesnelheid volgens de pick-up functie. Voor korreldiameters groter dan 300  $\mu\text{m}$  is de overeenstemming beter. In WAQ kan de gebruiker de gewenste pick-up functie kiezen.



### Opmerking

Het geldigheidsbereik voor de transportformulering gebaseerd op het bodemtransport (cf. Van Ledden) is:  $200 < d_{50} < 2000 \mu\text{m}$ .

Het geldigheidsbereik voor de pick-up functie is:  $130 < d_{50} < 1500 \mu\text{m}$ . en  $u = 0,5-1,0 \text{ m/s}$ . De figuren voor  $D^* = 1$  en  $D^* = 2$  zijn dus niet van toepassing. Verder kan uit Van Rijn (1993), Fig. 7.2.8, ontleend worden het geldigheidsbereik voor  $D^{0.3} T^{1.5}$  voor de verschillende korreldiameters  $D^*$  en dus het geldigheidsbereik voor  $T$  voor elke korreldiameter. Dit is in onderstaande figuur weergegeven:



Uit de figuur volgt dat voor  $300 < d_{50} < 300 \mu\text{m}$  de verschillen een factor twee kunnen zijn.

Aanvullende opmerkingen (Van Rijn, pers. comm.):

- De erosie van zand gebaseerd op het bodemtransport (methode gevolgd door Mathijs van Ledden) betreft een 'oudere' formulering. De pick-up functie verdient de voorkeur.
- De toename van de erosie met de korreldiameter is te verklaren uit het feit dat grotere korrels meer worden aangestroomd.
- Momenteel zitten er in een research versie van D3D ook het transport van zand en slib, zie Van Rijn (2007).



## C Notulen bijeenkomst Bram van Prooijen, Kees Kuijper, Johan de Kok

### C.1 Achtergronden

Bram van Prooijen werkt sinds december 2007 als onderzoeker bij de TUD. Momenteel houdt Bram zich bezig met de erosie van zand-slib mengsels incl. de effecten van biota. Doel van het gesprek is om informatie uit te wisselen met betrekking tot lopende en komende activiteiten op het gebied van zand-slib interactie en na te gaan hoe activiteiten bij de TUD en Deltares op elkaar kunnen worden afgestemd.

### C.2 Activiteiten elders

Volgens Bram lopen er bij de volgende instituten de volgende (voorgenomen) activiteiten op het gebied van water-bodemuitwisseling:

- NIOZ (binnen Building with Nature NTW 3.1) heeft een voorstel gemaakt gericht op het uitvoeren van metingen op de Noordzee (Thijs heeft dit voorstel). NIOZ maakt ook gebruik van modellen, o.a. het hydrodynamische model GETM (Generic Estuarine Transport Model) van Burchard et al.. 3D toepassingen zijn gericht op het ecosysteem van de Noordzee.
- STW-project (Eco-morphology of estuaries and tidal lagoons: Francesc Montserrat, Walter Jacobs en Bram van Prooijen) is vóór de zomer van 2009 gereed. Producten: lab-metingen+analyses van Walter (zie gesprek met Walter); veldmetingen+interpretatie van Francesc; modellering van Bram (zie onder).
- NIOO (binnen Building with Nature, NTW 2.3) heeft een voorstel gemaakt voor de metingen naar waterbodemitwisseling, start: 2009.
- Deltares (binnen Building with Nature, NTW 1.3) heeft een voorstel gemaakt voor implementatie van verschillende water-bodem-uitwisselingsconcepten: *Modeling mud dynamics on mudflats in estuarine and coastal areas*. Start 2009.
- Bas Borsje (TU Twente/Deltares) werkt ook aan effecten van de biologie op de bodem-wateruitwisseling, start: 2008 (?).

Om synergie te creëren uit de verschillende activiteiten op het gebied van water-bodem-uitwisseling zou het zinvol zijn om om korte termijn een dag(deel) te organiseren waarin alle partijen hun plannen uiteenzetten, en waar gezocht zal worden naar samenwerking. Bram zal contact opnemen met Han, Herman Ridderinkhof en Peter Herman.

Een generieke open-source water-bodem-uitwisselingsmodule zou voor iedere partij van belang zijn.

### C.3 Activiteiten TUD (Bram) op gebied van zand-slib formuleringen

Bram heeft een inventarisatie gemaakt van verschillende pick-up functies van zand. De benadering welke Mathijs van Ledden heeft gevolgd, afleiding op basis van *alleen bodemtransport*, werkt niet altijd goed, omdat het suspensief transport dan niet wordt meegenomen. Bovendien is de formulering niet in overeenstemming met metingen (Fernandez-Luque&Van Beek [1976] of Tsusjimoto [1980]). De nieuwe formulering volgens Van Rijn (2008) werkt niet goed voor slibtransport op de Noordzee, omdat deze formulering voor uniform zand/silt is bedoeld en niet voor slib dat in de porieën van het zand zit. De analyse van de pick-up functies wordt binnenkort afgerond.

Bram heeft o.a. de resultaten van het onderzoek van Walter Jacobs gebruikt om de erosie van een slibbodem na te rekenen. Aansluitend hierop zal eveneens de erosie van een zand-slib bodem worden berekend. Met de vaak gebruikte lineaire (Partheniades) formulering kan niet het afvlakken van het concentratieverloop worden gesimuleerd. Bram en Han hebben hierover een artikel geschreven en aangeboden aan het Journal of Geophysical Research (*A stochastic formulation for erosion of cohesive sediments*). Hierbij wordt uitgegaan van een stochastische beschrijving van de bodemschuifspanning en een bodem, welke is gediscretiseerd in een aantal klassen, elk met een eigen kritieke erosieschuifspanning. Met deze aanpak kan het allereerste begin van erosie en de afname van de erosiesnelheid gedurende het erosieproces beter worden beschreven. Een onderscheid maken tussen een niet-cohesief en een cohesief regime, conform de aanpak volgens Mathijs van Ledden, is volgens Bram wel zinnig. Bram prefereert om de erosie te beschrijven als functie van de parameter  $M(\tau_b - \tau_e)$  i.p.v.  $M\left(\frac{\tau_b - \tau_e}{\tau_e}\right)$ , om te voorkomen dat de erosiesnelheid oneindig groot wordt indien de kritieke erosieschuifspanning ( $\tau_e$ ) nadert tot nul.

Als vervolg op de paper zal worden gekeken naar: (i) zand-slib mengsels, (ii) meenemen van depositie en (iii) gebruik van meerdere pick-up functies. Bram zal ook de biologische aspecten op de bodem-wateruitwisseling meenemen.

#### Projecten voor 2009 en verder:

- Afronden STW-project: opzetten van een generieke water-bodem-uitwisselingsmodule, die in bestaande pakketten ingevoegd kan worden.
- Betrokken bij het BwN-project NTW 2.3. Bepaling van biologische effecten op erosie. Projectleider: Peter Herman. AIO zal in 2009 beginnen.
- Betrokken bij het BwN-project NTW 1.3. Implementatie van verschillende water-bodem-uitwisselingsformuleringen, oa bovenstaande stochastische formulering. Thijs van Kessel is projectleider en het zal in 2009 beginnen.
- Dagelijks begeleider van BwN-project NTW 1.2 naar morfologie van platen. Projectleider: Guus Stelling. AIO zal in 2009 beginnen.

#### Plannen:

- Experimenten naar erosie van slib uit zandige bodems. Dit zou gekoppeld moeten worden aan veldmetingen van het NIOZ. In samenwerking met MEDUSA zou het slibpercentage in de bodem bepaald kunnen worden. Han heeft een voorstel ingediend bij STW/waterdienst wat hier op aansluit.

### **C.4 Buffermodel**

Bij het buffermodel, zoals gebruikt voor de MV2-studie, communiceert de tweede (onderste) laag ook direct met de waterlaag: bij sedimentatie wordt een deel  $\alpha$  van het sediment vanuit de waterkolom “doorgeschoven” naar de tweede laag, terwijl de erosie van slib uit het zand in de tweede laag altijd optreedt, ongeacht of wel of niet sprake is van een volledig afdekkende sliblaag (= bovenste laag). Het model moet fysisch beter onderbouwd worden.

Voor wat betreft experimenteel onderzoek is nog niet duidelijk in welk kader dit zal worden opgepakt. Onder andere is van belang de vraag tot welke diepte slib uit een zandlaag wordt gespoeld.

### **C.5 Overig**

- Analyse suppletiemetingen zandwinning door HBR, RWS en Boskalis (zandwinpluimmodel met de vraag: waar blijft de baggerpluim?). Doel: reconstructie T1-beeld uit alle metingen. Hoe snel wordt slib geremobiliseerd (buffering in bodem)? Trachten om met MEDUSA vóór, tijdens en na zandwinning ruimtelijk beeld vast te leggen. Ook vóór en na een stormperiode. Effecten dienen groter dan 1% te zijn om dit met MEDUSA waarneembaar te maken. Hoe kunnen de bovengenoemde voorstellen aansluiten op de T0/T1-metingen en de data-modelassimilatie (Meinte).
- In hoeverre kan/moet consolidatie meegenomen worden?
- Wat zijn de slibvragen op rivieren (Kees Sloff)

### **C.6 Acties**

Uit bovenstaande volgt, dat er in diverse kaders veel gebeurt op het gebied van zand-slib. Bram stelt voor begin 2009 een dag te plannen met de diverse instituten die op dit gebied activiteiten ontplooiën (NIOZ, NIOO-CEME, Deltares, TUD, BwN, STW)

Bram neemt contact op met Han over experimenten naar erosie van slib uit zandige bodems. Hij houdt contact met Kees/Johan om te kijken of er co-financiering mogelijk is vanuit zandwinning/VOP-slib of andere projecten.



## D Notulen bijeenkomst Walter Jacobs, Kees Kuijper, Johan de Kok

### D.1 Achtergronden

Als onderdeel van VOP-slib (Z4773) zullen in 2008 in WAQ aanpassingen worden gedaan om het effect van slib in de (zand)bodem op de erosiesnelheid in rekening te brengen. De beschikbare formuleringen zullen op eenvoudige wijze worden aangepast, gebaseerd op het werk van Mathijs van Ledden:

- Onderscheid wordt gemaakt tussen een niet-cohesief en een cohesief regime;
- De kritieke erosieschuifspanning voor erosie wordt voor beide regimes afhankelijk gesteld van het slibgehalte;
- De erosieparameter ( $M_{nc}$ ) wordt in het niet-cohesieve regime volledig bepaald door de erosie van zand; het aanwezige slib in de poriën 'erodeert mee';
- De erosieparameter ( $M_c$ ) wordt in het cohesieve regime afhankelijk gesteld van het slibgehalte.

Deze benadering is in belangrijke mate empirisch en voor de toekomst zal gezocht moeten worden naar een meer onderbouwde fysische benadering.

De meest recente ontwikkelingen op het gebied van zand-slib hebben plaatsgevonden (en vinden nog plaats) op de TUD. Walter Jacobs rondt momenteel zijn proefschrift af. Zijn promotieonderzoek is vooral gericht op de erosie van een zand-slibbodem. Francesca Mietta werkt momenteel aan een flocculatiemodel, waarbij de flocculatie een functie is van de materiaaleigenschappen en de turbulentie. Verder werkt Bram van Prooijen als post-doc eveneens aan de TUD. Zijn activiteiten betreffen een inventarisatie van sedimenttransportformuleringen, implementatie in programma-codes en het toepassen ervan op watersystemen. In dit bespreekverslag wordt ingegaan op het promotiewerk, zoals toegelicht door Walter Jacobs.

### D.2 Bulkparameters zand-slib mengsels

Walter is in staat met de resultaten van zijn onderzoek uit te rekenen bij welk slibgehalte sprake is van de overgang van granulair naar cohesief gedrag van de bodem. Er is sprake van een granulair skelet, wanneer de zand en silt korrels met elkaar in contact zijn. Bij een cohesieve bodem worden de korrels omgeven door een slibmatrix. Met de volgende twee bulkparameters kan de bodem in termen van de kritieke erosieschuifspanning en de erosiesnelheid worden gekarakteriseerd:

1. pakkingsgraad van het sediment, welke de ruimte tussen de korrels aangeeft;
2. de plasticiteitsindex (PI), welke de 'kneedbaarheid' en daarmee de cohesiviteit beschrijft.

De pakkingsgraad geeft de porositeit van het bodemsediment als functie van het zandgehalte en het siltgehalte. De pakkingsgraad is maximaal (porositeit minimaal) voor een zeker zand- en siltgehalte van het betreffende sediment; het silt vult dan maximaal de poriën van het zand. Andere waarden voor het zand- en siltgehalte resulteren in een geringere pakking en dus in een grotere porositeit. De bepaling van de pakkingsgraad van sediment is een standaard geotechnische proef, welke bij Deltares kan worden uitgevoerd. De plasticiteitsindex geeft informatie over de cohesiviteit van het bodemsediment en is eveneens een standaard grondmechanische bepaling. De plasticiteitsindex is gecorreleerd aan de ongedraineerde sterkte van de

bodem. De bodem gedraagt zich 'zandig' voor waarden van de plasticiteitsindex tot 2. Voor waarden van PI tussen 2 en 7 is sprake van een zandig bed met slib in de poriën. In dat geval beïnvloeden beide sedimentfracties elkaar en is de kritieke erosieschuifspanning een functie van PI. Voor PI groter dan 7 bestaat de bodem uit een kleimatrix, waarbij zand en silt passief aanwezig zijn (als 'vulmateriaal').

### D.3 Erosie en consolidatie van zand-slib mengsels

Met de bovenbeschreven methodiek kan middels een erosievergelijking de erosiesnelheid worden bepaald. Tevens is op basis van het granulaire skelet (middels de pakingsgraad) en de plasticiteitsindex het consolidatiegedrag te voorspellen.

### D.4 Noordzee

De bodem van de Noordzee zal altijd bestaan uit een granulair skelet, waarbij zich slib in de poriën bevindt. Er is geen kleimatrix aanwezig en dus zal de bodem zich niet-cohesief gedragen. Wel kan er een belangrijke biologische invloed zijn (bioturbatie, zelfs tot 20 m waterdiepte). De menging in de bodem ten gevolge van bioturbatie heeft een grote invloed op de verblijftijd van het slib in het systeem; zonder bioturbatie wordt het slib tijdens stormperiodes direct geresuspendeerd. NIOO is momenteel bezig om de bioturbatie te kwantificeren. De verblijftijd wordt dus door zowel biologische als fysische factoren beïnvloed. Op basis van uitgevoerde metingen wordt de verblijftijd van slib in de Noordzee (voor de Nederlandse kust) op 2 jaren geschat.

### D.5 Relaties tussen parameters

- Voor een bepaald estuarium/gebied geldt, dat de verhouding klei-silt een constante waarde heeft. Dit komt waarschijnlijk, omdat silt tijdens het flocculatieproces wordt ingevangen in de slibvlokken. De flocculatie wordt vooral bepaald door de kleimineralogie en kan dus per gebied verschillen.
- Ook is in een watersysteem de verhouding organisch gehalte-kleifractie constant; het organische materiaal bindt zich aan de kleideeltjes.
- Verder is er sprake van een relatie tussen het kleigehalte en de bulkdichtheid van het sediment en een relatie tussen het slibpercentage en de plasticiteitsindex.
- Indien de plasticiteitsindex van alleen klei (dus zonder zand) bekend is, kan de plasticiteitsindex van een mengsel van klei en zand worden berekend (PI van zand is nul).

### D.6 Overige zaken

- Andrew Manning: flocculatie; veldmetingen m.b.t. vlokparameters.
- MEDUSA: hiermee kan een gebiedsdekkende kaart worden gemaakt m.b.t. bodemsamenstelling (slibgehalte; niet de dichtheid). Deze informatie is belangrijk voor de calibratie van modellen. Langdurige concentratiemetingen in combinatie met stroomsnelheidsmetingen in een (beperkt) aantal vaste locaties zijn dan ook essentieel.
- Kritieke erosieschuifspanning: met de aanpak van Van Rijn wordt voor zeer kleine korreldiameters de kritieke erosieschuifspanning onderschat. De geringe doorlatendheid bij kleine korreldiameters zorgt namelijk voor een toename van de kritieke erosieschuifspanning.  
Opmerking Bas van Maren: bij de meest recente transportformulering van Van Rijn (2004) is de ondergrens van het geldige bereik "opgerekt" van 100  $\mu\text{m}$  tot 10  $\mu\text{m}$ . Hierdoor wordt de kritieke erosieschuifspanning bij kleine korreldiameters niet meer onderschat.

- Bram van Prooijen maakt momenteel een overzicht van zand-slib procesformuleringen en het verbeteren/updaten van de Van Ledden formuleringen (o.a. biologische effecten). Hij zal zich ook bezighouden met toepassingen en het oplossen van numerieke problemen (bijv. het droogvallen van platen).
- Han: STW-voorstel zand-slib en voorstel binnen Building with Nature.
- Bij de TUD is een instrument ontwikkeld (momenteel operationeel), waarmee *lokaal* de dichtheid en de zand-slibverhouding kan worden gemeten op intergetijdengebieden (meetprincipe gebaseerd op het uitzenden van radioactieve straling).
- Aanvullende laboratoriummetingen zijn nodig voor de bepaling van transport van *fijn* sediment. Het mechanische gedrag moet dan worden gekarakteriseerd met de verhouding  $d_{10} / d_{90}$ , welke relateert aan de doorlatendheid ( $d_{10} / d_{90} \leftrightarrow$  doorlatendheid  $\leftrightarrow$  mechanisch gedrag).

### D.7 Consequenties voor toekomstige ontwikkelingen

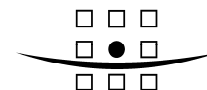
Toepassing van de hiervoor beschreven karakterisering van zand-slib bodems op een estuarien systeem (Westerschelde?) of kustsysteem (Noordzee?) zal aangeven hoe goed het concept voldoet. Bij de TUD zijn er plannen voor een dergelijke activiteit (Bram van Prooijen). Vanuit Deltares zou het concept, gebaseerd op het werk van Van Ledden, kunnen worden getoetst op hetzelfde watersysteem. Onderlinge vergelijking van beide concepten en vergelijking met observaties kan aangeven welke aanpak het meest geschikt is, bijvoorbeeld of een bodem bestaande uit slechts twee lagen (zoals in WAQ) niet te beperkend is..

Aandachtspunten voor deze vergelijking betreffen:

- Waterbeweging en concentraties:
  - Bijvoorbeeld eerst voor de Westerschelde;
  - Allereerst op meso-schaal (intergetijdengebied);
  - Op basis van een inventarisatie van bestaande en geschikte stromingsmodellen;
  - Inventarisatie van meetdata (NIOO, Rijkswaterstaat);
- Bodemprocessen op korte en lange termijn (bijvoorbeeld door consolidatie expliciet te beschouwen voor het tijdsafhankelijke gedrag) en op grote en kleine schaal;
- Inzet van nieuwe meettechnieken bij het vaststellen van de bodemeigenschappen:
  - Remote sensing;
  - Radiometrische sedimentologie. Dit is met een instrument dat gebruik maakt van een radioactieve bron (vergelijkbaar met de apparatuur zoals in gebruik bij MEDUSA). Momenteel wordt integraal over de bovenste 50 cm gemeten; het streven is deze dikte te verkleinen tot 10 m. Eventueel dient het apparaat geruime tijd in situ achter te kunnen blijven.



## **E Kennisvragen vanuit ingenieurspraktijk**



## Notitie

Aan : Thijs van Kessel (Deltares)  
Van : Thomas Vijverberg  
Datum : 9 januari 2009  
Kopie : archief  
Onze referentie : 9T9150.A0/N0001/903718/MJANS/Nijm

**Betreft : Voortschrijdend Onderzoeksprogramma Slib**

---

Deze notitie is opgesteld ten behoeve van het Voortschrijdend Onderzoeksprogramma Slib (VOP Slib) van Deltares. Dit onderzoeksprogramma heeft als doel het onderhouden en verder ontwikkeling van de kennisbasis op het gebied van slib. De verschillende onderzoeksvragen worden voornamelijk vanuit beheersvragen opgesteld. De link met de praktijk is hierdoor altijd aanwezig en praktijkproblemen dienen daardoor ook als input voor het programma. In 2007 zijn door Deltares interviews met beheerders gehouden om deze input vanuit de beheerders kant te verzamelen. Vanuit de ingenieurspraktijk is de input nog niet geleverd. Deltares heeft Royal Haskoning daarom gevraagd om van verschillende, regelmatig in de ingenieurspraktijk voorkomende slib gerelateerde projecten, op papier te zetten wat de algemene ervaring is bij deze projecten en welke kennisleemten er zijn. In deze notitie zal hierop in worden gegaan.

### Type projecten

De projecten kunnen grofweg in 4 categorieën ingedeeld worden.

#### 1. Saneringsonderzoeken waterbodems

In deze projecten speelt vaak de vraag wat te doen met vervuild slib in rivieren, plassen en havens. Enerzijds kan er worden opgedekt met zand en/of breuksteen, anderzijds kan het vervuilde slib worden afgegraven. Recent is hier veel vraag naar geweest bij verschillende projecten. Meestal gaat het hier dan om een goede afschatting te maken van de erosie en sedimentatie van de sliblaag en/of de afdeklaag onder belasting van scheepsgeïnduceerde stroming (schroefstraal werking), golven en stroming.

De effecten van schepen zijn vaak moeilijk in te schatten en hangen af van meerdere aannames, waardoor de berekeningen vaak uiteen kunnen lopen.

Een ander probleem is de relatieve onbekendheid met het dimensioneren van de afdekklagen voor vervuild slib. Met het beschermen van zand met breuksteen is meer ervaring en zijn goede handboeken aanwezig. Voor slib is dat echter niet het geval.

Bij het afgraven van vervuild slib ontstaat vaak een morslaag die blijft liggen. De vraag is vaak hoe erg dat is.

Uiteindelijk moet in deze gevallen vaak een uitspraak worden gedaan op basis van weinig gegevens van het slib (Soms wordt er alleen maar vermeld dat het 'dik' water is als de vraag opkomt wat de dichtheid is van de sliblaag). Hierdoor is het lastig om een betrouwbare schatting te maken van erosie en sedimentatie van de sliblaag, terwijl dit wel van belang is voor een juist advies.

Wellicht is prototype onderzoek of pilot studies een goed idee hiervoor.

## 2. Vertroebeling in waterkolom

Projecten waarbij vertroebeling in de waterkolom een rol speelt zijn voornamelijk gekoppeld aan ecologische problemen. Hierbij kan worden gedacht aan een min of meer natuurlijke oorzaak van vertroebeling (zoals het Markermeer), maar ook vertroebeling veroorzaakt door baggerwerken. Recent zijn een aantal projecten binnengekomen die betrekking hebben op het laatste geval, waarbij de verspreiding van zwevend stof onder invloed van stroming en golven moet worden onderzocht. Dit onderzoek wordt vaak uitgevoerd met behulp van mathematische modellen.

Het goed schematiseren van de invoer parameters is voor deze modellen cruciaal. Voor het zwevend stof geldt hiervoor dat de valsnelheid als belangrijke invoer moet worden opgegeven. Probleem hierbij is vaak de vertaling van de meetwaarden van het zwevend stof (als die al aanwezig zijn), zoals D50 of valsnelheid, naar modelinvoer. Vaak is namelijk een range aan korrelgroottes of valsnelheden aanwezig, maar kan er in de modellen maar met enkele sediment fracties gerekend worden. Calibratie van de modellen met behulp van meetgegevens dienen dan als oplossing en vaak gaat dit wel redelijk goed.

Als bron en puttermen (erosie en sedimentatie) ook meegenomen worden in de modellen komt echter weer het probleem om de hoek kijken als beschreven bij punt 1: het schematiseren van de belangrijke coëfficiënten.

## 3. Slibvangen

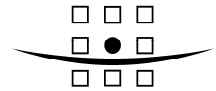
Bij het invangen van sediment in rivieren wordt vaak alleen maar rekening gehouden met zand. Bij problemen met aanzanding van nevengeulen kan slib ook een rol spelen. Vaak wordt hier echter niet expliciet rekening mee gehouden, omdat hierover weinig bekend is. Het invangen van slib speelt ook in uiterwaarden onder invloed van vegetatie. Effecten van verschillende soorten vegetatie zijn moeilijk in te schatten.

## 4. Aanslibbing in havens

In verleden zijn enkele studies gedaan naar het meest efficiënte ontwerp van havens in de Maas en de Waal tegen aanslibbing. De opdrachtgevers waren voornamelijk gemeenten (o.a. gebundeld in de Nederlandse Vereniging van Rivier Gemeenten) die het aanslibben van de havens hinderlijk vonden, ook omdat het slib vaak vervuild is. Vragen die speelden waren: Wat is de aanslibsnelheid? Waardoor wordt de aanslibbing veroorzaakt en hoe kan het voorkomen worden? De aanslibsnelheid is belangrijk om te weten om de onderhoudskosten van de havens te kunnen inschatten.

Echter, vaak de variatie in de modelvoorspellingen groot en in eerste instantie niet conform de realiteit. De inputfactoren voor de modellen moeten vaak erg overdreven worden om realistische resultaten te krijgen. Belangrijk in de analyse is het uitwisselmechanisme (debiet) van de hoofdstroom in de rivier met de haven. Verondersteld wordt dan dat het slib met dit debiet mee uitwisselt. Hierin zijn echter veel onzekerheden en kunnen de resultaten ver uit elkaar liggen. Ook 3D processen spelen een rol bij aanslibbing in deze havens, vaak wordt hier weinig rekening mee gehouden, omdat er geen detail gegevens bekend zijn.

Ook bij de aanslibbing in havens kan de invloed van schepen groot zijn. Schepen zorgen bijvoorbeeld voor opwoeling van het slib en kunnen lokaal de stroming beïnvloeden.



Deze effecten zijn (net als bij ander type projecten ) echter lastig om rekening mee te houden, omdat die voornamelijk zijn gebaseerd op aannames.

## 5. Behandeling van vervuild slib

Projecten waarbij vervuild slib een rol speelt kunnen worden ingedeeld in twee soorten:

### *Verspreiding van vervuiling richting oppervlaktewater*

Hierbij gaat het vaak om de vraag hoe de bijdrage van de vervuiling uit de bodem moet worden bepaald richting het oppervlaktewater. Hiervoor bestaat wel een richtlijn, maar deze is vaak erg warrig en geeft geen eenduidige methodiek voor verschillende situaties. Hierdoor ontstaat vaak discussie over de gekozen methode.

### *Storten van vervuild slib in zandwinputten*

Bij het storten van vervuild slib in zandwinputten is meestal de vraag wat het effect is op het oppervlaktewater en op het grondwater. Hiervoor zijn in het Besluit Bodem Kwaliteit eisen opgesteld, alleen geven die eisen vaak discussie.

Verder is het vaak onduidelijk welke parameters moeten worden ingevuld voor de analyses, omdat er weinig gegevens bekend zijn.

## **Algemeen**

In het algemeen kan worden gesteld dat bij de verschillende soorten projecten het vaak neerkomt op het maken van een goede afschatting van de erosie en sedimentatie van slib. Hiervoor moet een schatting worden gemaakt van de verschillende parameters, zoals kritische schuifspanning voor erosie en voor sedimentatie, de erosie coëfficiënt  $M$ , etc....

Voor deze parameters is veldonderzoek gewenst, maar bijna nooit aanwezig en het uitvoeren ervan is vaak te duur. Gevolg is vaak dat projecten hierop vastgelopen of dat de schattingen erg onzeker zijn.

Het kan wellicht helpen als er voor deze erosie en sedimentatie parameters een link kan worden gelegd met het gebied waar het project zich afspeelt. Wellicht dat ook een orde grote van de coëfficiënten voor elke gebied kan worden gegeven. Dit kan dan dienen als een soort handvat om de berekeningen te starten.

## **Toekomstige projecten**

Een voorbeeld van een type project dat op dit moment weinig wordt uitgevoerd, maar waar in de toekomst meer van wordt verwacht is uitwisseling van zoet en zout water. Hierbij kan worden gedacht aan energieopwekking of aan het project Afsluitdijk.

Zoet-zout uitwisseling kan invloed hebben op de valsnelheid van het zwevend stof in de waterkolom via het flocculatie proces. Gedegen kennis van de effecten hiervan en van het flocculatie proces is hierdoor wenselijk.

Nijmegen, 9 januari 2009

T. Vijverberg M.Sc.